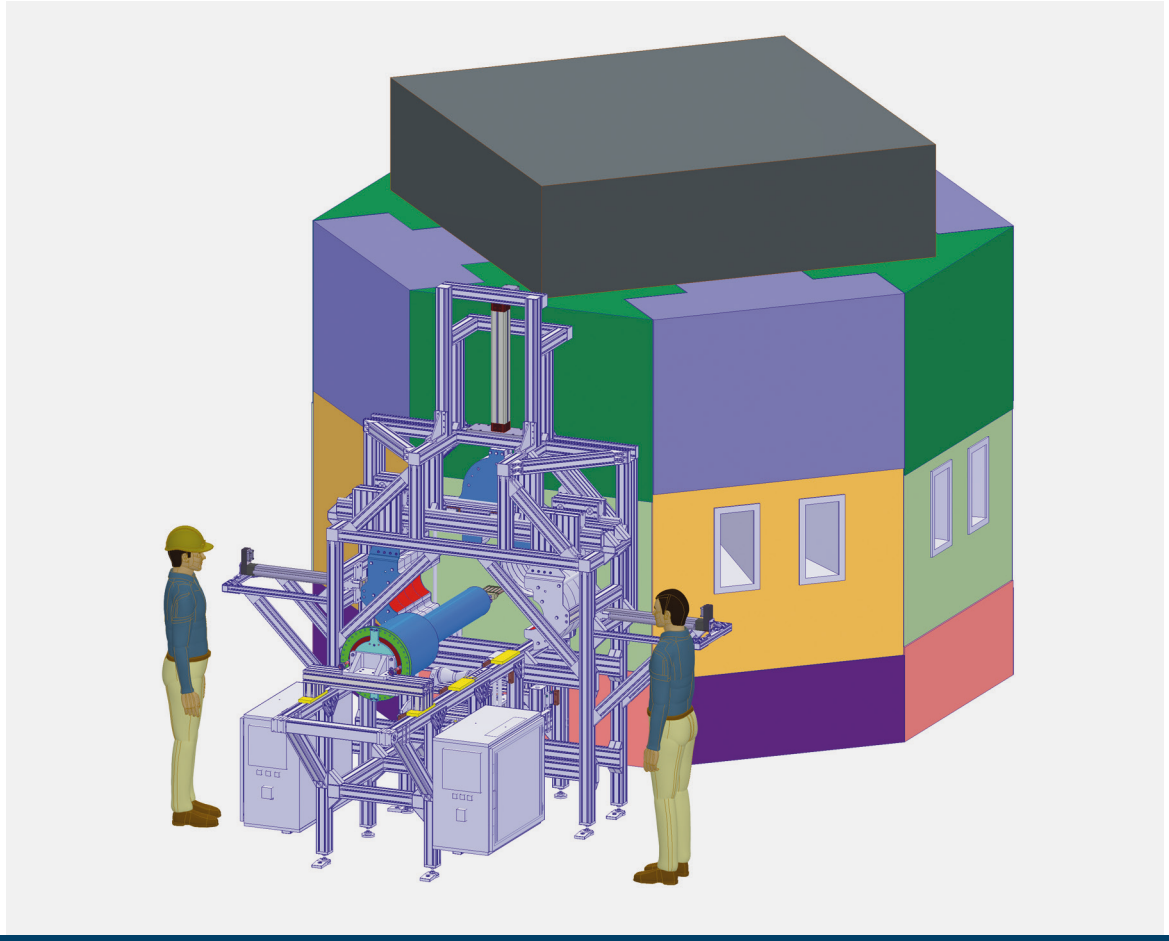

Technical Design Report HBS
Volume 2 – Target Stations and Moderators

J. Baggemann, E. Mauerhofer, U. Rücker, P. Zakalek (Vol. Eds.), T. Brückel, T. Gutberlet (Ser. Eds)

R. Achten, Y. Bessler, T. Gutberlet, R. Hanslik, H. Kleines, J. Li, K. Lieutenant, F. Löchte, I. Pechenizkiy, E. Vezhlev, J. Voigt, J. Wolters

Allgemeines / General
Band / Volume 9-02
ISBN 978-3-95806-710-3

Mitglied der Helmholtz-Gemeinschaft

JÜLICH
Forschungszentrum

Schriften des Forschungszentrums Jülich
Reihe Allgemeines / General Band / Volume 9-02

Forschungszentrum Jülich GmbH
Jülich Centre for Neutron Science (JCNS)
Quantenmaterialien und kollektive Phänomene (JCNS-2 / PGI-4)

Technical Design Report HBS
Volume 2 – Target Stations and Moderators

J. Baggemann, E. Mauerhofer, U. Rücker, P. Zakalek (Vol. Eds.)
T. Brückel, T. Gutberlet (Ser. Eds)

R. Achten, Y. Bessler, T. Gutberlet, R. Hanslik, H. Kleines,
J. Li, K. Lieutenant, F. Löchte, I. Pechenizkiy, E. Vezhlev,
J. Voigt, J. Wolters

Schriften des Forschungszentrums Jülich
Reihe Allgemeines / General Band / Volume 9-02

ISSN 1433-5565 ISBN 978-3-95806-710-3

Bibliografische Information der Deutschen Nationalbibliothek.
Die Deutsche Nationalbibliothek verzeichnet diese Publikation in der
Deutschen Nationalbibliografie; detaillierte Bibliografische Daten
sind im Internet über http://dnb.d-nb.de abrufbar.

Herausgeber und Vertrieb:	Forschungszentrum Jülich GmbH Zentralbibliothek, Verlag 52425 Jülich Tel.: +49 2461 61-5368 Fax: +49 2461 61-6103 zb-publikation@fz-juelich.de www.fz-juelich.de/zb
Umschlaggestaltung:	Grafische Medien, Forschungszentrum Jülich GmbH
Druck:	Grafische Medien, Forschungszentrum Jülich GmbH
Copyright:	Forschungszentrum Jülich 2023

Schriften des Forschungszentrums Jülich
Reihe Allgemeines / General, Band / Volume 9-02

ISSN 1433-5565
ISBN 978-3-95806-710-3

Vollständig frei verfügbar über das Publikationsportal des Forschungszentrums Jülich (JuSER)
unter www.fz-juelich.de/zb/openaccess.

CONTENTS

I.
INTRODUCTION

Accelerator-based neutron sources provide a versatile and effective opportunity to improve and spread neutron access in Europe and also a new route for the supply of neutrons to science and industry with leading-edge research infrastructures. The High-Brilliance neutron Source (HBS) project pushes the performance of such sources to the technological limits by employing state-of-the-art technologies in accelerator development, target and moderator design as well as beam extraction, beam optics and instrumentation. Based on a high current low energy proton accelerator, which produces powerful pulsed beams hitting a metal target (tantalum for HBS) to release a thermal neutron flux comparable to existing medium to high flux reactor sources, a variable suite of neutron instruments and applications can be served.

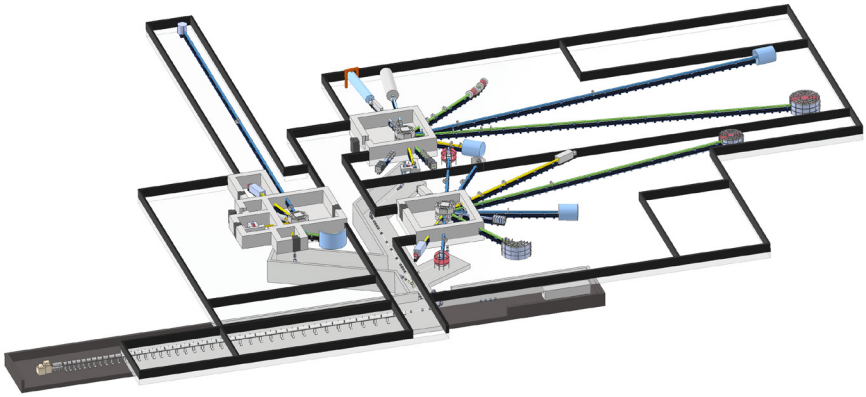

Figure I.1: *General layout of the HBS facility*

Main components of the HBS facility (Fig. I.1) are

- a dedicated proton accelerator (described in TDR Accelerator) with an optimized energy of 70 MeV and a current of 100 mA that is multiplexed to feed several target stations operated at different frequencies.
- a target – moderator combination that offers a pulsed neutron beam at optimal frequency, pulse duration and neutron spectrum to fulfil the needs of the corresponding instruments.
- a number of instruments (described in TDR Instrumentation) at each target station, typically around 6 to 8.

The construction of the buildings, organisation and sustainable operation of the facility are outlined in the TDR Infrastructure and Sustainability. This volume of the TDR series concentrates on the provision of neutrons by a target station which are delivered to the instruments.

I.1 Target requirements

The general purpose of a target station at a High-Current Accelerator-driven Neutron Source (HiCANS) like HBS (Fig. I.1) is to provide neutrons with the highest brightness possible to instruments built at such a target station. The requirements on the energy spectrum and the time structure of the neutron beam are set by the individual instruments described in the TDR "Instrumentation". Neutrons need therefore be produced, moderated and directed to the instruments which will be described in the following sections.

The neutrons at a HiCANS are released via nuclear reactions of protons with a suitable target material. The chosen target material should exhibit a high neutron yield, have a good combination of thermomechanical properties and show a high hydrogen solubility in order to withstand a high proton current. In the CDR [BBD$^+$20] an extensive material selection was done and tantalum was chosen as the material of choice especially due to its high blistering threshold. The requirements on the target are: (i) a minimum operational time of one year for a (ii) 70 MeV proton beam with a (iii) 1.43 mA average current and therefore (iv) a power deposition of 100 kW on an area of (v) 10 x 10 cm2. The technical realisation is described in detail in Section II.1.

The produced neutrons have a high energy in the MeV range and need to be moderated to the keV, eV or meV energy range depending on the instrument requirements. This happens in an optimised moderator / reflector assembly. The moderation needs to be done on a small time scale and a small volume in order to have a high flux density in the moderator / reflector setup from which neutrons can be extracted. This is realised with moderator materials mostly containing hydrogen, where the energy transfer is very large and therefore the moderation very efficient. As the moderators need to withstand a high heat load due to the large radiation level within the target station, water was chosen as the thermal moderator material. This is described in detail in Section II.4. Different materials can be chosen for a cryogenic moderator as the requirements on the energy spectra differ. Interesting materials are methane CH_4, mesitylene C_9H_{12} and liquid hydrogen H_2. These are described in detail Section II.5. The high energy neutrons as well as the byproducts of the nuclear reaction create a high radiation level surrounding the neutron releasing target. In order to protect the equipment and the people from radiation damage an adequate shielding is required following the principle of A Low As is Reasonable Achievable (ALARA). Two different areas regarding radiation level and required shielding are distinguished. The first area is the target room which is planned to be an exclusion zone during beam operation and a controlled area after beam shutdown. In order to protect equipment, like choppers or neutron guides inside the target room, the dose rate during target irradiation should be below 10^8 μSv/h. This requires a proper shielding around the neutron releasing target. After the beam shutdown the radiation level needs to be below 10 μSv/h so that work within the controlled area can be done. The second area is the neutron guide hall which will be designed as a surveillance area with a dose rate at the outside of the target room wall below 3 μSv/h, corresponding to annual dose rate of less than 1 mSv/a.

the entire thermal moderator and is penetrated by the extraction channels. The moderators are intrinsic parts of the instruments.

I.2 Instrument requirements

A target station at a facility for neutron instruments needs to fulfill the requirements of the individual instruments. Thus, in the following a short overview of typical instruments and their specific requirements will be given.

As a user facility the HBS covers a wide range of neutron applications:

- Neutron scattering to find out, where atoms and spins are and how they move.
- Neutron imaging and analytics to look deep below the surface of things without destroying them and determine the constituting elements.

The former makes use of slow neutrons emitted from moderators. Within the slow neutron regime, we distinguish thermal neutrons with a kinetic energy 10 meV $< E <$ 200 meV and cold neutrons 10 meV$< E <$ 0.2 meV. Thermal neutrons are used to resolve the nuclear and magnetic structure of materials with sub Å precision. The dynamic range, that can be probed with them, covers acoustic and optical phonons in crystalline materials or more generally vibrational motions in condensed matter. Also the magnetic excitations in materials with high ordering temperatures and therefore a high application potential fall within this energy range.

The lower energy cold neutrons are used to determine structural and spin correlations on longer time and length scales. Typical examples are polymer system or biological samples where individual building blocks exceed the nm range. Also human-made structures such as nanoparticles or artificial superlattices are probed by cold neutrons. Dynamics, that can be probed partially exclusively by neutrons, include the gapped magnetic excitations in unconventional superconductors or topologically protected systems. Relaxation and diffusion phenomena ranging from ps up to ns with a special emphasis on the motion of light elements require the highest wavelength resolution. Even longer times can be probed by spin echo methods, which can relax the wavelength resolution but depend on a spectrum covering very low energies down to 0.1 meV.

Imaging applications benefit from the huge penetration power of neutrons. For slow neutrons, the transmission properties can depend on the wavelength or the polarization, which allows one to vary the contrast e.g. of regions with different crystalline structure or of different magnetic domains. The application of imaging methods extends over a very wide range of scientific disciplines from engineering over geology to cultural heritage. This broad applicability is shared by neutron analytics methods, which rely on the absorption of the neutron and the subsequent decay of the excited nucleus and detection of the decay products. They are element- or actually isotope-specific, which allows a non-destructive analysis deep below the surface of bulky or precious specimens.

Scattering applications. The time-of-flight t the neutrons need to travel across a distance L determines the neutron wavelength λ:

$$\lambda = \frac{h}{m_n}\frac{t}{L} \tag{I.1}$$

with the neutron mass m_n and the Planck constant h. Therefore neutrons that arrive at a certain distance L from the moderator e.g. at the sample or at the detector within the periodicity of the source f_{src}^{-1} cover the bandwidth

$$\Delta\lambda = \frac{h}{m_n}\left(L \times f_{\mathrm{src}}\right)^{-1} \tag{I.2}$$

with the wavelength resolution determined by the pulse length of the source τ_{src}. This is shown in Fig. I.2 in the top panel for two pulse length $\tau_{96Hz} = 250\mu$s and $\tau_{24Hz} = 667\mu$s for distances from 5 to 100 m, while the bandwidth as function of the instrument length is given in the bottom panel.

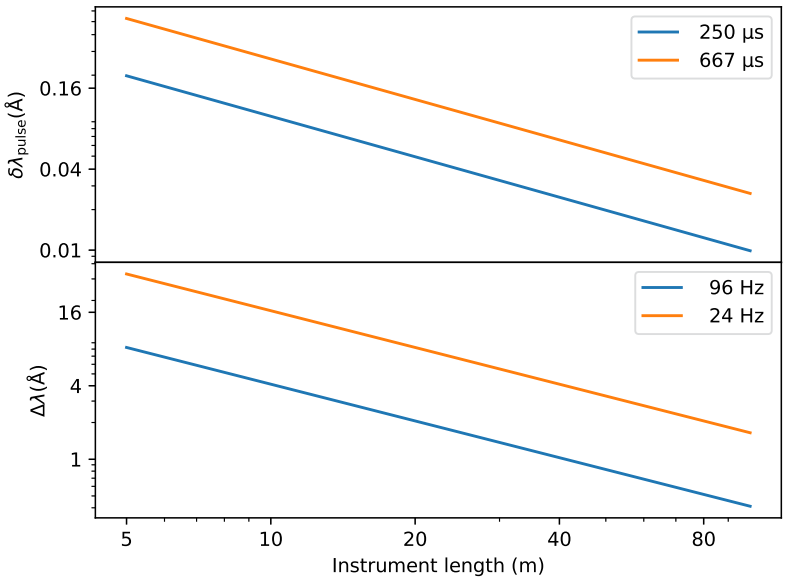

Figure I.2: *Top panel: Wavelength resolution due to the moderator pulse length as a function of the instrument length for a 250 μs and 667 μs moderator pulse. Bottom panel: Neutron bandwidth for the source repetition rate of 96 Hz and 24 Hz as a function of the instrument length.*

Exploring these figures one can identify the requirements for the different neutron scattering applications with respect to the pulse timing. Soft matter samples, e.g. from biology or polymer research, consist of entities with structure sizes ranging from nm to μm. Small angle scattering is a standard tool to probe the correlations within this length scale. Neutrons play here a special role due to the high sensitivity to hydrogen and other light elements and the possibility to label fractions of the sample by substitution of hydrogen with deuterium, to highlight different functional groups. In small angle scattering, the momentum transfer resolution and hence the range, across which correlations can be probed, are dominated by the angular contribution to the resolution function. The wavelength resolution can be relaxed to increase the intensity. The required wavelength resolution is indicated in Fig. I.2, showing that SANS instruments and reflectometers require approximately 20-30 m for a pulse length of 0.7 ms.

Often only neutron scattering can elucidate the ordering of spins and their fluctuations and excitations. Despite the progress of resonant x-ray scattering methods, neutron scattering is the method of choice to compare with theoretical models due to the fully understood interaction cross section that allow a comparison between theory and experiment on a absolute scale. Typically, spin correlations extend over less than 100 nm. This requires a wavelength resolution $\delta\lambda \approx 0.05$ Å, which can be realized by an instrument length of 20 m for a pulse length of 0.25 ms. The corresponding bandwidth $\Delta\lambda \approx 2$ Å provides a continuous covering of large areas in reciprocal space. For many applications a band 2 Å$< \lambda <$ 4 Å will be used, which just covers the most intense part of a cold moderator spectrum. Both effects lead to very efficient measurements of magnetic order and disorder in novel materials.

A higher resolution is required to resolve coherent excitations in condensed matter, which today are typically probed by three axis spectroscopy (TAS) and chopper spectrometers. As the energy resolution is proportional to λ^3, these instruments require a higher wavelength resolution. Still for a instrument length of 50 to 60 m the resolution just due to the pulse becomes finer than the resolution of existing instruments. The corresponding narrow bandwidth confines the dynamic range of such instruments. To cover a larger dynamic range requires the scanning of the initial neutron band, similar to scans performed today at TAS instruments.

High resolution powder diffraction or backscattering spectroscopy require an even narrower wavelength resolution. The former aims e.g. at resolving subtle changes of lattice constants at structural phase transitions. That requires a wavelength resolution $\delta d/d \approx 10^{-3}$. The latter probes the broadening of the quasi-elastic scattering due to nuclear motions on the ns timescale, requiring μeV energy resolution. To achieve an even narrower wavelength resolution one could increase the instrument length further and further. Alternatively, a chopper as close to the moderator as possible can be introduced. Then the wavelength resolution is controlled by the time the chopper transmits neutron, which is typically short compared to the pulse length of the moderator. The resolution is therefore independent of the moderator pulse length. The instrument needs then a certain length, until the band passing through the pulse shaping chopper covers again the full timeframe of the instrument. Pulse shaping is most effective for a flat broad pulse with steep rising and falling edges. Therefore high resolution instruments require a low repetition rate and a long neutron pulse.

Imaging Applications. At the HBS we envision neutron imaging applications using the full range of the spectrum from MeV to meV. Fast and resonance neutrons are needed to penetrate deep into complex samples. Existing instruments use the integrated flux of the neutron source. At the HBS even the high energy methods aim at making the data more unique by applying time-of-flight also to the imaging with fast neutrons. For that a time resolution in the µs regime is required. As the pulse in this energy regime is governed nearly completely by the proton pulse shape, we can introduce a specific pulse pattern to distinguish between nuclear resonances and hence add some information about the isotopic contents of the illuminated sample.

Imaging with slow neutrons allows higher spatial resolution. Using the thermal or the cold spectral range, certain isotope show significant changes of the transmission with wavelength. Methods that use a wavelength depending transmission, e.g. Bragg edge imaging, require a wavelength resolution similar to the diffractometers described above.

Neutron analytics applications. Existing applications rely largely on the integrated flux provided by the neutron source. The pulsed nature of the source will allow to efficiently discriminate the background. As a consequence the high signal-to-noise ratio similar to existing instrumentation can be realized. Combining the time-of-flight analysis with the prompt gamma spectroscopy extends the capabilities: the position in the gamma spectrum provides the information about the isotope composition of the specimen. The intensity variation of a certain gamma line with the time-of-flight and hence neutron energy can then be associated with the distribution of this isotope within the specimen. For that it is sufficient to distinguish neutron energy groups, which can be achieved with a ms long neutron pulse.

In summary, to cover the full range of neutron applications, the HBS needs dedicated target stations to serve best the different instrument requirements. A long pulse station is ideal both for low and and very high resolution applications, the latter by use of pulse shaping choppers. It will also host applications that ask for a wide initial neutron band. A medium pulse source provides the required resolution for many cold neutron applications without complex chopper systems, providing a high value for money for many applications, where neutron play a leading or even unique role. The ideal filling of cryogenic moderators constraints the extraction for neutrons in the energy regime above 1 eV. The third target station meets the demands of all applications, which are extremely relevant for imaging and neutron analytics.

II.
TARGET STATIONS

In what follows, the technical design of the target stations with all its components is described. It has to be emphasized that the design is not only based on simulations, but that all major components have been realized, tested individually and as an ensemble in a test-set up the JULIC neutron test platform [BGB+23, ZAB+23] (see II.6.5).

II.1 Neutron target

The target releases free neutrons via the nuclear reaction of the impinging protons with the target below the spallation threshold energy. It is the heart of the facility as well as the bottleneck, since it has to withstand a high volumetric heat deposition. Since there was no target concept that could be adapted to the needs of the HiCANS HBS, an entirely new target concept has been developed. Known risks of existing targets (e.g. blistering, hydrogen embrittlement) have been analyzed and systematically minimized during the development process.

II.1.1 Target requirements and engineering design

The goal of the development process is to develop a neutron releasing target which is able to sustain a 70 MeV proton beam with a thermal power of 100 kW which illuminates an area of 100 cm^2 of the target surface. Furthermore, the time averaged neutron output is supposed to be maximised (more details in chapter II.1.5) and the targets lifetime should be at least 1 year (chapter II.1.6). The target is supposed to be designed as reliable as possible since 5000 operation hours per year are required and the total mass of the target should be minimized in order to reduce the amount of activated material (both discussed in chapter II.1.1). A special focus was placed on known weak spots from existing low energy targets, on comments collected at workshops during the development phase as well as potential risks identified during the development process. These include in particular blistering, mechanical stress and bounded regions (each discussed in chapter chapter II.1.1) as well as possible water erosion and possible burn out (both discussed in Chapter II.1.4).

The target will be placed inside the accelerator vacuum. For that reason, the target must be vacuum tight. Since the HBS benefits from a compact target in terms of brilliance and usable neutron yield the target is supposed to be as compact as possible.

The actual result of the target development process is shown in figure II.1. The detailed description of the geometry is discussed in chapter II.1.1. The target consists of three parts, the main body, a 180° turnaround and an adapter for inlet and outlet. The main body converts the impinging proton beam into free neutrons, dissipates the reaction heat via water cooling channels and stops the proton beam

inside an additional water layer, the so-called beam stop layer. The 180° turnaround part collects the water behind the cooling structure and reverse the direction of the coolant water flow back towards the main body into the beam stop layer. Both parts, the main body and the 180° turnaround are each fabricated out of one single tantalum piece. The adapter for inlet and outlet enables the connection of a common water supply line and a water drain. This adapter is made out of a tantalum-aluminium bimetal plate. This bimetal plate is made from a thin tantalum layer (2 mm) and a thick aluminium layer (several cm), both bounded via explosion cladding. Tests have shown that this bimetal plate is able to fulfil all requirements in terms of mechanical stability and leak tightness. The use of this bimetal adapter allows the welding of the tantalum main body to the bimetal adapter on one side and the welding of the bimetal adapter to the aluminium tubes on the opposite side.

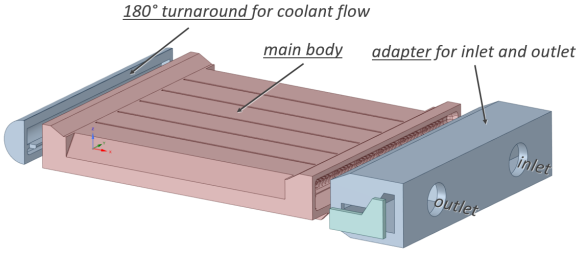

Figure II.1: *Assembly of the 3 parts of the HiCANS HBS Target: 180° turnaround for coolant flow, main body and adapter for inlet and outlet*

II.1.1.1 Target material, properties

At the high-powered accelerator-driven neutron source, the release of neutrons is based on the interaction of protons with the atomic nuclei of the tantalum target material, such as (p,n)-reactions, below the spallation threshold. Additionally, to the considerations regarding the neutron yield, the target material must exhibit, besides a high melting point, a suitable combination of thermo-mechanical properties such as high thermal conductivity, low thermal expansion coefficient to reduce thermal and particularly fatigue stresses, good elasticity and ductility and high yield strength to act as a solid target. These properties are very important since the target has to withstand a range of temperature differences and stresses. Furthermore, high hydrogen solubility i.e. a high blistering threshold, low chemical reactivity and low radiation damageability are required for physico-chemical stability. From materials studies in the field of target development for spallation sources [Bau10, FGT14] we identify within the material range of $70 < Z < 82$, tantalum as the most promising materials for the design of a high performance HBS-target. The neutron yield calculated from the irradiation of the material with 70 Mev protons is shown in Table II.1. Relevant properties of tantalum for target development are given in Table II.2.

Tantalum is a hard and ductile high density (16.656 g cm^{-3} at 20 ^{o}C [Car08]) material with a very good workability. It is suitable for joining technologies, mechanically workable and capable for EDM. It is outstanding in its performance to resist corrosion within the highly resistant refractory metals and tantalum is inert to practically all organic and inorganic substances. The melting point of tantalum is in the upper range (2996 ^{o}C [Car08]), the average thermal conductivity is in the medium range (57.55 W m^{-1} K^{-1} at 20 ^{o}C [Car08]) and an thermal expansion coefficient is also in the medium range ($6.5 \cdot 10^{-6}$ K^{-1} at 20 ^{o}C [Car08]) in comparison with other metals. When soft and recrystallized, its elastic modulus is 179 GPa and its yield stress is in the range of 172 MPa [Car08] and 210 MPa [inhouse tests at ZEA-1 in Jülich] at 20 ^{o}C. In the presence of protons or fast neutron irradiation, tantalum shows hardening with reduced ductility [SLK^{+}18, UC95, CBB^{+}03a] only after a high radiation exposure. Pure tantalum exhibits excellent ductility even after proton-induced

irradiation of at least 11 DPA. [CBB+03a] [Ull03] and neutron-induced damage of at least 0.14 DPA [CBB+03a]. Furthermore, tantalum has a very high hydrogen solubility (0.76 H/W at 100 °C and 1 atm [SMM91]) and blistering threshold ($> 230 \cdot 10^{22}$ m^{-2} [ABB+10]). Moreover, no corrosion occurs when in contact with water under irradiation [SLK+18].

	Protons	
Element	Thickness [mm]	Neutron yield $10^{14}\mathrm{s}^{-1}\mathrm{mA}^{-1}$
Ta	5.07	9.0

Table II.1: *Neutron yield analytically calculated for the irradiation of tantalum with protons and with energy of 70 MeV. The thickness of the material is set to fully stop the ions.*

Element	Melting point °C	Thermal conductivity $\mathrm{Wm}^{-1}\mathrm{K}^{-1}$	Yield stress MPa	Blistering threshold $10^{22}\mathrm{m}^{-2}$
Ta (soft, recrystallized)	2996	57.55	172 - 210	$\geq$ 230 [ABB+10]

Table II.2: *Relevant properties of tantalum for target development. The blistering threshold describes the proton fluence.*

Hence, tantalum exhibits strong characteristics under irradiation to withstand blistering due to hydrogen implantation from a high intensity proton beam. In particular, its capacity to store large amounts of hydrogen to suppress blistering should is a benefit for the target lifetime. Due to the combination of suitable thermal, mechanical, chemical and irradiation properties of tantalum (soft, recrystallized), it is the material of choice among all material candidates for neutron targets.

II.1.1.2 Engineering design, mechanical properties

The HiCANS HBS target design is a compact all-solid target made of tantalum and aluminium without any moving parts which minimises the volume and significantly reduces the probability of failure. The total amount of tantalum is 3.2 kg. The tantalum mass of the 180° turnaround part is 0.32 kg, the tantalum mass of the main body is 2.75 kg and the tantalum mass of the adapter for inlet and outlet is 0.13 kg. The amount of tantalum of the adapter for inlet and outlet is reduced by approximately 1.2 kg of tantalum by replacing the bulk of the tantalum with aluminium due to the usage of tantalum-aluminium bimetal. (more details in chapter II.1.7).

The final design of the main body is shown in Figure II.2. This photo shows the first 1:1 model of the final design made of aluminium for fabrication testing. The target is shown in correct mounting direction, the proton beam hits the target at the bottom side. The target consists of three layers. The first layer in the direction of the proton beam is the neutron producing layer which consists of solid tantalum with an water cooling structure. The cooling structure consists of six almost identical micro channel segments which are cooled by parallel flow. This neutron producing layer has a thickness of 5.8 mm. The thickness of the layer as well as the geometry of the water cooling structure ensure that each proton at each position has the same energy loss when penetrating the layer. The proton range in water is 6 to 7 times higher than in tantalum which cause shorter stopping ranges in the tantalum bridges in between to micro channel segments and higher effective stopping ranges inside the segments. The different effective stopping ranges are compensated by grooves parallel to the micro channel segments at the bottom surface of the target. The geometry of the neutron producing

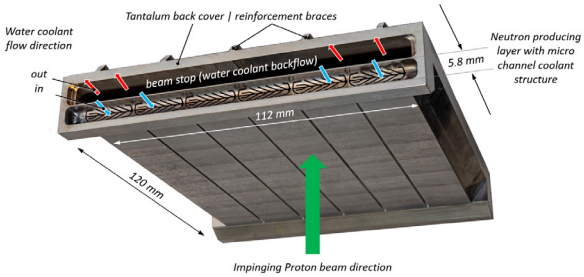

Figure II.2: *Basic design of HBS target: photo of the 1:1 aluminum mock-up*

layer finally leads to the effect that almost all protons leave this layer with an energy below 30 MeV (95%) and an average of the proton energy of 20 MeV. Hence the Bragg peak is placed behind the neutron producing tantalum layer. On the one hand this reduces the risk of hydrogen blistering since the majority of the protons exits the tantalum. A more detailed description of the neutronics can be found in chapter II.1.5. The protons are stopped inside the following water layer. This so-called beam stop ensures that the protons cannot cause any damage to the adjacent installations. Moreover the beam stop adds an significant contribution to the heat removal since the highest heat release density inside the tantalum takes place at the upper slice of the neutron producing layer. This layer is cooled by the adjacent beam stop in addition to the internal micro cooling structure. A more detailed discussion of the cooling concept is given in chapter II.1.2. The tantalum back cover safely separates the water beam stop from the adjacent accelerator vacuum. Since there is a strong pressure difference between the water and the vacuum, stiffening ribs are placed at the back side in order to reinforce its stability.

The technical drawings of the target main body can be found in the Appendix A.2. An overview of the relevant details is shown in the cross section in Figure II.3. The shown cross section has a total height of 21 mm and a total width of 127 mm. The water pressure at the inlet of the target is 7 bar (total pressure) and the pressure loss within the target is 2.5 bar. The target itself is operated inside vacuum. The wall thickness is 0.75 mm at the thinnest areas between the water coolant and the outer vacuum. Various measures have been taken in order to keep the stresses within the permissible tolerances despite the cooling water pressure and the low wall thicknesses. Each micro channel segment is just 18 mm short in order to reduce the tensile stresses in the solid tantalum bridges between the micro channels caused by the water pressure. However, there is no possibility to place any structural support within the beam stop area to prevent the entire beam stop cover and the neutron producing target layer from bending. To counteract high stresses in the beam stop cover, a material thickness of 3.5 mm was chosen and the cover is reinforced by stiffening ribs on the top side. Bending of the neutron producing target layer would lead to high local stresses in the channel structure close to the flanks if the stiffness of the flanks is too high. Therefor the wall thickness was optimized at the flanks and the geometry of the microchannels close to the flanks was adapted to reduce local stresses in the target.

II.1.2 Target cooling

The development of the target is driven by two basic requirements. The target should be as compact as possible the target should safely withstand a high proton current resp. a high thermal load. Both requirements together result inevitably in a high thermal power density release inside the target. The additional requirement for a simple as well as reliable solution has focused the development on a solution without moving components as well as water as a coolant. Compared to many liquid metals,

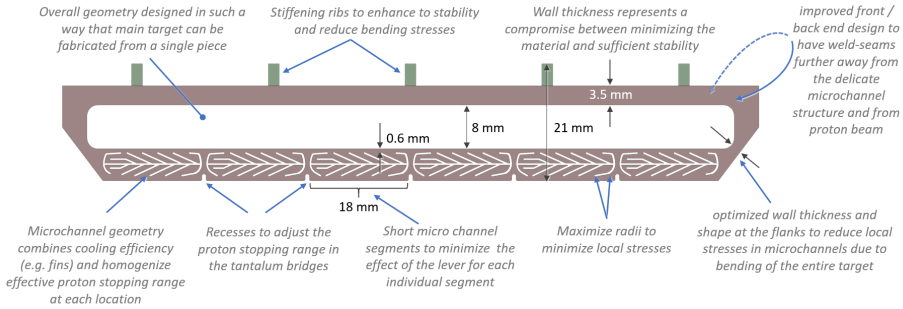

Figure II.3: *Cross-section through the targets main body: design features*

gases, melts or solutions, water has the advantages of being non-toxic, having low corrosivity, is always available, is virtually cost-free and being easy to handle. In addition, water has good cooling properties such as a, compared to gases, high heat capacity at low pressure and a, compared to melts, relatively low viscosity, and the behaviour of water is known in any state. The avoidance of all moving or rotating components, such as the rotating ESS target wheel that distributes the pulses to multiple targets, significantly increases compactness, reduces potential sources of abrasion as well as sources of faults, but in return increases cooling and thermomechanical demands.

As a solution for the heat dissipation, an internal micro channel structure has been developed. The micro channel structure is the result of a comprehensive design evolution, starting from heat dissipation and static strength [Din23], through manufacturing processes, thermomechanical optimization performed by ZEA-1 and neutronic optimization [Din23]. The final design of the mircochannel structure is shown in Fig. II.3. The microchannels are located in the first neutron producing layer, where about 80 % of the energy of the proton beam is released as heat. The major part of the remaining energy of the proton beam is placed directly as heat in the cooling water of the beam stop above.

As a result of an intensive parameter study, the parameters of cooling within the micro channels have been set to 8 m/s average velocity which results in a mass flow of 1.3 kg/s and an inlet pressure of about 6.5 bar absolute pressure.

The path of the cooling water through the target is shown in Fig. II.4. The supply adapter connects a conventional pipe to the target and distributes the flow to all micro channels via its first chamber. As the water coolant flows through the micro channels, the water absorbs the heat from the target and warms up by approx. 20 K. The flow is returned in the 180 degree turnaround adapter. On the way back, the flow passes the back of the target. It fulfills two functions here. The return flow stops the proton beam and absorbs the hydrogen atoms. In this way, surrounding structures are protected from embrittlement. In addition, the return flow cools the back side of the neutron producing layer of the target. This region has the highest heat load since it is close to the protons Bragg peak. [1] The back flow is collected in the second chamber of the supply adapter and guided to a second conventional pipe.

II.1.3 Computational design and verification

The design and optimization of the target is carried out iteratively between neutronic calculations and fluid-mechanical simulations and subsequent mechanical calculations. In the following, the final results of the fluid-mechanical and thermo-mechanical calculations are presented.

[1] The energy loss per penetration depth is a function of the proton energy. This means that for a mono-energetic proton beam the protons are stopped inside a small interval at the position of the so called Bragg peak

Fluid dynamical analysis

The pulsed, resp. transient operation will significantly increase maximum temperatures in the target compared to steady-state conditions with a time-averaged heat deposition. Both available frequencies, 24 Hz and 96 Hz, have the same duty cycle and the same peak thermal power of 6.3 MW within the pulse. The 24 Hz pulse is four times longer than the 96 Hz pulse and thus has the same average thermal power. Thus, the thermal load on the target at the 24 Hz station is significantly higher. The maximum temperature increment during one pulse at 24 Hz is about 76 °C but the maximum temperature is only about 151 °C despite the extreme power density of 50 kW/cm² during the pulse. The maximum temperature is located at the top side of the middle bridge close to the end of the target in direction of the micro channel flow due to heat up of the water coolant.

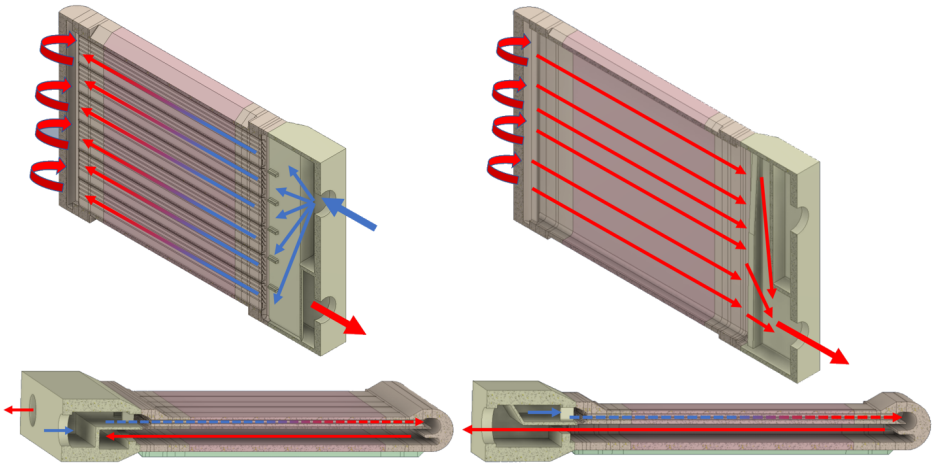

Figure II.4: *Schematic illustration of the coolant flow. left side: inflow (blue) into adapter and widening the flow to the target width - flow through the micro channels (blue to red); right side: turnaround and feed the beam stop*

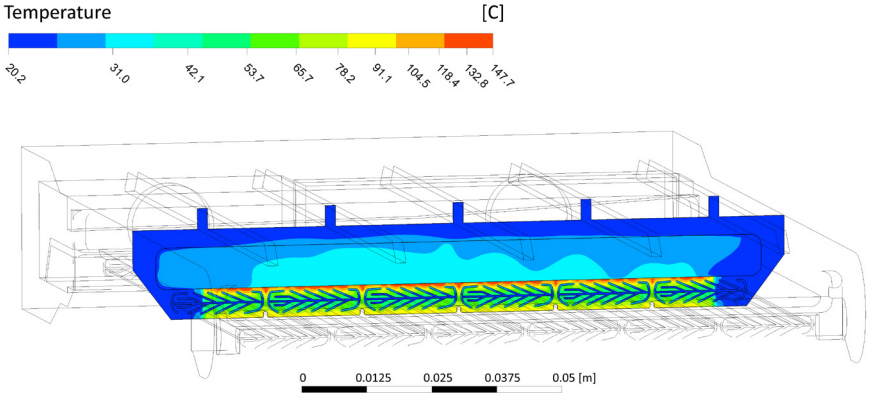

Figure II.5: *Temperature distribution at the center of the target at the end of a proton pulse (result from a CFD simulation)*

The efficiency of the micro channel cooling is demonstrated by the temperature distribution inside the target at the centre of the target where the maximum temperature is about 147 °C at the end of a proton pulse (Figure II.5). It can be seen that the temperature distribution within the target is very homogeneous since the micro cooling structure almost acts like a volumetric heat sink. Local hot spots are avoided which also minimises the temperature-induced stresses. However, there are warmer regions at the top side of the neutron producing layer. These regions result from the more intense heat load at the Bragg peak although this area gains additional heat dissipation due to the back flow of water. The water heats up by 20 K as it flows through the target, the interface heat flux goes up to 6.3 MW/m² inside the micro channel structure. Due to this high heat flux, it can be assumed that nucleate boiling will start locally. This condition is seen as uncritical for the following reasons: due to the subcooled flow, the bubbles will disappear immediately after detaching from the wall and the subcooled boiling will significantly increase the local heat transfer. Compared to the 3 bar pressure drop inside the micro channels, the pressure loss due to possible local subcooled boiling is probably negligible. Experiments have indicated that the safety factor is at least 2 with respect to reaching the critical heat flux and resulting burnout (see Section II.1.4).

The velocity distribution inside the target is shown in Fig. II.6. The average velocity inside the channels is set to 8 m/s however the local velocity varies between approx. 6 and up to 12.9 m/s. Inside the beam dump the velocities are significant smaller with values between 0 and 3 m/s since the free flow cross section of the combined micro channels is much smaller than the free flow cross section of the back flow through the beam dump. The high minimum velocities within the micro channels illustrate the great strength of this cooling structure. The laminar sublayer, which usually generates high thermal resistance due to stagnant flow in the near wall region, does almost not occur inside micro channels. As a result, the micro channels cooling has a high heat transfer of approx. 1E+7 W/m²/K which causes small temperature differences between the coolant and the target and hence low temperatures at all.

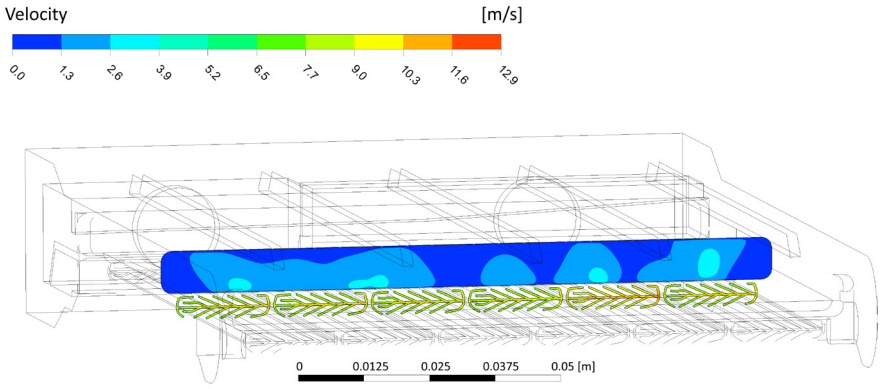

Figure II.6: *Velocity field at the center of the target inside micro channels and beam dump (result from a CFD simulation)*

Thermo-mechanical analysis

The actual mechanical stresses inside the target are shown in Fig. II.7 for thermo-mechanical loads. The simulation was performed with ANSYS mechanical 2022 R2 and a linear elastic material model was used here. The thermo-mechanical loads (temperature distribution and pressure) are taken from a previous CFD simulation (see Section II.1.3). The left side of Fig II.7 colourises the equivalent stresses

on the outer surface of the target and shows the deformation. The discussed outward bending of the bottom neutron producing layer is clearly visible and the stress-reducing measures show their positive effects. The entire bent surfaces as well as the majority of the target volume are within the permissible stress limits. However, there are some local regions which exceed the limit and which require a closer look. The most critical areas are highlighted in the right side of Fig. II.7. All are located in the tips of the micro channels. The estimated radius at these tips is half the channel width, 0.175 mm. The small radius leads to peak stresses in the linear elastic simulation, which can be relieved by local plastic deformations under real conditions.

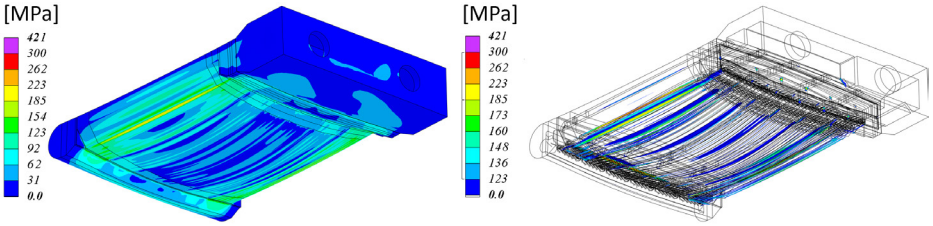

Figure II.7: *left side: equivalent stress at HBS target during full operation caused by thermo-mechanical loads (linear elastic); right side: equivalent stresses above 185 MPa highlighted*

Fig. II.8 shows the result of the stress linearization at the maximum local stress for mechanical loads only. The maximum equivalent stress is 410 MPa, in contrast to 421 MPa in Fig. II.7 where thermal stains partially release locations with high notch stresses. For the further stress analysis, the simulation with the highest stresses is selected in order to be able to make conservative statements. Both mentioned values are beyond the yield stress of tantalum. The major part of the stress is peak stress which can be self limited and do not endanger the structural integrity with respect to plastic collapse. However, even the non self limiting membrane and bending stress do slightly exceed the yield stress. In order to assess these stresses and to prove sufficient stiffness of the target, a simulation with plastic deformation is carried out.

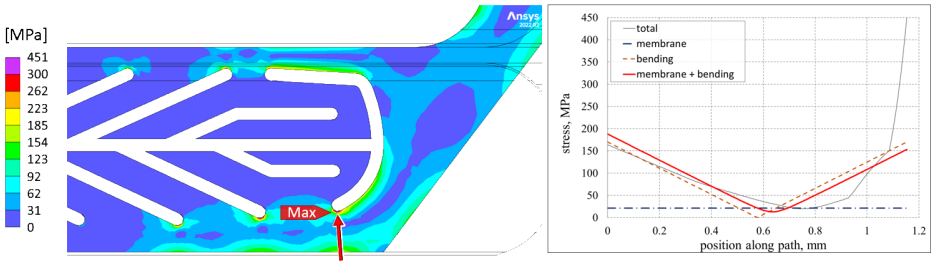

Figure II.8: *left side: path for stress linearization at maximum local stress (linear elastic); right side: result of the stress linearization: membrane + bending stress is slightly above the yield stress: 188 MPa*

The results from the mechanical simulation with ideal plastic behaviour are shown in Fig. II.9. This type of simulation requires a multiple of computational time, nevertheless, it allows the relief of stress peaks through localised plastic deformation. This behaviour is typical for ductile or toughness-hardened materials such as tantalum. The design limit for equivalent plastic strain is usually assumed to be 1 percent in case of ductile materials, for which the elongation at break is usually larger than 10 percent. Left side of Fig. II.9 shows the equivalent plastic strain obtained from the same realistic

mechanical loads used for Fig. II.7. The largest plastic strain occurs at the tips of the fins as well as in the bounding layer between the target main body and the connector. However, all plastic strains are well below 1 percent. In order to explore the limits of the mechanical load capacity, the same simulation has been repeated up to plastic collapse that occurs at a load factor of 8.9 The result is shown at the right side of Fig. II.9. Although plastic collapse will not occur at this extreme load, high plastic strains will lead to fracture. The load factor that will just lead to plastic strains in the range of 10 % is about 2.3 (c.p. figure). Here the shear force in the bridges in between the cooling channels caused by the bending of the target is responsible for the maximum plastic strain. From these investigations it can be concluded that the target has a sufficient high load-bearing reserve against a water pressure of at least a factor 2.3.

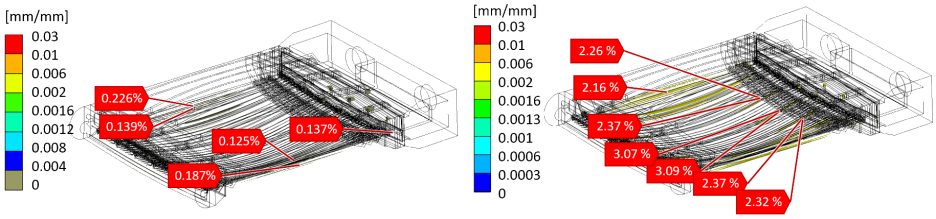

Figure II.9: *Equivalent plastic strain (elastic - ideal plastic). left side: simulation based on realistic mechanical loads; right side: simulation based on twofold mechanical overload*

In addition to the steady-state stresses discussed so far, a transient thermo-mechanical simulation is required. This enables a statement to be made about possible fatigue phenomena in the material due to pulsed operation and thus effects on the lifetime of the target. The thermal CFX simulation (see Section II.1.3) has shown that local temperature fluctuations of up to 76 K are expected in pulsed operation. Subsequent thermo-mechanical simulations calculate the changes of the equivalent stresses due to the temperature fluctuations in pulsed operation between the state before and after the pulse. For simplicity, these changes of the equivalent stresses between the state before and after the pulse are just called equivalent stresses differences. These simulation results show that the local maxima between the state before and after the pulse are located at two places: In the flow direction at the beginning and at the end of the target, respectively, exactly in the boundary region of the heat input. Furthermore, the simulations show a strong dependence of the maximum local equivalent stress differences on the Gaussian distribution in the boundary region of the heat input. The result of a simulation without Gaussian distribution in the boundary regions (homogeneous heat input on 10 cm x 10 cm) is shown at Figure II.10. This simulation with sharp, rectangular boundaries of the heat input leads to maximum local equivalent stress differences of 267 Mpa between the states before and after the pulse. The same simulation with 10 mm boundary region in the heat input (3 sigma = 10 mm) leads to a reduction of the maximum equivalent stress difference by 25 MPa to approx. 242 MPa between the states before and after the pulse. The fatigue strength of tantalum (soft, annealed) is given in the literature [UC95] as 240 MPa for plates at 25 °C. Thus, the Gaussian distribution of the thermal load in the flow direction is relevant for the fatigue strength of the target. With a boundary region of about 10 mm, the maximum equivalent stress between the state before and after the pulse is close to the fatigue strength of tantalum. In conclusion, continuous fatigue operation of the target is possible with a sufficiently large boundary region of heat input. Necessary thermo-mechanical investigations of softer boundary regions (3 Simga = 30 mm) are in progress.

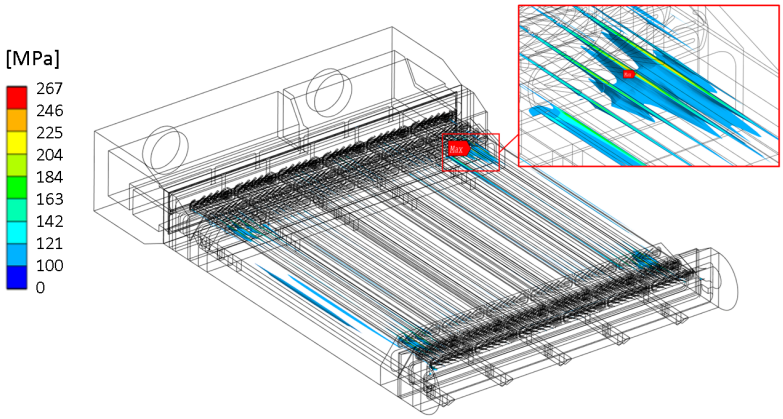

Figure II.10: *Equivalent Stress inside the target caused by temperature differences between the states before and after the pulse (without Gaussian distribution in the boundary regions of the heat load region*

II.1.4 Experimental Validation

The ability of the cooling system to reliably dissipate a heat load of 1 kW/cm² has been successfully demonstrated in the JUDITH-2 experimental facility at IEK-4 in Forschungszentrum Jülich. It should be mentioned that the experiment has been performed with the previous target design. However, the results are transferable to the current geometry, since the relevant parameters, micro channel thickness, coolant pressure and flow velocity, have not changed. The basic design of the JUDITH-2 facility is shown in the right side of figure II.11. The facility basically consists of an electron gun facility, equipped with a vacuum chamber, an infrared camera (IR) and a cooling circuit. The special characteristic of the heat release in a target by an electron gun compared to a proton beam is shown in the left side of Fig. II.11. The proton beam penetrates the entire target and thus the heat is released throughout the entire target. In contrast, the electron beam penetrates solely the first few micrometers of the tantalum and thus the entire heat is released at the surface. In this way, only about one fourth to one third of the micro channel surface contributes to the cooling and thus the interface heat fluxes are significant higher as well as the maximum surface temperatures. The power was rammed up in small steps and each new power level was held for a certain time to achieve constant conditions in each case. The electron gun creates a beam with a Gaussian shape with a diameter of approx. 6 mm which scans in the megahertz regime over the targets surface. Using this process up to 48 kW were focused at a surface of 48 cm² in order to meet the design heat load of 1 kW/cm².

Finally, the HBS target was able to withstand a heat load of 1 kW/cm² despite to very conservative surface heat load of the electron gun. The heat distribution at the targets surface was recorded among others over 0.5 seconds by the infrared camera. These images were used in order to validate the CFD simulations, presented in section II.1.3. A brief glance at the comparison is shown in Fig. II.12. It is noteworthy that the surface temperature is not homogeneous neither at the IR cam not at the CFD simulation. The reasons for the inhomogeneous surface temperature are the cooling structure as well as the water heat up. The cooler region at the surface are above the micro channel structures while the warmer regions are above the bridges between the single micro channel elements. Furthermore the left side of the images is colder than the right side since the water flows in this direction and heats up while it absorbes the heat.

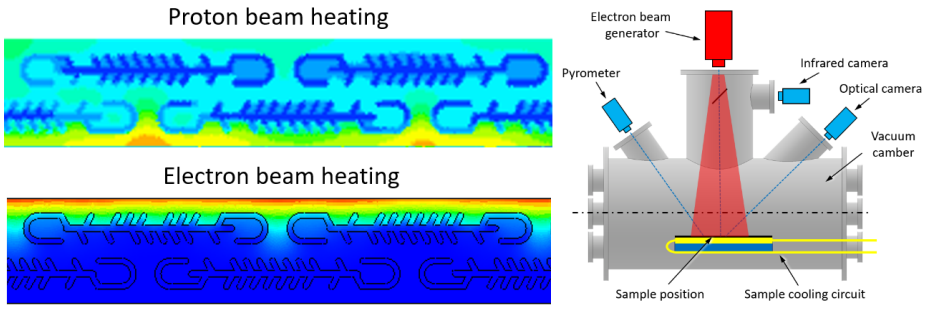

Exemplary temperature distribution from CFD *Judith-2 basic design*

Figure II.11: *Schematic view of the JUDITH-2 facility. left side: simulated exemplary temperature distribution inside target heated up by proton beam (top side) and electron gun (bottom side), right side: JUDITH-2 basic design, figure inspired by [SHK+ 09], electron gun heats cooled target from top, infrared camera records surface temperature*

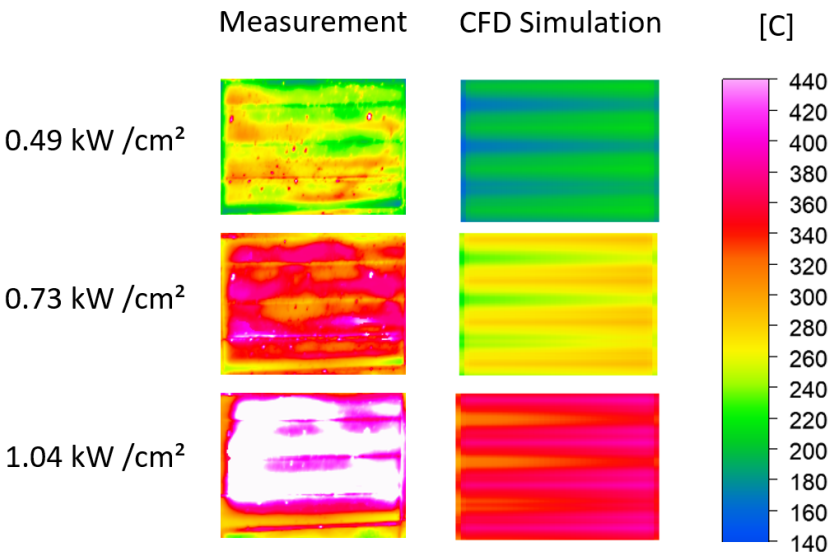

Figure II.12: *Brief glance at the surface temperature distribution of the target at different heat loads, measured results (left) vs. simulation results (right)*

Overall, the comparison between the measured and simulated profiles shows a very good qualitative and a good quantitative agreement. However, the absolute deviations of the mean surface temperatures are almost constant around 70 K. [BBR+23] This deviation is due to inaccuracies in the manufacturing process of the first HBS target. The channels were widened by 20 % (0.08 mm), the wall thickness at the target surface was increased by up to 25 % (0.16 mm) and one fin-channel per segment was clogged by tantalum brazing material. The evaluation of this test has contributed to the identification of manufacturing problems. The manufacturing of the current target design has been completely rethought and fundamentally revised, see Chapter II.1.7. An analysis of the current

manufacturing tolerances shows that the current deviations are now in the hundreds of millimetres range [Din23].

The erosion resistance of the micro channel against the high water velocity of 8 m/s was demonstrated by a 6 week durance experiment. The setup for that test is shown in Fig. II.13. Deionized water flow through the previous target design with a micro channel arrangement comparable to the current arrangement. The velocity inside the micro channels was 8 m/s, the total pressure was 4 bar at the inlet of the micro channels and the average water temperatures was 30 °C. The tantalum target was weighed with a precision balance before and after the experiment. The pressure loss within the micro channels was monitored with a pressure gauge during the experiment and finally the tantalum content in the water was measured with inductively coupled plasma - mass spectrometry for 5 times during the experiment. There was no significant changes in weight observed, nor change of the pressure loss inside the micro channels and no significant tantalum content inside the coolant measured [BBR+23]. This test is consistent with published studies on the erosion resistance of tantalum to water, e.g. at [CDD17], performed at significantly higher velocities (34 m/s) and longer study periods (4.5 month).

II.1.5 Neutronics

The geometry of the target is interatively optimized in terms of neutronics, heat dissipation and mechanics. In the context of neutronic optimization, the arrangement of the cooling channels was a particular focus, since the stopping power of the protons in the tantalum is significantly greater than in the cooling water. The goal of the optimization was to maximize the neutron yield, homogenize the thermal heat release, and minimize the protons stopped in the tantalum as well as minimize the amount of heat released inside the tantalum. The number of protons stopped in the tantalum is minimized by reducing the thickness of the neutron producing tantalum layer. This reduces the risk of embrittlement and blistering. The neutron yield is maximized by increasing the thickness of the neutron producing layer in order to use all possible reaction channels, hence all particles leaving the neutron producing tantalum layer have energies below the dominant neutron producing reaction

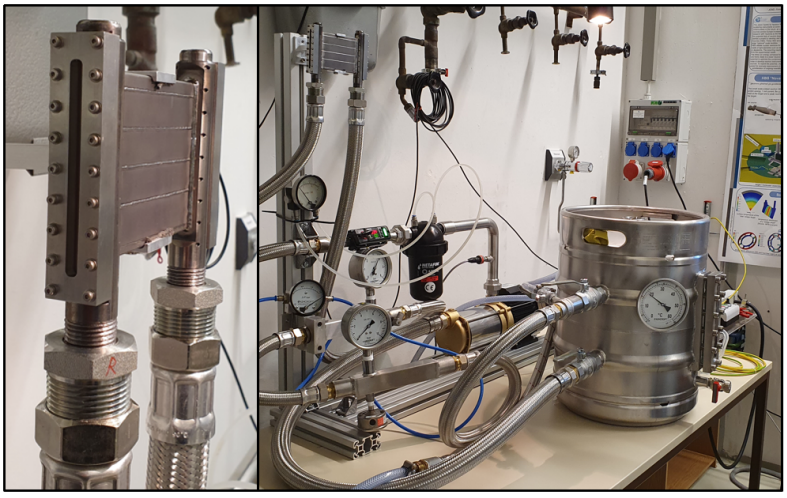

Figure II.13: Simple setup for the 6 week endurance experiment to measure the endurace resistance of the tantalum cooling structure against the water erosion (right) and detailed view to the tested first target design (left)

threshold. Neutron release from the reaction is dominated by (p, 4N) and (p, 3N) when the proton energy is more than 20 MeV. Although there are possibilities of (p, N) or (p, 2N) when th energy is between 7 and 15MeV, the contribution is quite low compared to (p, 4N) and (p, 3N). The amount of heat released inside the tantalum is minimized by, in turn, increasing the energies of the protons leaving the neutron producing layer. Finally, the design goal is achieved when all particles leaving the neutron producing tantalum layer have almost exactly 17 MeV. In order to reach that goal, the geometry of the target surface as well as the geometry of the coolant channels, which allows a local fine adjustment of the neutron exit energy, are designed in order to ensure that each proton at each position leaves the same amount of energy while travelling through the neutron releasing layer.

A few highlights of the successful neutronic optimization is shown in Figure II.14. The protons travels from the positive x-axis towards the negative x-axis. The interface between the neutron prodcing tantalum layer and the water beam stop behind the target is at x = 0 cm. The right side of Figure II.14 shows the optimization result in terms of minimization of the stopped protons inside the tantalum. Only 4.6 % of the protons are stopped inside the tantalum layer which does not cause a risk if one consider the hydrogen storage ability as well as hydrogen diffusion ability of tantalum. The major part of the protons, 94.6 %, are stopped in the following water beam stop and by that the Bragg peak is directly placed inside the water coolant. The remaining 0.5 % of the proton beam is stopped inside the tantalum back wall. The neutron production of this target is as high as 99% of a target which stops all protons.

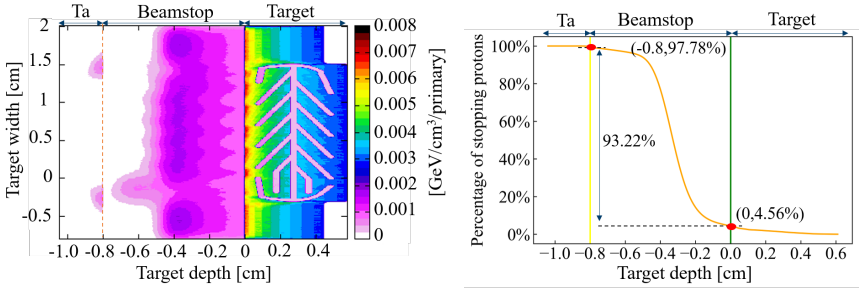

Figure II.14: distribution of energy deposition by protons (right) and percentage of stopped protons (left) each along target depth, protons travels from right side to left side

Left side of Figure II.14 shows the deposited proton energy. The effective proton stopping range is higher at the micro channel segments compared to the solid bridges between the micro channel segments. For that reason, the thickness of the bridges are reduced by recesses at the target surface (Right side in left picture at figure II.14). The energy deposition is homogeneous across at the micro channel segment and homogeneous across the bridges which reduces the temperature induced stresses. The main energy deposition is close to the interface between the tantalum target and the water beam stop since in this region the protons have the lowest energy. The adjacent beam stop offers additions cooling which helps to remove this heat load.

II.1.6 Radiation damage and target lifetime

The proton- and neutron-induced material damage in tantalum was investigated in detail by means of numerical simulations. The code FLUKA was used to extract information on the number of displacements per atoms (dpa) resulting from atomic rearrangements, energy deposition and neutron spectral data. Average and peak annual displacement doses were calculated from the displacement rates (dpa/s) for a continuous operation mode of HBS in a full power year (fpy, 70 MeV, 1.43 mA,

12.52 Ah). The results obtained for a bare tantalum target (5 mm thickness) are given in Table II.3 [OML$^+$21]. They show that the displacements produced by neutrons are negligible compared to that induced by protons. The simulations indicate the rear of the target i.e. the exit side of primary protons as the most vulnerable area, with the highest number of atomic displacements due to Bragg peak. The distributions of the average dpa induced by protons and neutrons, respectively, within the designed HBS tantalum target are showed in Figure II.15. While dpa caused by neutrons is almost homogeneously distributed over the entire material, the dpa caused by protons increases towards lower proton energy and is maximum at the interface between the neutron producing layer and the coolant of the proton beam stop. The resulting average annual dose induced by protons, 1.94 dpa/fpy, is a factor 2 lower than in the case of the bare tantalum target owing to the deposition of the proton energy (Bragg peak) in the coolant of the beam stop. The average annual dose induced by neutrons, 0.14 dpa/fyp, is the same as obtained for the bare target. Based on obtained average damage rates in order to account for the whole bulk of the material and two reference dpa values, one referring to proton damages (11 dpa [CBB$^+$03b]) and one to neutron damages (0.14 dpa [BM08]), minimum lifetimes of 2.6 (33 Ah) and 0.8 years (9.8 Ah), respectively, were estimated for the bare tantalum target [OML$^+$21]. In the case of the designed HBS target, minimum lifetimes are estimated to 5.7 (33 Ah) and 1.2 years (9.8 Ah), respectively. However, since the lower lifetimes derived from neutron doses are most probably attributed to a material weakening (premature embrittlement [BM08]) as a consequence of oxygen uptake during pre-irradiation treatment, the lifetimes based on protons should be taken as more accurate. Based on the damage induced by protons, indeed the main agents here, a conservative minimum lifetime of 2.6 years (33 Ah) is proposed. This value remains reasonable when considering frame irradiation conditions.Since the temperature achieved in the targets keeps within a moderate frame and the target must be replaced at regular intervals anyway, a critical failure before the proposed time is very unlikely.

Displacement rate R_d [10^{-8} dpa/s]				Annual dose [dpa/fpy]			
Average		Peak		Average		Peak	
p^+	n	p^+	n	p^+	n	p^+	n
13.32	0.57	37.82	0.63	4.20	0.18	11.93	0.20

Table II.3: *FLUKA numerical results for the calculated damage rates R_d and annual doses. Values for R_d are obtained by scaling the damage per source proton with the number of protons incident on the Ta target per second, i.e. 1.43 mA. Annual doses represent the extent of atomic displacements accumulated over one whole year in continuous operation mode, i.e. full power year (fpy).*

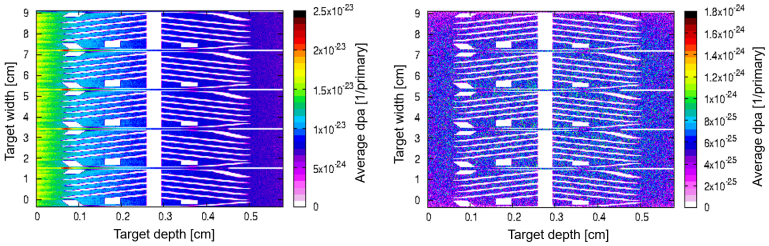

Figure II.15: *Proton induced (left) and neutron induced (right) displacements per atom inside target, protons travels from right to left.*

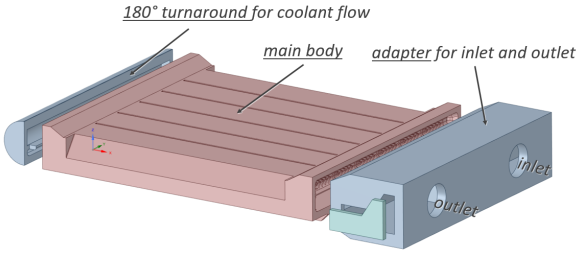

Figure II.16: *Assembly of the 3 parts of the HiCANS HBS Target: 180° turnaround for coolant flow, main body and adapter for inlet and outlet*

II.1.7 Target manufacturing, installation and handling

The target is manufactured in three parts. The three parts are the 180° turnaround adapter for coolant flow, the main body and the adapter for inlet and outlet, each shown in Figure II.16. A detailed description of the function of the individual parts can be found in Chapter II.1.1. The 180° turnaround adapter and the adapter for inlet and outlet are simple milled parts, both can be milled from a single piece of tantalum. Due to the complex internal structure of the adapter for inlet and outlet, it requires additional access for the milling cutter on both sides. After completion of the milling work, these accesses are each welded with a cover. The adapter for inlet and outlet also offers the possibility of reducing the total amount of tantalum by approx. 1 kg to 3.4 kg. The main body must be made of tantalum as an efficient and reliable neutron source. Due to the high melting point of tantalum, all welded-on parts should also be made of tantalum. Since the 180° turnaround adapter weighs only 320 g, no substitutions are considered for this target component. On the other hand the adapter for inlet and outlet weighs 1.32 kg. This must be connected to water pipes made of aluminium. The possibility of explosive cladding between tantalum and aluminium is being investigated as part of a feasibility study. In this process, 3 mm tantalum is bonded to a solid aluminium layer, shown at left side of Figure II.17. Such a stable connection enables reliable welding of the adapter for inlet and outlet to the tantalum target on one side and the necessary aluminium pipes on the opposite side. As part of this feasibility study, a 40 cm x 40 cm explosion clad plate of tantalum and aluminium has been ordered from a commercial supplier and is currently being tested for vacuum tightness, strength and fatigue resistance at the joint edge.

The main body has already been successfully manufactured from aluminium for production testing,

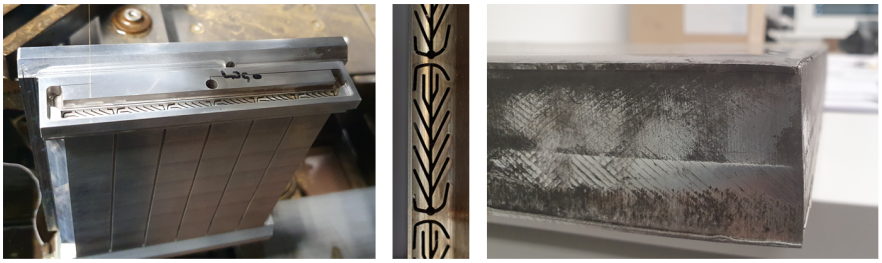

Figure II.17: *Left side: Manufacturing the target main body prototype via wire erosion out of one solid aluminium piece; centre: enlarged view of the micro channel structure with outdated start hole positions; right side: test sample of explosion clad plate of tantalum (3 mm on the top) and aluminium (50 mm on the bottom)*

including measurement of the production tolerances. In addition to milling, the two main manufacturing processes are sinking Electrical Discharge Machining (EDM) and wire EDM. Both processes are non-contact, and on the basis of previous experience in production, it is assumed that the knowledge gained from EDM of aluminium will be largely transferable to EDM of tantalum. The wire erosion process of the aluminium prototype target is shown at right side of Figure II.17, micro channels successfull eroded and test inside tantalum are shown in Figure II.18. The start holes for the wire erosion process are fabricated via sinker EDM. Tests have shown that copper zinc electrodes can be used to erode holes with a diameter of 0.6 mm over the entire height of 160 mm. Correctly positioned, holes up to 0.8 mm disappear within the cooling structure. The following wire EDM machine can automatically insert the wire through these start holes.

The successful joining of two tantalum components as well as the vacuum tightness and pressure resistance of numerous welds proves the feasibility of joining tantalum components. It has been successfully demonstrated on the, now outdated, first HBS target design. The cooling structure of this old design was made exclusively with wire EDM. This requires the wire to be inserted laterally into each segment, shown at top left side of Figure II.18. These entree channels are sealed with tantalum weld, shown at the bottom left of Figure II.18. Right side of Figure II.18 shows the successfully joining of the outdated tantalum main body with two tantalum coolant supply tubes. All welds have been welded under helium protective gas atmosphere as well as with the addition of pure tantal wire without any other impurities. The target shown here has been used for all experiments shown in chapter II.1.4.

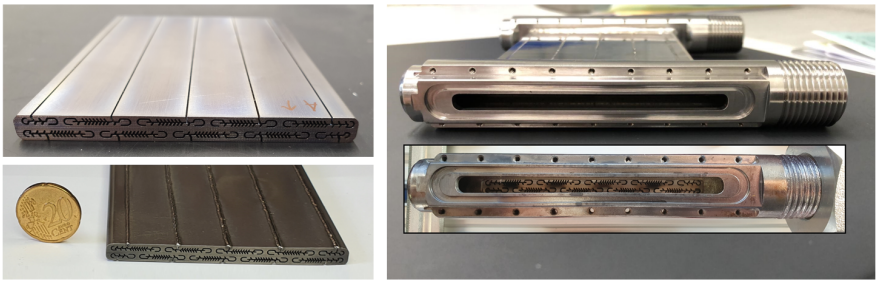

Figure II.18: *Top left: tantalum target with outdated design after wire erosion process; bottom left: weld lateral entrees from wire erosion; right side: welded tantalum target to tantalum supply tubes (outdated design)*

Connections, tubings

The coolant supply to the target takes place via two aluminium pipes with 15 mm inner diameter welded to the adapter for inlet and outlet. Both pipes run through the target plug and both pipes are equipped with connectors at the outer side of the TMR shielding for the primary cooling circuit, shown in Figure II.19. At this position conventional couplings with elastomer seals can be used since the radiation exposure is sufficient low. There are no removable connections used inside the TMR shielding in order to reduce the risk of coolant leakage. The water pipes are stored inside the intermediate storage together with the attached target and target plug after the envisaged lifetime of one year. The usage of aluminium pipes reduces the amount of activated material. A parallel offset of the piping near the center of the target plug prevents a gap in the shielding due to the piping and ensures the shielding effect.

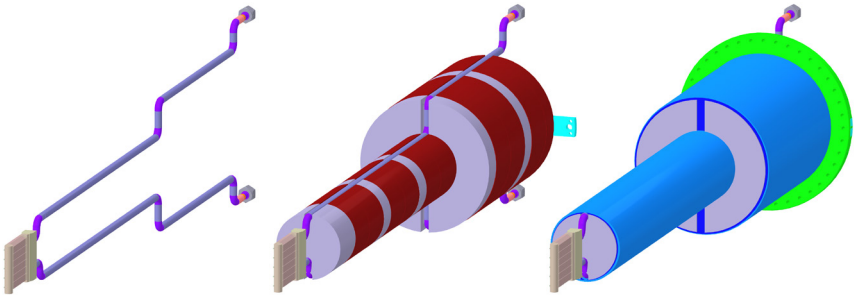

Figure II.19: Coolant supply inside target plug; target with coolant pipes (left); including sandwich shielding layers of borated PE and lead (center); including aluminium plug housing and flange (light green) for closing the accelerator vacuum (right)

Coolant, pumps, cooling control

Each target is equipped with a closed primary cooling circuit and a secondary cooling circuit in order to ensure the safe containment of tritium due to tritium diffusion out of the target and in case of leakage. A sump in the bottom is able to absorb the entire water of the primary cooling system in case of leakage. The total amount of water coolant inside the primary circuit is be kept very low at 70 to 100 l. The heat transfer from the primary cooling circuit to the secondary cooling circuit takes places via a compact water/water - counter flow heat exchanger inside the targer bunker. The location ensures that the entire primary cooling circuit is located inside the target bunker and that no activity can escape to the outside in the event of a loss of coolant accident. The primary circuit is driven by two pumps connected in parallel. Both pumps operate at 50 % capacity and each pump can operate the cooling circuit alone in case of failure or maintenance of the other. A 10 micron mesh filter is placed between the pump and the target to protect its cooling structure from possible cooling water contamination and clogging. The heat exchanger is located downstream of the target, followed by a tank that serves both as a pressurizer and as a feed tank for the pumps. In addition to the system pressure, the temperatures and the filling level of the cooling system, the conductivity of the water and the pH value are measured continuously in order to detect any deviation from the required condition at an early stage.

II.1.8 Target activation

The activity of the radionuclides produced by interaction of protons and neutrons with the tantalum target and the cooling water is simulated for an incident proton beam of 70 MeV and an average current of 1.44 mA (90 mA peak current, 1.6% duty cycle, 100 kW average power) and for irradiation times of 30, 90, 180 and 360 days using the FLUKA particle transport code with the cross section databases ENDF/B-VII, JENDL and JEFF. The neutron producing part of the target is modelled without microchannel structure and its thickness is reduced to 4.45 mm to yield an proton energy deposition of 70 % into the water dump. The thickness of the back wall of the target is increased to 4.5 mm to conserve a total mass of tantalum of 4.5 kg. The target is embedded in a thermal moderator made of polyethylene and a lead reflector. The target is cooled by flowing 70 litres water through the target with a mass flow of 1.3 kg s^{-1}. The volume of water inside the target is 152 cm^3. The radionuclides formed and their activity at the end of the irradiation of the tantalum target and cooling water are listed in Table II.4 and Table II.5, respectively. The build up of the activity during irradiation and the decay of the activity from the end of the irradiation are shown for the tantalum target and the cooling water in Figure II.20 and Figure II.21, respectively. The total activity, dose rate, decay heat and heat deposition at the end of irradiation and for a decay time of one week from the end of irradiation are given in Table II.6. The decay heat is calculated from the total energy (Q-value) released by the radioactive decay. The dose rate is calculated with the SISy software (Strahlenschutz-Informationssystem version 2.6.0) for radiation protection. The heat deposited in the tantalum target is determined with the FLUKA code.

The total activity of the target increases slightly from 0.60 to 0.76 PBq for increasing irradiation time and is one to two orders of magnitude lower than that of a spallation target. The overall activity of the radionuclides with a half-life less than some hours represents 60% to 77% of the total activity depending on the irradiation time. For a decay time of one week from the end of irradiation the total activity decreases by factors ranging between 8.7 and 3.6 and is mainly related to the medium and long lived radionuclides like ^{182}Ta ($T_{1/2}$= 114.4 d),^{178}W ($T_{1/2}$= 21.6 d), ^{179}Ta ($T_{1/2}$= 1.82 y), ^{175}Hf ($T_{1/2}$= 70 d), ^{177}Ta ($T_{1/2}$= 56.6 h) and ^{181}W ($T_{1/2}$= 121.2 d). However, ^{182}Ta generates 75% to 88% of the dose rate and 68% to 86% of the decay heat. Therefore, ^{182}Ta is the major source of radiation to consider for shielding issues in particularly for the target replacement that will be performed during the week following the end of irradiation. Depending on the irradiation time the heat deposited in the tantalum target ranges from only 28 W to 42 W and therefore no cooling of the target is further needed during its exchange and storage.

Due to the high activity generated at the end of irradiation, the replacement and storage of the target including the target-plug can be done only by remote control using an appropriated transport cask as shielding to maintain an acceptable local dose rate during the operation. The main radionuclides, the total activity, the decay heat and the dose rate after 1, 3, 5 and 10 years decay time from the end of target irradiation are listed in Table II.7. Up to a decay time of 1 years ^{179}Ta ($T_{1/2}$=1.82 y) and ^{182}Ta ($T_{1/2}$=114.4 d) are the main radionuclides. Afterwards, the long-lived radionuclide ^{179}Ta becomes predominant. The spent targets including the target plug as shielding can be stored over the full period of operation of HBS (around 30 years) in a dedicated long-term storage facility. This will require about 100 individual storage positions. Alternatively, the spent targets can be separated from the target plug after a decay time of 5 years in a hot cell and transfered into a cask of type MOSAIK (MII-15EI with 5 cm lead shielding) which can receive about 30 to 40 targets. Depending on the target irradiation time, the dose rate at the cask surface ranges between 1 μSv/h and 7 μSv/h for one stored spent tantalum target. For the cask transport, a dose rate at the cask surface lower than 500 μSv/h or 2 mSv/h must be ensured.

The total activity of the cooling water is mainly due to the short-lived radionuclides like ^{12}B ($T_{1/2}$= 20.2 ms), ^{13}N ($T_{1/2}$= 9.96 m), ^{16}N ($T_{1/2}$= 7.13 s) and ^{15}O ($T_{1/2}$= 2.04 m), and reaches a value 4.93 TBq independently of irradiation time. For a decay time of one week from the end of irradiation the

Irradiation parameters					
Isotope	Half life	30 d	90 d	180 d	360 d
^{3}H	12.33 y	3.80E+09	1.13E+10	2.25E+10	4.44E+10
^{171m}Yb	5.25 ms	1.52E+10	1.52E+10	1.52E+10	1.52E+10
^{171}Lu	8.24 d	1.28E+10	1.40E+10	1.41E+10	1.42E+10
^{172}Lu	6.7 d	2.72E+11	3.56E+11	3.72E+11	4.01E+11
^{172m}Lu	3.7 m	2.69E+11	2.69E+11	2.69E+11	2.69E+11
^{173}Lu	1.37 y	3.60E+10	1.09E+11	2.09E+11	3.83E+11
^{174}Lu	3.31 y	6.38E+08	2.07E+09	4.15E+09	8.29E+09
^{174m}Lu	142 d	1.16E+09	3.09E+09	4.97E+09	7.04E+09
^{176m}Lu	3.63 h	1.21E+09	1.21E+09	1.21E+09	1.21E+09
^{178}Lu	28.4 m	1.21E+09	1.21E+09	1.21E+09	1.21E+09
^{171}Hf	12.1 h	1.46E+10	1.46E+10	1.46E+10	1.46E+10
^{172}Hf	1.87 y	2.45E+10	7.14E+10	1.37E+11	2.50E+11
^{173}Hf	23.6 h	1.44E+12	1.44E+12	1.44E+12	1.44E+12
^{175}Hf	70 d	4.79E+12	1.13E+13	1.60E+13	1.88E+13
^{178m}Hf	4 s	1.57E+13	1.57E+13	1.57E+13	1.57E+13
^{179m}Hf	18.7 s	2.71E+11	2.71E+11	2.71E+11	2.71E+11
^{179m2}Hf	25 d	1.71E+09	2.79E+09	3.04E+09	3.04E+09
^{180m}Hf	5.5 h	6.07E+09	6.07E+09	6.07E+09	6.07E+09
^{181}Hf	42.4 d	1.83E+10	3.64E+10	4.48E+10	4.72E+10
^{173}Ta	3.14 h	1.46E+10	1.46E+10	1.46E+10	1.46E+10
^{174}Ta	1.05 h	1.85E+12	1.85E+12	1.85E+12	1.85E+12
^{175}Ta	10.5 h	2.34E+13	2.34E+13	2.34E+13	2.34E+13
^{176}Ta	8.09 h	6.55E+13	6.55E+13	6.55E+13	6.55E+13
^{176m}Ta	3.05 h	2.98E+10	2.98E+10	2.98E+10	2.98E+10
^{177}Ta	56.6 h	6.60E+13	6.94E+13	7.24E+13	7.52E+13
^{178}Ta	9.31 m	1.57E+13	1.57E+13	1.57E+13	1.57E+13
^{178m}Ta	2.36 h	7.25E+13	7.25E+13	7.25E+13	7.25E+13
^{179}Ta	1.82 y	2.39E+12	6.97E+12	1.33E+13	2.44E+13
^{179m}Ta	9 ms	5.25E+13	5.25E+13	5.25E+13	5.25E+13
^{180}Ta	8.15 h	2.13E+13	2.13E+13	2.13E+13	2.13E+13
^{182}Ta	114.4 d	2.10E+13	5.33E+13	8.43E+13	1.13E+14
^{182m}Ta	283 ms	4.33E+11	4.33E+11	4.33E+11	4.33E+11
^{182m2}Ta	15.8 m	1.12E+09	1.12E+09	1.12E+09	1.12E+09
^{174}W	31 m	1.69E+12	1.69E+12	1.69E+12	1.69E+12
^{175}W	35.2 m	2.16E+13	2.16E+13	2.16E+13	2.16E+13
^{176}W	2.5 h	5.86E+13	5.86E+13	5.86E+13	5.86E+13
^{177}W	2.25 h	5.95E+13	5.95E+13	5.95E+13	5.95E+13
^{178}W	21.6 d	4.10E+13	6.27E+13	6.62E+13	6.64E+13
^{179}W	37.05 m	4.81E+13	4.81E+13	4.81E+13	4.81E+13
^{180m}W	5.47 ms	1.85E+11	1.85E+11	1.85E+11	1.85E+11
^{181}W	121.2 d	5.73E+11	1.46E+12	2.34E+12	3.17E+13

Table II.4: *Activity (Bq) of main radionuclides produced at the end of the irradiation of the 4.5 kg tantalum target. The proton energy is 70 MeV and the average current 1.44 mA.*

total activity decreases by 3 to 4 orders of magnitude and is mainly related to ^{7}Be ($T_{1/2}$= 53.1 d) and ^{3}H ($T_{1/2}$= 12.33 y). The dose rate is in the range of some μSv/h. Depending on the irradiation time the activity concentration of tritium ranges between 800 Bq/g and 9,000 Bq/g and is higher than

Irradiation parameters					
Isotope	Half life	30 d	90 d	180 d	360 d
^{3}H	12.33 y	5.44E+07	1.62E+08	3.23E+08	6.37E+08
^{7}Be	53.1 d	6.02E+08	1.28E+09	1.68E+09	1.85E+09
^{12}B	20.2 ms	2.47E+12	2.47E+12	2.47E+12	2.47E+12
^{11}C	20.4 m	4.41E+09	4.41E+09	4.41E+09	4.41E+09
^{13}N	9.96 m	1.28E+12	1.28E+12	1.28E+12	1.28E+12
^{16}N	7.13 s	3.19E+11	3.19E+11	3.19E+11	3.19E+11
^{15}O	2.04 m	7.77E+11	7.77E+11	7.77E+11	7.77E+11
^{17}F	64.5 s	1.63E+09	1.63E+09	1.63E+09	1.63E+09
^{18}F	1.83 h	6.29E+10	6.29E+10	6.29E+10	6.29E+10

Table II.5: *Activity (Bq) of radionuclides produced at the end of the irradiation of the 70 L cooling water. The proton energy is 70 MeV and the average current 1.44 mA.*

Irradiation parameters				
	30 d 1.05 Ah	90 d 3.15 Ah	180 d 6.30 Ah	360 d 12.61 Ah
Tantalum target - EOI				
Activity (PBq)	0.60	0.67	0.71	0.76
Dose rate (Sv/h)	62.6	69.9	76.4	82.4
Decay heat (W)	136.6	147.8	158.1	167.1
Heat deposition (W)	28.0	33.1	37.7	42.1
Tantalum target - 1 week after EOI				
Activity (PBq)	0.069	0.13	0.17	0.21
Dose rate (Sv/h)	5.2	12.1	18.3	23.9
Decay heat (W)	8.5	18.6	28.0	36.6
Heat deposition (W)				17.4
Cooling water - EOI				
Activity (TBq)	4.93	4.93	4.93	4.93
Dose rate (Sv/h)	0.27	0.34	0.34	0.34
Decay heat (W)	5.9	6.7	6.7	6.7
Cooling water - 1 week after EOI				
Activity (GBq)	0.60	1.33	1.86	2.32
Dose rate (μSv/h)	4.4	9.5	12.5	13.7
Decay heat (mW)	0.08	0.16	0.21	0.23

Table II.6: *Total Activity, dose rate, decay heat and heat deposition obtained at the end of the irradiation (EOI) and for a decay time of 1 week after the end of irradiation for the 4.5 kg tantalum target and the 70 L cooling water. The proton energy is 70 MeV and the average current 1.44 mA. The dose rate is given for a distance of 1 meter in free air. 1 PBq corresponds to 10^{15} Bq, 1 TBq to 10^{12} Bq and 1 GBq to 10^{9} Bq.*

the value for unrestricted release, 100 Bq/g. Therefore, the water will be collected in an appropriated thank before further processing. The total volume of cooling water over the full period of HBS is estimated to 6,500 L.

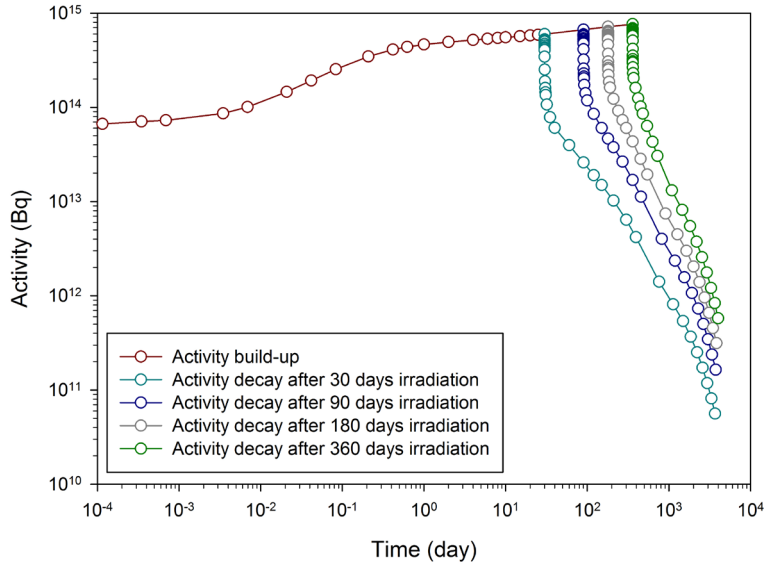

Figure II.20: *Target activity*

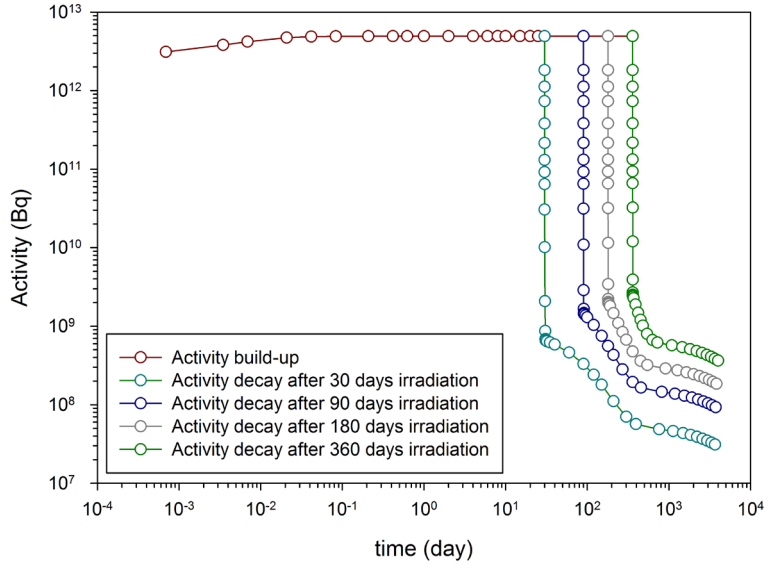

Figure II.21: *Water activity*

	1 yr	3 yr	5 yr	10 yr
Irradiation 30 d, 1.05 Ah				
Radionuclides	55.1% ^{182}Ta 39.1% ^{179}Ta 5.8%(^{175}H, ^{181}W, ^{173}Lu, ^{172}Hf, ^{3}H)	94.1% ^{179}Ta 3.4% ^{182}Ta 2.5%(^{172}Hf, ^{173}Lu, ^{3}H, ^{181}W)	97.3% ^{179}Ta 2.7%(^{172}Hf, ^{173}Lu, ^{3}H)	94.4% ^{179}Ta 3.9% ^{3}H 1.7% (^{172}Hf, ^{173}Lu)
Activity (TBq)	4.17	0.81	0.37	0.056
Decay heat (mW)	723	25.8	8.3	1.25
Dose rate (mSv/h)	473	12.8	3.5	0.51
Irradiation 90 d, 3.15 Ah				
Radionuclides	52.1% ^{182}Ta 42.4% ^{179}Ta 5.5%(^{175}H, ^{181}W, ^{173}Lu, ^{172}Hf, ^{3}H)	94.5% ^{179}Ta 3% ^{182}Ta 2.5%(^{172}Hf, ^{173}Lu, ^{3}H, ^{181}W)	97.2% ^{179}Ta 2.8%(^{172}Hf, ^{173}Lu, ^{3}H)	93.9% ^{179}Ta 3.9% ^{3}H 2.2% (^{172}Hf, ^{173}Lu)
Activity (TBq)	11.2	2.35	1.07	0.16
Decay heat (mW)	1850	72.4	24.4	3.6
Dose rate (mSv/h)	1206	35.4	10.3	1.5
Irradiation 180 d, 6.30 Ah				
Radionuclides	47.9% ^{182}Ta 47.1% ^{179}Ta 5%(^{175}H, ^{181}W, ^{173}Lu, ^{172}Hf, ^{3}H)	94.9% ^{179}Ta 2.5% ^{182}Ta 2.6%(^{172}Hf, ^{173}Lu, ^{3}H, ^{181}W)	97.1% ^{179}Ta 2.9%(^{172}Hf, ^{173}Lu, ^{3}H)	94.2% ^{179}Ta 4.1% ^{3}H 1.7% (^{172}Hf, ^{173}Lu)
Activity (TBq)	19.3	4.5	2.0	0.31
Decay heat (mW)	2954	132	46.5	6.9
Dose rate (mSv/h)	1919	63.1	19.5	2.8
Irradiation 360 d, 12.61 Ah				
Radionuclides	54.6% ^{179}Ta 40.8% ^{182}Ta 4.6%(^{175}H, ^{181}W, ^{173}Lu, ^{172}Hf, ^{3}H)	95.5% ^{179}Ta 2.7% ^{182}Ta 2.7%(^{172}Hf, ^{173}Lu, ^{3}H, ^{181}W)	97.0% ^{179}Ta 3%(^{172}Hf, ^{173}Lu, ^{3}H)	94.1% ^{179}Ta 4.3% ^{3}H 1.6% (^{172}Hf, ^{173}Lu)
Activity (TBq)	30.4	8.1	3.7	0.58
Decay heat (mW)	4058	225	85	12.7
Dose rate (mSv/h)	2612	105	35.7	5.3

Table II.7: *Radionuclides, activity, decay heat and dose rate obtained for various decay times after the end of the irradiation of the 4.5 kg tantalum target. The percentage in front of the radionuclide represents the fraction of the activity given bellow. The dose rate is given for a distance of 1 meter from the target unshielded. 1 TBq corresponds to 10^{12} Bq.*

II.2 Target support systems

The target is operated in the vacuum of the high energy beam transport in the centre of the 1.5 meter thick shield of the target station. Two special components have been developed to ensure reliable operation and to ensure safe target changes. First, the so-called L-tube, in which the target is operated and which forms the last section of the proton beam line. Second, the target plug, with which the target is positioned, supplied and safely exchanged.

II.2.1 Target plug and target vacuum housing

The target is placed inside the target station into a tube shaped like a "L", the so called L-tube, during operation. The L-tube of the HBS target station prototype is shown exemplary at Figure II.22. These pictures are shown since it is the only existing version of such a L-tube. Technical drawings of the L-tube fabricated for the HBS target station prototype can be found in the Appendix A.4. The major difference between this prototype L-tube and the HBS L-tube is the alignment of the proton beamline. In case of the HBS, the proton flight path runs upwards from the ground floor towards the target inside the center of the TMR and hence the proton beamline is aligned vertically. In case of HBS prototype the proton flight path and hence the proton beamline is aligned horizontally. In both cases, the L-tube enables the positioning of the target plug together with the bound target inside the centre of the TMR within the accelerator vacuum as well as enables a safe vacuum sealing outside the radiation field. The L-tube consists of two different vacuum jacket cylinders made of aluminium and arranged at a right angle to each other. The smaller cylinder is the continuation of the proton beamline into the center of the TMR. The lager cylinder can mount a target plug with the bound neutron target.

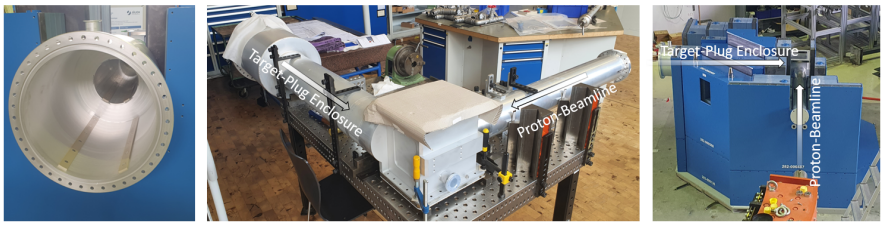

Figure II.22: *left: look into the enclosure for the target plug of the L-tube; centre: L-tube (design of the 10 kW HBS prototype) which carries the target plug and continues the proton beam line; right side: L-tube inside partly build up target station prototype*

The target plug is designed for precise positioning of the target inside the target station, to enable an easy handling of the exchange of the target and to ensure a safe vacuum sealing. The target plug which is designed and fabricated for the HBS TMR prototype is shown in Fig. II.23. The target plug consists of an outer vacuum jacket cylinder made of aluminium with inner shielding and water supply lines to feet the bound neutron target at the front side.

II.2.1.1 Technical requirements and engineering design

The following requirements are placed on the target and its enclosure and hence implemented accordingly:

The target is operated in the accelerator vacuum without an ion beam window because a significant, small single-digit percentage of the proton energy would be blocked by a potential window due to the low energy of the proton beam. Hence, the target is directly operated inside the accelerator vacuum

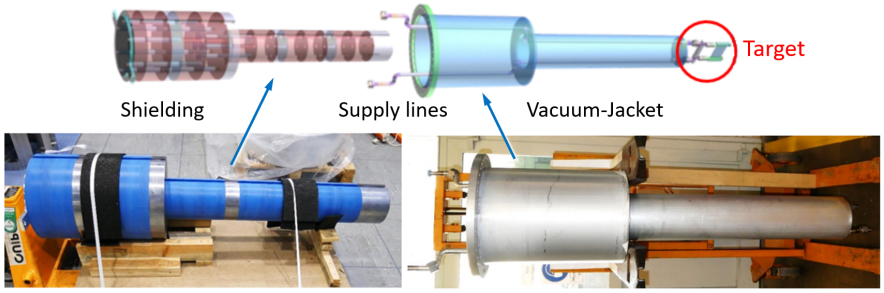

Figure II.23: *Construction of the target plug (HBS prototype design): sandwich shielding composed of borated polyethylene layers and lead layers enclosed by aluminium vacuum jacket with outer flange, target is bound at front side, water coolant supply lines run through recess inside the shielding)*

at $2{\cdot}10^{-7}$ mbar. For this purpose, the L-tube forms the outer vacuum jacket, and the target and target plug form the inner vacuum jacket. The detachable vacuum seal between the two components is located on the flange outside the shielding (Fig. II.24). This prevents possible embrittlement of the sealing by the radiation field of the target and also enables safe mounting. The target itself is materially bonded to the supply lines resp. the 5 mm thick aluminum shell of the plug. The target plug is assembled in a non-hot workshop, this is where the required vacuum tests of each fresh unit are performed and documented.

A detachable connection of the coolant supply lines in the accelerator vacuum close to the high radiation field of the target would be a potential source of failure or leakage. For that reason, any detachable connections between the primary coolant circuit and the target are placed outside the shielding and hence outside the high radiation field. The transition from tantalum target material to aluminium (supply line material) is made via two friction-welded dapaters (tantalum-to-steel to aluminum), each of which is milled out to form the first piece of the supply tubes on the target. As an alternative to friction welding adapters, a direct material transition from aluminum to tantalum via explosion cladding is currently being investigated. If the result of the explosive cladding meets the mechanical and vacuum requirements, the material transition will already take place in the adapter for the inlet and outlet of the target.

Just as consequently as with Target Plug, potential sources of failure are also avoided in the design of the L-tube. For this reason, all accesses to the diagnostic box from the prototype, which can still be seen in figure II.22, are removed and all joints are welded instead. This measure minimises the risk of leaks by careful control of the manufacturing process and to reduce the volume from the diagnostic box to the target chamber. Previous measurements in the target chamber (e.g. current measurement, beam position) are performed outside the target bunker.

The target must be placed as close as possible to the thermal moderator to enable the moderator to cover a large solid angle and to be located within the maximum of the neutron flux. The thermal moderator itself is located outside the accelerator vacuum. For this reason the neutron window of the vacuum must be as close as possible to the target. Two primary measures are taken to meet this requirement. The structure reinforcing struts on the back of the target are kept as small as possible in height to minimise the distance between the neutron producing volume and the neutron window. In addition, the L-tube has a special shape in the area of the target which enables the positioning of the target at a minor distance of 5 mm to the flat neutron window. Unintentional rotation of the target by the cylindrical bearing surface of the target plug is prevented by guide rails in the L-tube and corresponding grooves in the target plug.

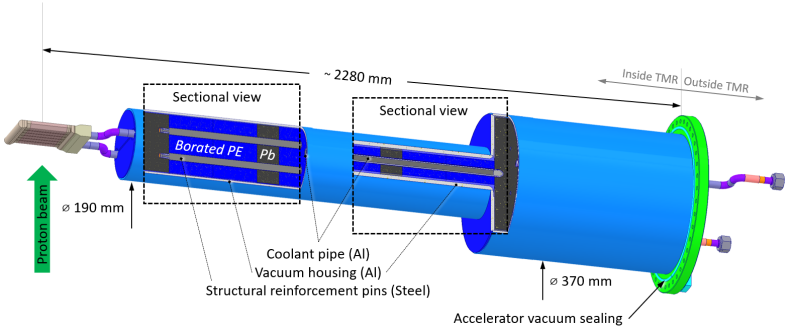

Figure II.24: *Design of the target plug with neutron-producing target at the front (left) and cooling water connections (left). The two sectional views into the interior show the layered shielding maintained by steel pins (left sectional view) and one cooling water line through a groove on the outside of the shielding (right sectional view). The entire plug is surrounded by an aluminium shell.*

In the event of a leakage in the cooling water circuit, the target is separated from the beam transport by a fast-closing shutter to protect the accelerator. The guaranteed closing time of available shutters is 10 mS. A possible leak is detected via the vacuum pressure. In order to minimise the response time of the fast closing shutter there is a direct wiring between pressure sensor and the shutter, parallel to the control system. Such a protective measure is state of the art, it is implemented e.g. at the Low Energy Neutron Source (LENS) at Indiana University.

Furthermore, a fail-safe and fast solution for replacing the highly activated target after operation by a new target is required. This requirement had a major impact on the design of the target plug and the L-tube; the exchange process is described in detail in Chapter II.3.

II.2.1.2 Drawings, manufacturing, installation, handling

L-tube. The L-tube consists of a vacuum box made of aluminium, from which two aluminium tubes extend at right angles to each other. The first tube is a vertically aligned aluminium tube with an inner diameter of 150 mm and a length of approx. 4 m which forms the extension of the high energy proton beam transport line. The second tube is a horizontally aligned aluminium tube with 210 mm in diameter which forms the insert for the target plug. The diameter of this horizontal tube increases to 280 mm in 1.2 meters distance from the vacuum box. All wall thicknesses of the tubes are 5 mm wide, the vacuum box has a wall thickness of 10 mm. The outer ends of the pipes are made of CF flanges of steel in order to make the sealing surfaces durable. The transition of the materials is state of the art, it can be done with friction weld adapter as well as with explosion cladding. The steel flanges are located outside the primary shielding in each case.

The rectangular vacuum box holds the target during operation. The box is machined from a solid material of high strength aluminium alloy with a wall thickness of 10 mm. The cover is welded on. The minimal distance of the vacuum box to the target is 5 mm which is in the direction where the moderator-reflector assembly is positioned (see II.4). The neutrons exit the vacuum box at this back side with a reduced aluminium wall thickness of 3 mm. The aluminium tubes are made of thick-walled pre-products of 6061-T6, which are first lathed with oversize, then welded to the vacuum box and milled to the final dimensions after welding to compensate for deformations caused by welding. Two Teflon slide rails are mounted in each of the two horizontal tubes and fixed by radial drilled drilling in which helicoils are assembled. These serve to lighten the movement of the target plug and

to protect the L-tube from abrasion.

Target Plug. The target plug will become fully assembled and tested for vacuum tightness in the workshop. It consists of a borated polyethylene and lead layered inner shield (1), a vacuum-tight aluminium shell (2) and the target itself (3) with welded-on supply lines.

The three tantalum parts of the target (3) are joined by electron beam welding and tested for leak tightness first. A joint is made from tantalum via steel to aluminum by friction welding for the transition from the target material tantalum to the aluminium of the cooling water lines and pressure tested with 1.43 * PD (PD > PO according to PED). A direct transition from tantalum to aluminum by explosion cladding is under consideration as a alternative; however the necessary material investigations are still in progress, please see chapter 1.1.2. Friction welding adapter are produced out of the friction welded joint and welded to the adapter for inlet and outlet at the target. The cooling water lines of the target consist of DN 20 aluminium lines. The water lines become pre-bent and weld to the friction weld adapter at the target.

The inner shielding (1) consists of layered discs of lead and borated polyethylene in the same configuration as the TMR shielding. For structural reinforcement, the shielding elements are hold together with tension hooks. The borated PE is supplied in large sheets with 135 mm thickness and cut to size by water jet cutter, including the two outer recesses for the water pipes. Each small disc is also provided with 4 holes for mounting the tension hooks, each large disc is provided with 6 holes for mounting the tension hooks. For the lead elements, 80 mm high rods with two diameters (180 mm and 360 mm) were used. These blanks are milled to size and recesses are milled out for the water pipes. In addition four holes are drilled into the 180 mm lead disks for the tension hooks and six holes are drilled into each 360 mm disk. The 360 mm diameter disc which bounds to the small diameter disks is one exception, this disc receives 10 holes for tension hooks. The first part of the shielding disks is assembled and pressed together by 4 tensions hooks (upper left of side picture II.25). The remaining shielding disks are assembled to the first part with 6 additional tension hooks and a docking plate for the target-plug exchange is mounted at the back side. Finally, the pre-bent DN 20 cooling water lines attached to the target are pulled over the grooves of the inner shielding.

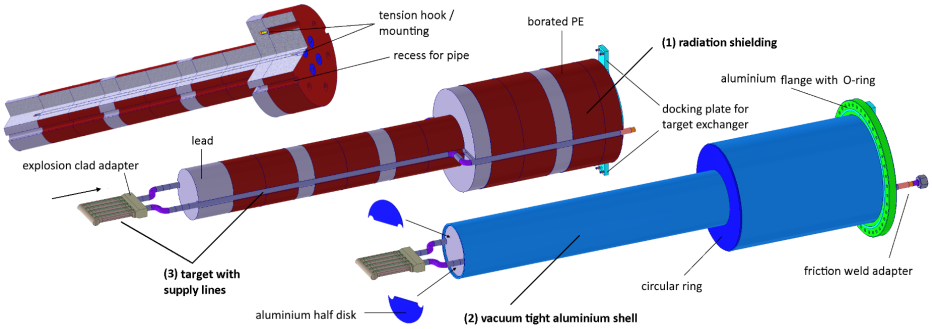

Figure II.25: *Schematic assembly of the target plug: Layered shielding with grooves for cooling lines inside (top left), Target with adapter to aluminum lines (center), Aluminum vacuum shell with conventional O-ring flange and water connection (bottom right)*

The outer aluminium shell (2) of the target plug, including the O-ring at the rear, are made of aluminium. The cylinder wall is made from two thick-walled aluminium semi-finished products with 190 mm and 370 mm, which are lathe in advance with slight oversize. In addition, a 5 mm thick circular ring disc for the front side of the step, a 10 mm thick disk for the back side of the plug, and two 5 mm thick aluminium half discs with a diameter of 190 mm and 1 hole each are fabricated for

the front of the target plug. The two aluminium cylinder walls are welded together with the circular ring disk in between and lathed to size afterwards and hence become the cylindrical cover. This pre-made cylindrical cover is slid over the inner shielding with the water pipes and the attached target. The two aluminium half disks are weld to the front side of aluminium shell and weld to the cooling pipes. The CF flange is slid over the entire assembly and weld to the docking plate as well as to the back side disk. Connectors for the primary cooling system are welded on the friction weld adapter at the back side. Finally, tolerances and tightness are checked and the alignment of the target can be slightly readjusted.

II.2.1.3 Pumps, vacuum control

The proton-carrying side of the L-tube exits the shielding of the target station at the bottom. The transition from L-tube to HEBT (High Energy Beam Transport) takes place in the room below the target bunker. The L-tube ends in a crosshead, which is connected on the opposite underside first to a shutter and then to the HEBT. By closing the shutter, the vacuum of the L-tube is separated from the vacuum of the HEBT. Furthermore, a vent valve, pressure sensor, scroll pump and turbo pump are connected to the crosshead to vent the L-tube section for a target change or to evacuate it after insertion of the target plug. The L-tube should be operated at $2{\cdot}10^{-7}$ mbar. The entire control of the L-tube vacuum is managed by the control system, detailed description in chapter II.7. The safety concept provides that the shutter can only be opened if a vacuum is applied on both sides.

II.2.1.4 Sensors, safety measures

The target monitoring pursues two main objectives. First, it has to be ensured that the target is operated within safe parameters to ensure a safe and reliable operation. Second, any structural damage of the target shall be detected as quick as possible in order to avoid danger to persons and equipment.

The target is monitored indirectly via the cooling water of the primary coolant circuits and the vacuum pressure. The temperature, the pressure loss inside the target plug, the total pressure, the activity, the pH value and the electrical conductivity are monitored in the cooling water. The detectors are located at the pump station of the primary cooling circuit in the media supply room below the target bunker. In addition, temperature sensors are attached to the coolant supply lines inside the target plug. Due to the pulsed ion beam, temperature fluctuations and pressure surges occur in the target. Nevertheless, constant values are measured at the detectors at the pump station, since the coolant water travels 5 m in the pipes from the target to the detectors and the fluctuations are averaged out over this distance which takes about 1.6 s. The average temperature increase of the cooling water is 20 °C while it flows through the target in full-load operation. The stable temperature difference is a necessary indicator of stable operation. The pressure loss through the entire target plug and the attached coolant pipes from the pump station and back to the pump station is dominated by the pressure loss inside the micro channel structure in the target and hence a possible clogging of these channels as well as partial clogging is detectable via the pressure loss. A possible widening of these micro channel caused by water erosion is detectable via the coolant water pressure loss too, however such a possible tantalum erosion is detected much earlier by measuring the conductivity. Each clogging has a negative effect on the heat transfer as well as on the homogeneity of the heat removal inside the target and hence the pressure loss must be monitored continuously. The absolute cooling water pressure in the target must be between 3 bar and 6 bar in order to limit local boiling phenomena and to prevent cavitation at the exit of the micro channels by sufficiently high pressure on the one hand and to limit local stresses by low pressure on the other hand.

The primary coolant circuit is slightly activated by neutrons or contaminated by outgassed or eroded activated isotoped from the target. In particular a constant increase in tritium activity in the cooling

water is expected over the operating time of a target. The monitoring of the tritium activity is a mandatory requirement for the operating license. Monitoring of the radioactivity in the cooling water also provides an early indicator of structural damage caused by micro-cracks caused by load changes, which can lead an increase of the activity due to outgassing of trapped hydrogen. The measurement of the pH value in the primary cooling circuit is primarily used to control the pH value regulation. This is done to protect the aluminum alloys in the cooling circuit from corrosion. The electrical conductivity serves as an indicator for the degree of pollution of the water. This should be extremely low during normal operation. However, abrasion due to erosion, outgassing, externally introduced material and especially corrosion can never be completely prevented and are favored by unfavorable operating parameters. Constant monitoring of the electrical conductivity of the cooling water serves as an early indication system and enables continuous improvement of the operating parameters with regard to wear reduction over the operating time.

Monitoring the vacuum pressure at the interface between the L-tube and the HEBT is necessary because there is no vacuum separation by windows between the two components. The increase in pressure is the earliest alert signal in the event of a cooling water leak from the target into the vacuum. For this reason, the pressure monitoring at the interface between the L-tube and the HEBT is hard-wired to a fast closing shutter in addition to the connection to the control system. The fast closing shutter separates the HEBT in the event of a pressure rise from a leaking target, thus preventing contamination of the beam transport by water.

II.3 Target handling

The lifetime of the target under full operation was estimated to 2.62 years owing to radiation damage [OML+21]. The main irradiated part of the target is made of tantalum, which will be highly activated due to the isotope ^{182}Ta with a half-life of 114 days. In order to minimise the activity, the dose rate and radiation heat, the target will be operated for a period of one year which is lower than the target lifetime. After one year of full beam power operation the target will have an activation of 0.76 PBq. The target handling is related to the following processes: extraction of the spent target from the target station, transport of the spent target to the interim storage facility (or to the hot cell), storage of the spent target, insertion of a fresh target into the target station. To protect operators and local staff, all the tasks mentioned above must be carried out remotely and the spent target must be completely surrounded by an appropriate shielding anytime.

II.3.1 Target handling tool

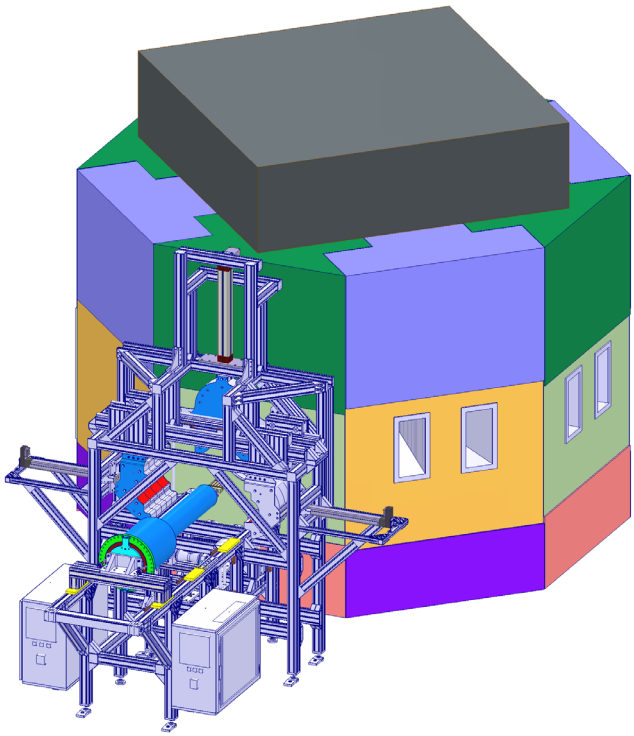

Figure II.26: Handling tool in front of HBS target station, of which the target unit is pulled out

The extraction of the spent target from the target station can start about one week after the switch-off of the proton beam. During this waiting time of one week, necessary for the activity decay of short-lived radionuclides, the target is still cooled. Afterwards, the cooling is stopped, the water is pumped out of cooling loop and the target plug pipes are dried and disconnected from the cooling circuit. Then, the target handling tool is positioned in front of the target plug and connected to it via an interface adapter (Figure II.26).

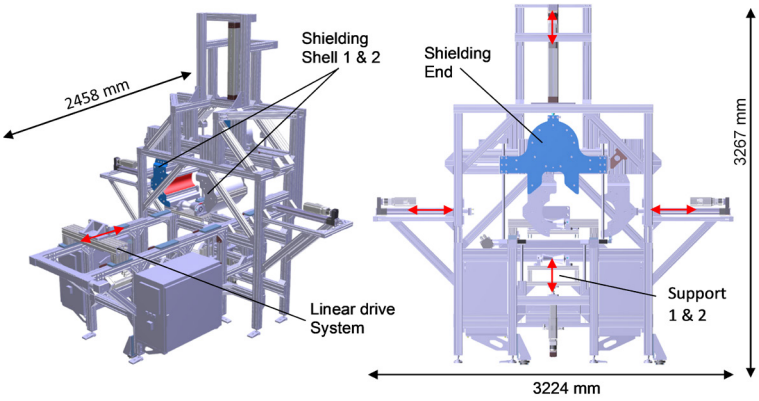

Figure II.27: *Isometric and back CAD view of HBS target handling tool design*

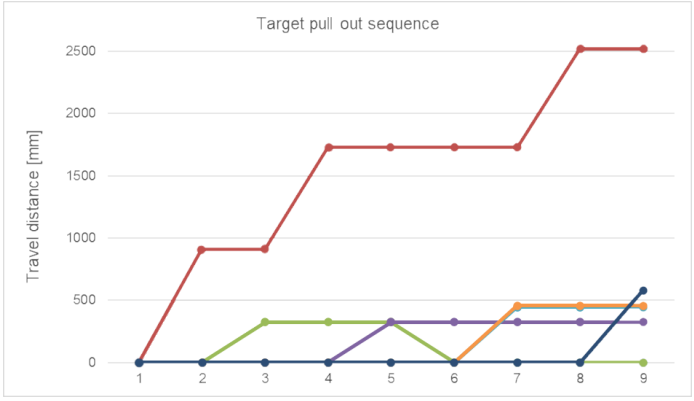

Figure II.28: *Flowchart of HBS handling tool: pulling out sequence with linear drive system in red, support drives in green and purple, shielding shells in orange and front shielding in blue*

The target handling tool is equipped with three movable 300 mm thick lead elements in order to shield the spent target. The contact dose rate at outer surface of the lead elements is 2 mSv/h and corresponds to a dose rate of about 5 μSv/h at one meter distance. The target plug is extracted from the target station using the linear drive system shown in Figure II.27. The target plug is supported from below when being extracted in order to prevent tipping. This is performed with two synchronised lifting cylinders that support the target plug radially. The movements of the lead elements are synchronised with three lifting cylinders to ensure a permanent shielding of the spent target.

Figure II.28 shows the synchronised movements of the three lift cylinders for the lead elements, the linear actuator for the axial movement, and the two lift cylinders for supporting the unit to prevent tilting. The linear driving system (red line in Figure II.28) extracts the target plug automatically in three steps (1 & 3 & 7). To support the heavy and long target plug, two support drives (green and purple line in Figure II.28) move up from below, as illustrated in step 2 & 4, while the axial movement takes place. To shield the spent target, two lead shells (orange line in Figure II.28) first move sideways, shown in step 6 just before the target moves out of the target station, whereby the shells elements surround the target radially. Finally, when the target plug is fully extracted from the target station,

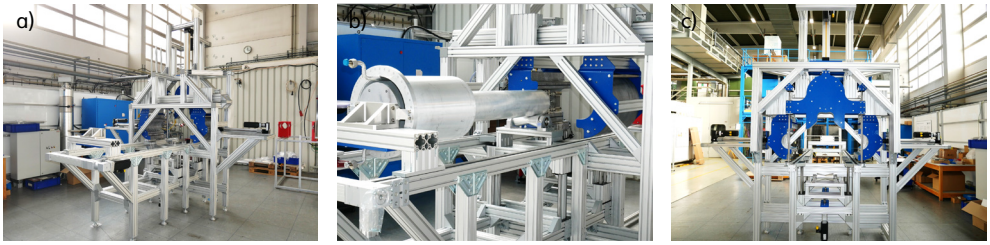

Figure II.29: Picture of the partially assembled target extraction tool: a) isometric view; b) prototype with target plug and target; c) back view

a lead plate (blue line in Figure II.28) is moved down, as shown in step 8, to completely shield the spent target. To insert a fresh target into the target station, the sequence shown in Figure II.28 has to be done in the reverse order.

A prototype of the target handling tool was manufactured and tested at the target station test facility in Jülich. Figure II.29 shows three pictures of the partially assembled target extraction tool prototype. The picture shows an isometric view of the handling tool without target (a); a section with target (b) and the backside of the handling tool (c). This prototype allows full-scale testing of the critical handling sequence with and without the activated tantalum target.

II.3.2 Target transport

In order to prepare the target plug for a save transport first a robot fixes all shielding shells by screws. The target plug is clamped by the shielding shells with the help of an appropriate groove at the front part of the target plug. In next step, the extracted target plug together with the target shielding is decoupled from the target handling tool by the robot. Afterwards the whole structure is placed onto an omni-wheel mobile platform [KMT^{+}16] from e.g. KUKA using the crane inside the target room (see Fig. II.30). The mobile platform is remotely controlled and allows easy passage through gates and corridors especially with the possibility of omni-directional movement.

The three target rooms, the target storage area and the hot cell are all connected trough the transport corridor which is.

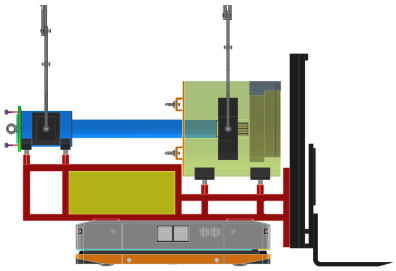

Figure II.30: Target plug and shielding on the mobile platform for transportation

II.3.3 Target storage

Due to the long lived isotopes ^{182}Ta ($Ta_{1/2}$ = 114.4 d) and ^{179}Ta ($Ta_{1/2}$ = 1.82 y) and the high target activity in the order of PBq, the targets need to be stored in a save environment. This is done in the interim storage area where pits in the concrete ground floor are used to store the activated targets as shown in Figure II.31. Within the expected operation time of 30 years and a target change every year for each of the three target stations, a total number of 90 pits equidistant of one meter are required. This results in a total floor space necessary for the storage area of 100 m^2. The pits have a diameter of 400 mm and a length of 2500 mm in which the whole target including target plug and shielding as described in section 2.1.2 can be placed. The pits are clad with 2 mm steel. The pits will be closed with a 20 mm thick steel lid.

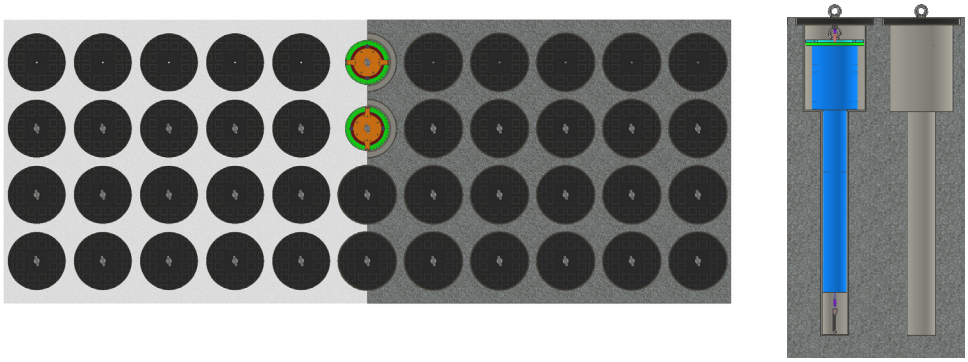

Figure II.31: *Storage area (left) and storage pit with and without target plug (right).*

The rotation from a horizontal position of the target plug on the mobile platform into a vertical position is done with an automated machine like VEAB BS103 I as shown in Figure II.32 positioned in the interim storage area. A rotary arm grabs the target plug from the mobile transport platform by its gripper as shown in Figure II.32. It rotates the whole structure so that the target plug is facing up and places it on the floor. The rotated target plug is than picked up by the manipulator mounted on the crane with the help of the robot system which is also used to release the screws required for the save transport and the rotation of the target plug.

The targets can be inserted or extracted from the pits with a manipulator mounted on a crane within the interim storage area. The manipulator has three arms as shown in Figure II.33. One arm for the target plug and one for each of the lead half shells. The outer two arms can be moved radially taking the lead shells with them allowing to lower the target plug into the pit. The mobile platform described in the previous section is used to remove the shielding plate and can be used in an emergency to move the shielding shells as shown in Figure II.33.

The general process is therefore as follows:

1. The shielding plate is removed by the mobile platform which is equipped with adequate forks.
2. The target plug is lowered as much as possible to place the activated target into the pit until the outer target plug structure touches the shielding shells.
3. The shielding shells can be moved radially by the manipulator hanging on the crane. As the target is already place far into the pit, the outer structure is still well shielded.
4. The target plug is further lowered until it lies on the concrete step.

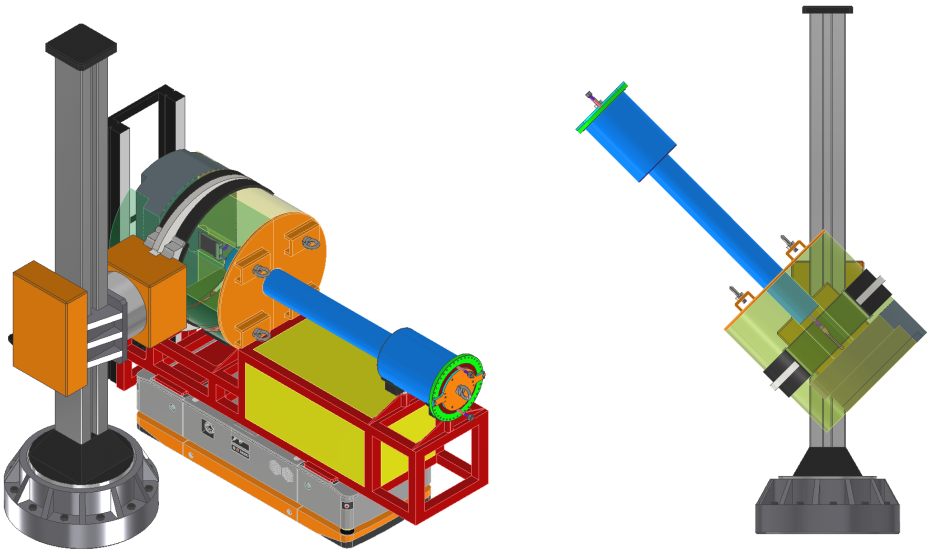

Figure II.32: Rotation from a horizontal position of the target plug on the mobile platform into a vertical position with automated machine VEAB BS103 I

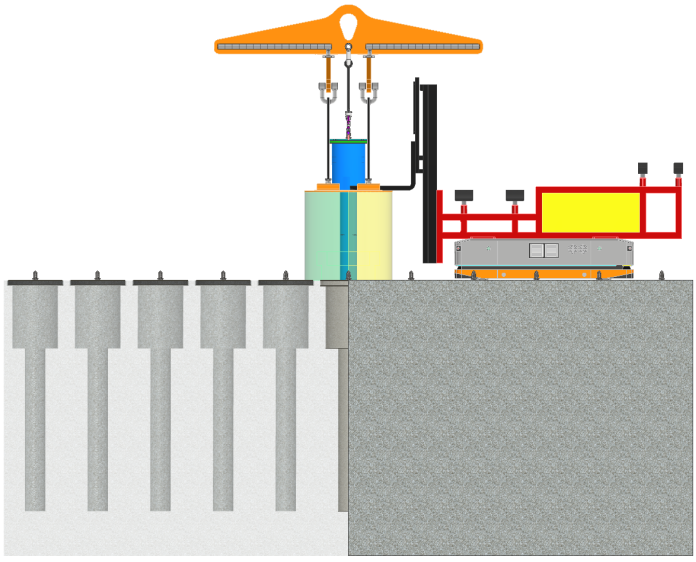

Figure II.33: Insertion or extraction of target plug from the pits with a manipulator mounted on a crane

5. The robot releases the manipulator from the target plug and places a hick steel lid on the pit.

We propose a solution how a handling, the transport and the storage of an activated target can be achieved without technical details because the process involves heavy industry supported by robotic

to reduce the dose rate for the workers. We described an operational process requiring discussions with companies having experience in this field of technology. In a following design update phase the process will be therefore reevaluated as a whole process and a complete solution will be given.

II.4 Thermal Moderator and Reflector

The thermal moderator / reflector unit has the purpose to convert the primary neutron energy spectrum to a thermal spectrum and to allow the extraction of neutron beams towards the experimental stations outside the shielding block. The thermal moderator is the first material dedicated to interact with the primary neutrons and therefore has to accept the majority of the energy of the primary neutrons. At a source of the power level of HBS this requires active cooling of the moderator, as shown in Section II.4.3, so that water has been chosen as moderator material.

Due to the small target volume of HBS compared to fission reactor or spallation neutron sources, a large fraction of the solid angle of the neutron emission from the target can be covered by a small thermal moderator of only a few liters of volume. This makes it possible to confine the thermal neutron cloud in this volume, so that the density of the thermal neutron cloud (normalized to the number of primary neutrons produced) is by orders of magnitude higher than in reactors or spallation sources. This is a massive gain in efficiency of primary neutron usage compared to the earlier research neutron source concepts.

The HBS concept provides a high flexibility concerning the assignment and usage of individual neutron beams. The moderator-reflector unit has been designed with materials that hardly activate in the neutron field (see Section II.4.2) and it has no shielding function outside the operation of the target station. That implies that the moderator-reflector unit can easily be removed and replaced within less than a week of work, once the activated target has been brought out of the target station. This flexibility allows to use a design that can strongly depend on the current instrumentation operated at the individual target station with the opportunity to exchange it to adapt to future requirements.

The design presented here offers the usage of 12 individual neutron beams. All beam tubes have a diameter of 6 cm that allow the extraction of thermal beams or the introduction of a cryogenic moderator (see section II.5) to further reduce the energy spectrum of the neutrons delivered to the instruments. The beam tubes have been arranged in two levels, so that the voids due to the beam tubes are sufficiently distributed that every beam tube is surrounded by thermal moderator material to feed thermal neutrons into it. The design presented contains three penetrating (end-to-end) beam tubes towards six beam ports that can host an elongated para-H_2 cold source.

Based on the technical design presented, variations with different arrangements and geometries can easily be derived without the risk of new technological problems. In the event that instruments are to be rearranged or moderators changed to gain intensity or modify the spectrum, the design can be adapted readily to the instrumentation to be built. The accessibility of the thermal moderator allows such modifications any time, so that potential drawbacks in the efficiency of the design could be removed by corresponding improvements or modifications to the design presented here. This offers the perspective of future upgrades.

As the HBS is a pulsed neutron source, the materials of the moderator and reflector are chosen to moderate and store the neutrons on a time scale comparable to the proton pulse delivered to the target station. Hence, different pulse lengths and repetition rates require modifications in the moderator geometry and material composition to optimize the performance. The design presented here uses a neutron reflector made of lead for an efficient reflexion of fast neutrons without prolongation of the pulse's time structure. This is the optimized solution for the 96 Hz target stations. The long pulses produced in the 24 Hz target station are less sensitive to an prolongation due to thermal neutrons travelling in the reflector.

The thickness of the reflector has been increased above the volume that is useful to reflect fast neutrons into the thermal moderator region because lead is also a good shielding material for the fastest neutrons produced at the target. Increasing the size of the reflector, especially in the vertical direction, has helped to reduce the shielding thickness required for the operation of the target stations.

II.4.1 Position and geometry of TMR

Figure II.34 shows how the thermal moderator-reflector assembly is integrated in the shielding block with the target assembly and the proton beam tube. The figure shows a cut through the lower layer of extraction channels. It can be seen that this layer is ultimately close to the target which is embedded in the green tube just below the moderator. Figure II.35 shows the horizontal cut through the two layers of extraction channels. The yellow area is the volume filled with light water for moderation

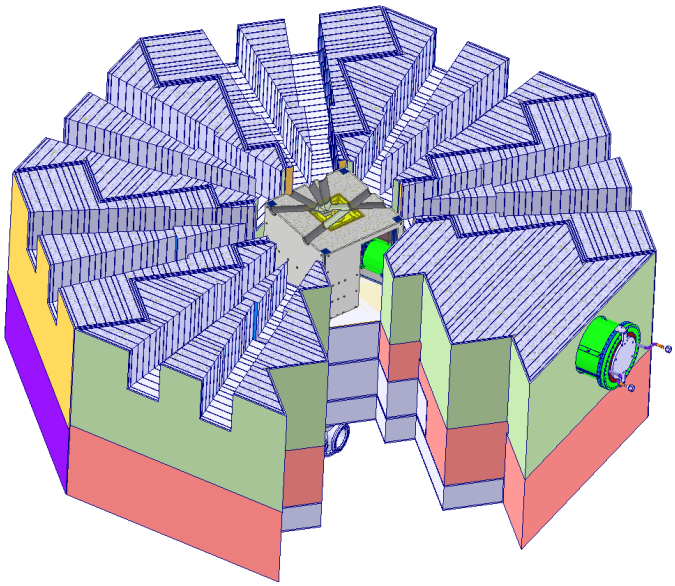

Figure II.34: *Position of the thermal moderator-reflector assembly inside the target station shielding (lead shielding between inner reflector and shielding elements removed for better visibility)*

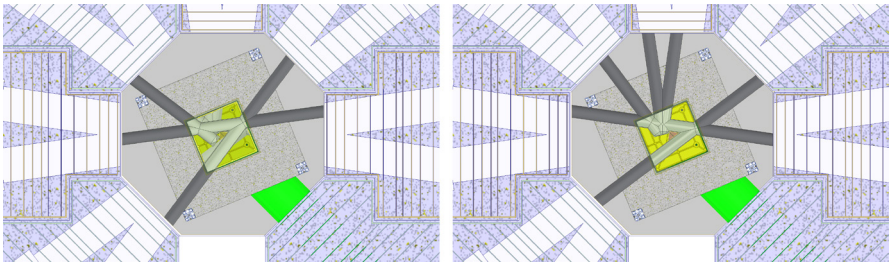

Figure II.35: *Cuts through the two layers of extraction channels in the thermal moderator reflector assembly (left: upper layer, right: lower layer)*

of the fast neutrons. Its size is 265 x 265 x 190 mm^2. The gray square around it is the lead reflector with outer dimensions of 700 x 700 x 1000 mm^2 which fully encloses the thermal moderator and the target chamber. Both are penetrated by the extraction channels which all have 60 mm diameter and are arranged in two layers of 60 mm and 130 mm distance above the target. As can be seen from figure II.35, a geometry has been created where every beam port in the shielding matches with one extraction channel in the moderator-reflector assembly. The extraction channels are off-centered from the axes of the beamports to have enough moderator material in the centre of the thermal moderator to be able to catch most of the primary neutrons close to the flux maximum.

The geometry has been optimized to guarantee equivalent flux conditions on all twelve beam ports on the expense of a somewhat reduced flux on all positions. Other optimizations serving less beam ports allow a higher flux on some of them and can be realized using the same approach. For this reason, we describe here the technologically most demanding solution, while the flux values calculated for the instruments described in Volume 3 of this TDR are based on a thermal moderator - reflector assembly serving only six beam ports but with higher intensities.

This moderator design has four continuous extraction channels which each can be equipped with a cold moderator serving two instruments at both ends of the extraction channel. The other four extraction channels are blind and can be used to extract thermal beams or three of them may share a short cold source, e.g. using a solid CH_4 cold moderator insert.

II.4.2 Materials

Light water has been chosen as thermal moderator material because it has a high proton density yielding efficient moderation of neutrons and it can be circulated in a cooling loop to remove the excessive heat imposed by the strong radiation close to the target.

As the thermal moderator is located at the place of highest neutron flux of the facility, it is necessary to consider the activation of all materials of the moderator and reflector in the intense neutron radiation. The thermal moderator is operated with a total volume of 60 l of light water. For an irradiation time of 1 year the activity concentration of tritium reaches 200 Bq/g and is higher than the value for unrestricted release of 100 Bq/g. Therefore, the moderator water will be collected in an appropriate tank for storage and decay before further processing. The total volume of moderator water over the full period of HBS is estimated to 5500 l.

The structural materials of the water vessel and the extraction channels inserted are made of aluminium alloys with magnesium as alloying addition. These materials are reasonably machinable, weldable and castable to realize the complex geometry which is required, while they are not very sensitive to irradiation, have a sufficiently good thermal conductivity and do not produce long-living isotopes by activation in the neutron field. In addition, these materials are common in mechanical engineering and economic. Also the profiles and screws used for the assembly as well as the water connection tubes are fabricated from aluminium alloyed with magnesium and silicon.

As the reflector material, pure lead for the massive parts and an alloy of lead with calcium or tin as addition for the casted parts around the extraction channels have been chosen. Lead has a high scattering cross section for fast neutrons and a low moderation effect, so that the mobility of the scattered neutrons remains high on their way back to the thermal moderator region to avoid elongation of the neutron pulse length.

II.4.3 Radiation heating, cooling requirements

To be able to assess the necessity of moderator and reflector cooling we have performed simulations of the energy deposition (radiation heating) for prompt neutron and gamma radiation within the

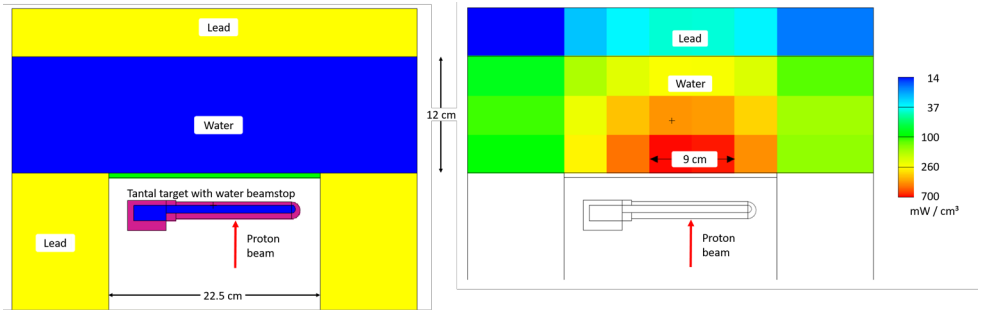

Figure II.36: *Vertical cut through the model geometry (left) and simulated energy deposition in the thermal moderator and the first layer of the lead reflector due to neutron and prompt gamma irradiation (right)*

close vicinity of the target: namely, the light water thermal moderator and the first layer of the lead reflector surrounding the moderator were of particular interest. For that purpose, we have prepared a simplified model of the TMR assembly, where we neglected the beam extraction channels, cold moderator inserts, and constructional parts. Only a thin 1 cm aluminum layer was added between the proton beam tube and the thermal moderator to simulate the energy deposition in the moderator housing. The simulation was performed for prompt neutron and gamma-ray contributions using the fmesh energy deposition tally of MCNP6, where the mesh size was set to cuboids of 3.5 x 4 x 4.5 cm^3. As it can be seen from figure II.36 the highest energy load is to be expected within the first few cm of the moderator right above the target where the maximum of the fast neutron flux arrives. Directly above the target a radiation power of ca. 700 mW / cm^3 of water is deposited. The 4 cm thick water layer above the target receives the integrated power of 1 kW of radiation energy. Additionally, the heat deposition due to the gamma-ray emission going along with the decay of activated materials (delayed radiation) during the operation of the facility should be considered, though in the water moderator this effect is expected to be negligible compared to the prompt contribution. This amount of radiation heating clearly requires a cooling circuit with forced circulation.

The heat deposition in the lead reflector is about a factor 20 lower. Due to the high thermal conductivity of pure lead this amount of heat can be removed by convectional cooling at the surfaces of the reflector.

II.4.4 Design concept of the thermal moderator

The light water thermal moderator needs a confinement to keep the liquid phase in the desired geometry for the proper shaping of the thermal neutron field. This tank consists of the outer vessel, the extraction channels penetrating the vessel, a void towards the target used for feeding the primary neutrons more efficiently into the upper layer of extraction channels and service elements for connecting the water cooling circuit.

Figure II.37 shows the main elements of the water vessel for the thermal moderator. The outer vessel consists of three shells (6, 7, and 8) from the lower boundary to the centre of the lower level of extraction channels to the centre of the upper level of extraction channels to finally the top. To achieve thin walls while keeping sufficient mechanical strength and stiffness, a layout with reinforcing ribs (5) and weight reduction pockets (4) in between has been foreseen. This can be manufactured by mechanical milling of the main body and chemical milling of the pockets. In the lower shell one can see a deep drawn void shell (10) as a guide for fast neutrons towards the moderator surrounding the upper level of extraction channels.

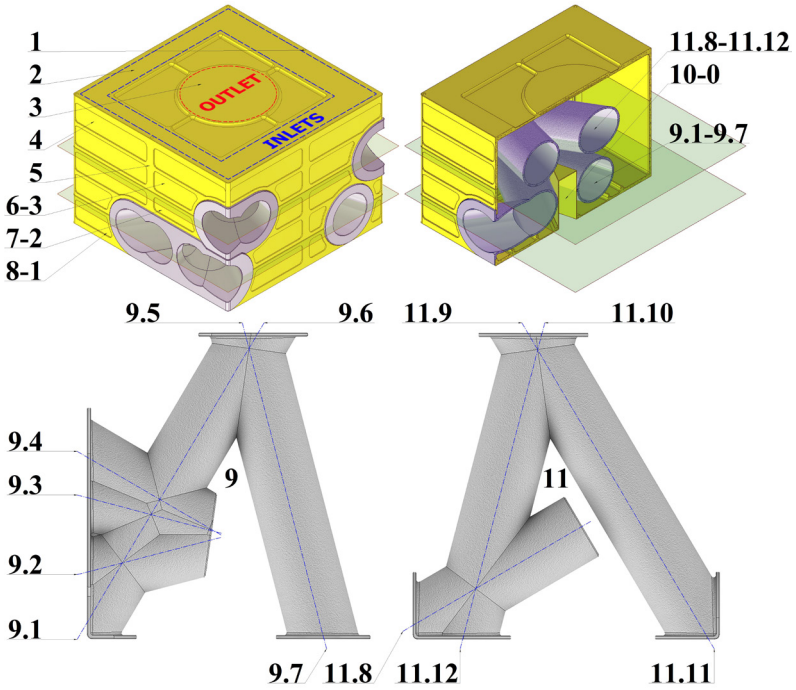

Figure II.37: *Light water tank used as confinement of the liquid thermal moderator. Upper left: main view, upper right: vertical cross section, bottom left: extraction channels of the lower level, bottom right: extraction channels of the upper level. The numbers indicating the individual components are explained in the main text.*

The extraction channels of both levels are manufactured separately (9 and 11). The system of intersecting thin-walled cylindrical channels (9.1-9.7 for the lower layer and 11.8-11.12 for the upper layer) is made with a combined lost-wax casting technology. The lost-wax casting is used to define the outer geometry of the complex channel systems. In the next step a deep drilling of the cast body realizes the desired thickness of the thin walls of the extraction channels. In a third step mechanical milling defines the contact surfaces towards the shells.

The inner surfaces of the shells as well as the outer surfaces of the tube assemblies need an electrolytic oxidation step producing an 50 μm thick oxide layer to prevent corrosion occurring due to contact with the moderator water. The welding surfaces need to be protected against the oxidation.

For the adjusted assembly of these six parts openings for aluminium assembly pins and holes for locking screws (1) are foreseen to be able to properly assemble all these parts to the desired precision, where they are welded to form a single closed tank. During the first welding steps of the channels to the shell, a removable auxiliary construction will define the precise position of the axes of the inner channels with respect to the base of the shell. Welding between the different aluminum alloy parts will be performed under inert gas. Water connections will be mounted in the areas indicated (2 and 3).

Figure II.38 shows the water flow and temperature distribution in the light water thermal moderator and the walls of the tank. The geometry has been simplified to 2 dimensions to reduce the calculation time. The outer dimensions of the moderator tank, the deep-drawn void and two extraction channels in each level have been modeled together with one (case II) or two (case I) inlets at the boundaries

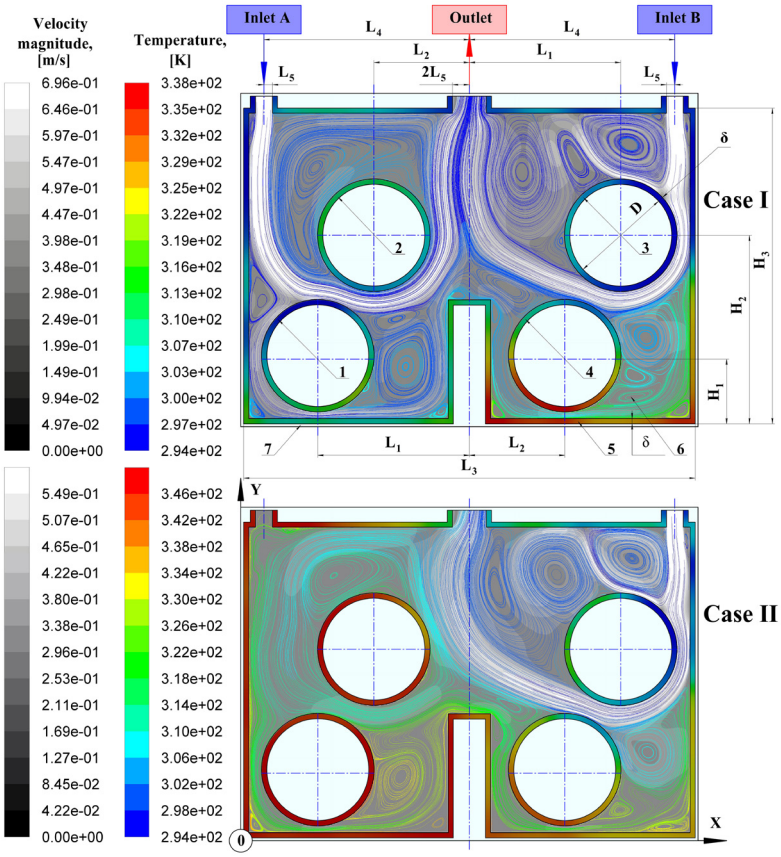

Figure II.38: Pseudo-2-dimensional model of the water flow in the thermal moderator tank. Case I (top): water input at both sides, water output in the centre. Case II (bottom): Only one water input at one side.

of the container's top plate and the only outlet in the centre. The water at the inlet is assumed to flow with 0.5 m/s and have an initial temperature of 294 K.

The heating has been assumed to be 30% above the simulation values presented in section II.4.3. Although all water connections are mounted at the top plate, the water flow reaches the lower surface of the moderator tank with reasonable velocity to remove the heat. According to this simplified simulation, the water temperature never increases above 340 K, even in case II at the side opposite to the inlet. This simulation proves with sufficient safety margin that the moderator water will not start boiling and all heat deposited by the radiation can be removed properly.

II.4.5 Design concept of the reflector

Figure II.39 shows all main design elements of the thermal moderator integrated in the lead reflector and all the periphery necessary for assembly and operation. In addition, the position of the moderator - reflector assembly with respect to the target and the target handling tube is shown.

The four figures in the second line show the different levels of neutronic elements with respect to the

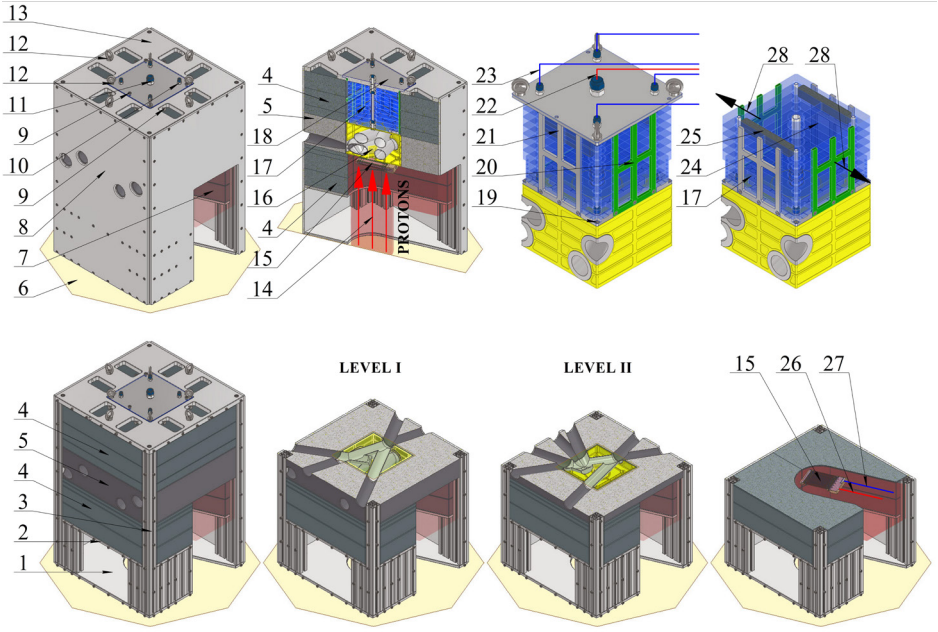

Figure II.39: *Main design elements of the reflector and its periphery. The numbers indicating the individual components are explained in the text.*

reflector assembly. Two support platforms (1 and 2) align the reflector around the proton beam tube and around the target chamber well centred on the octogonal base (6) of the central volume inside the shielding. The lower part of the reflector surrounds the target (15) and the opening towards the target handling tube and the target cooling circuit (26, 27). Above this, there are the two levels of extraction channels aligned with the extraction channels in the thermal moderator tank and the top part of the reflector.

This top part is relatively complex to allow for the mounting of an alignment gear for alignment of the thermal moderator unit inside the reflector block. For this reason, it is again separated into an inner part including the thermal moderator tank ("Cargo cabin") and an outer part covering the reflector surrounding the extraction levels.

The main structural element of the reflector assembly is a four-pillar system of strength hot-extruded hollow columns (3) made of aluminium alloy EN AW 6060 serving for the correct spatial positioning of all components and holding of three aluminium platforms (1, 2, and 13) which carry the main weight of the lead reflector. The reflector elements 4 (without extraction channels) and 5 (with neutron beam extraction channels) surround the target tube and the Cargo cabin including the thermal moderator. The design of the lower (1) and intermediate (2) platforms provides a port for enveloping the peripheral elements of the target (15) which makes it possible to install or remove the thermal moderator - reflector assembly through the upper removable block of the shielding (orange part in figure II.52) without the necessity of disassembling any of the adjacent units. The upper platform (13) with the square central opening and the peripheral openings serves to close the strength contour and organizes the precise positioning of the Cargo cabin by means of a system of alignment screws (9). The shell (8) serves to close the strength contour in transverse directions to avoid the risk of movement of the lead reflector elements. The strength contour surrounds a volume of 670 x 670 x 1000 mm^3. Its components are connected by means of threaded aluminium joints. This frame

system allows the reflector to be subjected to static and quasi-static mechanical loads in the working position and during installation with a lifting device while avoiding any critical deformations.

The Cargo cabin as the central element of the thermal moderator - reflector assembly (shown in the top row in the third and fourth figures) is a self-supporting structure containing the upper part of the reflector, the thermal moderator and a support transferring all weight forces onto the top holding plate (13), thus avoiding to transmit the weight of the lead reflector on the aluminium tank of the thermal moderator. The autonomous Cargo cabin with a total weight of 225 kg and overall dimensions of 265 x 265 x 460 mm^3 is designed to enable the convenient operative input and removal of the thermal moderator into and out of its operation position in the centre of the reflector assembly by means of an external crane access. The cabin is structurally realized in the form of a frame made of demountable (20) and fixed (21) aluminium plates connected from above by the support aluminium platform (18). This support platform is also used as the location of the double-sided aluminium fittings of the moderator water inlet (10) and outlet (11) system with the pipelines (22, 23). The transport elements (12) and the adjustment screws (9) are also connected to this support plate. The reflector inside the Cargo cabin consists of demountable (24) and fixed (17) lead plates allowing to install the reflector around the pre-installed water tubes of the thermal moderator. The bottom plate of the reflector part in the Cargo cabin offers a threaded joint with the thermal moderator tank (19) This structural assembly holds the entire weight of the Cargo cabin by the top plate, i.e. there is no mechanical loading of the water tank of the thermal moderator.

The total weight of the thermal moderator - reflector assembly is 3750 kg. This does not impose any issues concerning the mounting of the assembly when the target vacuum tube is already installed.

II.5 Cryogenic moderators

Cryogenic moderators are used to produce neutron beams with energies between 1 and 10 meV, i.e. with wavelengths above 2 Å. To reach these low neutron energies, interaction with a suitable moderator material at cryogenic temperatures is required. At these temperatures, it is mainly the interaction of neutrons with the molecular excitations of the moderator material that is relevant for the transfer of energy from thermal neutrons to the moderator material in order to reduce the energy of the neutrons to the desired level.

The HBS offers cryogenic moderators feeding one or two instruments with dedicated spectral, pulse shape, and angular emission characteristics. In this sense, the cold moderator is no longer part of the neutron source, but an intrinsic part of the instrument and can be optimized individually during the design process of every instrument. This also implies that a variety of cold source designs can be offered by the instrument designers to optimize beam size, neutron spectrum, and intensity according to the requirements.

The cryogenic moderators developed for the HBS are moderator plug cryostats. The cryogenic moderator vessel is enclosed in a cylindrical vacuum vessel with typically 6 cm outer diameter made of aluminium. The supply lines as well as the neutron extraction optics are enclosed in a moderator plug (see Section II.6.2) that can be placed inside one of the extraction channels of the target station shielding (see Section II.6). The vacuum vessel together with the cryogenic moderator vessel then can be mounted inside one of the beamtubes of the thermal moderator assembly (see Section II.4.4). With this arrangement, full flexibility of the choice of cryogenic moderators for the instrument attached to the extraction plug is available. In addition, two instruments attached to the opposite ends of an end-to-end extraction channel can share a single cryogenic moderator. In this case, the second extraction plug will contain the neutron optics only.

II.5.1 Moderator materials

Suitable materials for cryogenic moderators are liquids or solids containing a high density of hydrogen or (with limitations) deuterium atoms. As the interaction between neutrons and cryogenic moderators involves molecular excitations, the structure and dynamic spectrum of the materials have a strong influence on performance.

The materials currently under consideration are solid mesitylene, solid methane, and liquid hydrogen. The deuterated cryogenic moderator materials need a much larger volume and cannot be fitted into the 6 cm diameter extraction channels. They would need a complete re-engineering of the thermal moderator.

- **Solid mesitylene** C_9H_{12} is an easy-to-handle choice. Mesitylene is liquid at room temperature and freezes at 228 K. It can be contained in a simple Al vessel with a liquid supply tube that is connected to a closed-cycle cooler by a thermal conductor. This technology has proven to deliver neutron spectra with an average neutron temperature below 50 K [Str20].

- **Solid methane** CH_4 is a very efficient cold moderator that can moderate neutrons down to very low temperatures, if the solid methane is kept below 10 K. To achieve sufficiently low temperatures with sufficient cooling power, liquid helium is used as a coolant. Solid methane shows radiation damage problems in high-power neutron sources, but at the power level of HBS we expect to be able to operate a solid methane moderator for at least a day [KLJ+17].

- **Liquid hydrogen** H_2 at a temperature of 18 K can be condensed and kept cold using a commercially available closed-cycle cryostat. Together with a cryopump, a cooling circuit without the use of an additional coolant can be realized. The hydrogen molecule has two molecular

nuclear spin states: the singlet para-hydrogen S=0 state and the triplet ortho-hydrogen S=1 state. The lowest excitation for cooling neutrons is a spin excitation which is only available for ortho-hydrogen. As the ground state of the molecule is para-hydrogen, the liquid will slowly convert into para-hydrogen which reduces the probability to produce very cold neutrons. A regular refreshment of the gas at temperatures above 100 K can avoid this problem.

- **Liquid para-hydrogen** p-H_2 is a very special and useful cold moderator material. Due to the forbidden excitation at energies below 3 meV, the scattering probability for cold neutrons is about one order of magnitude lower than for thermal neutrons, which means that thermal neutrons entering from the side into a cylindrical "finger moderator" are efficiently moderated and the cold neutrons can easily exit the finger moderator in the direction of the cylinder axis. Therefore, cold neutrons can be extracted from a great depth in the moderator volume. In the latest neutron para-hydrogen moderators, e.g. the one designed for the ESS [ZKMT20], the size of the moderator volume has been reduced in one dimension, resulting in an 2-3 fold increase in the brightness. An additional gain factor can be realized if a second dimension is also reduced, resulting in a cylindrical cryogenic volume with a diameter of up to 30 mm and a length of at least 100 mm, as it is presented here.

The use of individual moderators for each instrument allows the optimization of the extraction of cold neutrons in the direction of the instrument. A compact one-dimensional cold moderator can be placed inside the thermal moderator at a position where it is fed with thermal neutrons in an optimized way from all sides, while the cold neutrons are extracted only in one (or two) direction(s) through an extraction channel towards the instrument.

II.5.2 Cryostat designs

Four concepts for cold moderators with different cryogenic materials have been developed to date. All moderator materials have already been qualified experimentally (to be published), the para-hydrogen cryostat with the cryocooler and the recirculating pump is fully assembled and will be used in first experiments during summer 2023. What is in common for all cryostats is that they consist of an in-pile part where the moderator material is kept at low temperatures to interact with the neutrons and a main cryostat outside of the shielding where heat-removal, the preparation of the gas to be condensed (if necessary), and the circulation / refreshing of the moderator is realized. The in-pile part is described in Section II.6.2.

II.5.2.1 Liquid para-hydrogen cryostat

A closed-cycle system for a liquid para-hydrogen moderator has been designed which can be operated with a moderator plug inside one of the extraction ducts of the target shielding. The elongated moderator vessel needs to be placed inside a penetrating extraction channel because of its length. It allows stable operation to take place continuously for several weeks, is easy to use and requires low maintenance. The schematic in Appendix A.3 shows all the components of the system. It contains a closed gas circuit with a buffer vessel that takes all the hydrogen in the warm state and from which the liquid hydrogen filling of the moderator volume and the supply tubing can be condensed. The gas management system is only used for storage of the hydrogen inventory at high temperatures and safety features. If all components are at room temperature, the pressure in the system is 18 bar.

The cryogenic system is based on a cryocooler SRDK-500B from Sumitomo Heavy Industries which has a continuous cooling capacity of 40 W at 18 K temperature. This cooling capacity is sufficient to compensate for all the heat intake of the complete liquid hydrogen moderator circuit. Together with a cryopump which is designed to circulate liquid hydrogen at temperatures between 16 K and 20 K,

a closed-loop moderator has been designed. It consists of the main cryostat and the moderator plug cryostat connected with a cryogenic transfer line.

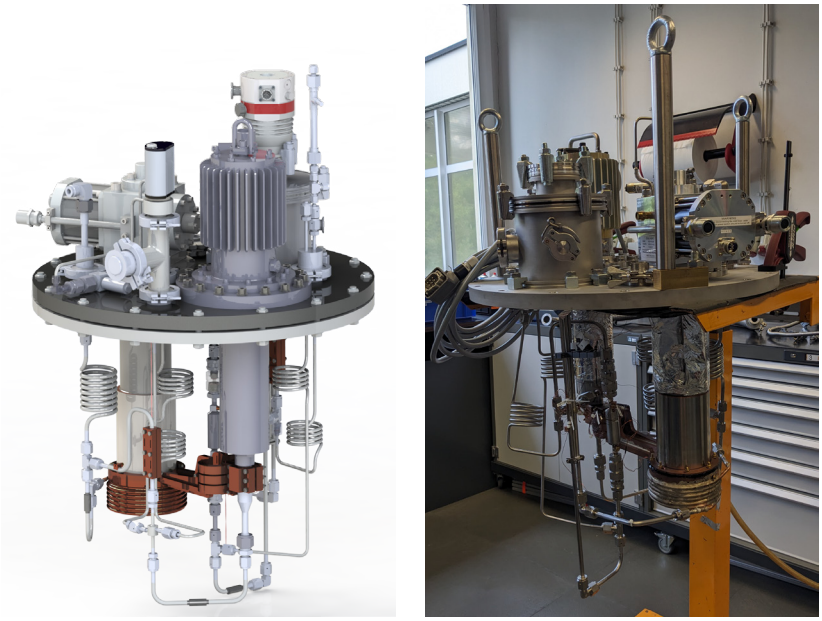

Figure II.40: *Left: Design of the para-hydrogen main cryostat (courtesy of S. Eisenhut). Right: Assembly.*

The important components of the main cryostat (shown in Figure II.40) are the cryocooler, the cryopump, and the paramagnetic ortho-para converter. At temperatures below 21 K the converter produces para-hydrogen with a purity >99.8%.

The main cryostat is connected to the moderator plug (see Section II.6.2) with a vacuum-insulated liquid hydrogen transfer line. The para-hydrogen circuit itself is used as the coolant for the entire in-pile part of the cryostat including the moderator volume. This makes a simple moderator cryostat possible that consists only of the moderator vessel with inlet and outlet tube and the vacuum insulation cover around. To make use of the low scattering cross section of cold neutrons in para-hydrogen, an elongated moderator volume is used as shown in Figure II.41. The dimensions of the cylindrical moderator volume are 10 - 14 cm in length and 2 - 4 cm in diameter, depending on the instrument requirements. Smaller diameter moderators deliver higher brilliance, larger diameter moderators deliver higher integral flux.

Due to the simplicity of operation of this cryostat and the efficiency of cold neutron production in a 1-dimensional para-hydrogen moderator, this type of cold source is considered as a workhorse cold moderator.

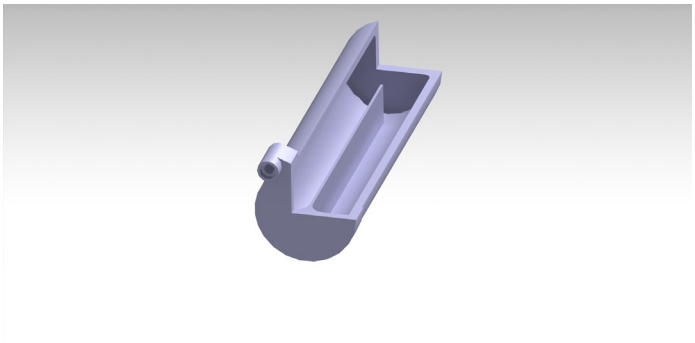

Figure II.41: Moderator vessel for para-hydrogen without vacuum insulation cover (courtesy of A. Schwab)

II.5.2.2 Ortho/para-hydrogen mixing cryostat

The ortho/para-hydrogen mixing cryostat is designed to provide a well-defined mixture of liquid ortho-hydrogen and liquid para-hydrogen in the moderator volume. Due to the continuous natural conversion of ortho-hydrogen into para-hydrogen at low temperatures (with a timescale of several hours) the content of the moderator volume needs to be refreshed continuously. For this reason, a cryostat providing two parallel flow channels for natural hydrogen (75% ortho- and 25% para-hydrogen) and pure para-hydrogen (>99.8%) with adjustable flows regulated by two mass-flow controllers at room temperature has been designed. A triple heat exchanger between liquid helium and both hydrogen lines provides the cooling of both gas streams. In one of the tubes, the catalytic conversion form natural hydrogen to para-hydrogen takes place with a paramagnetic catalyst at cryogenic temperature [EKB+20].

Figure II.42 shows the complete assembly with mixing cryostat and vacuum extension containing the moderator volume. Both gas streams are mixed before the entrance of the moderator volume. This is an aluminium vessel for the moderator material surrounded with a helium gas cooling labyrinth, where the condensation takes place at temperatures below 20 K.

At the gas exhaust, the ortho/para ratio in the evaporated gas leaving the moderator volume is controlled by a speed-of-sound measurement. This result is the input for a feedback loop for the mass-flow control of both gas input streams thus maintaining a constant and adjustable ortho/para-hydrogen mixture. With the adjustment of this mixture, the temperature of the neutron spectrum and the extraction depth from the moderator volume can both be adjusted to the requirements of the instrument. Due to the variation of the extraction depth when changing the ortho/para ratio, the dimensions of the moderator vessel need to be adapted to the mostly used working range.

Figure II.43 shows the neutron spectra measured with the ortho/para-hydrogen mixing cryostat filled with different ratios between liquid ortho- and para-hydrogen. It can be seen that the ratio between ortho- and para-hydrogen can be controlled well better than 1% and that the full range between 25% and 99.9% para-hydrogen fraction can be realized.

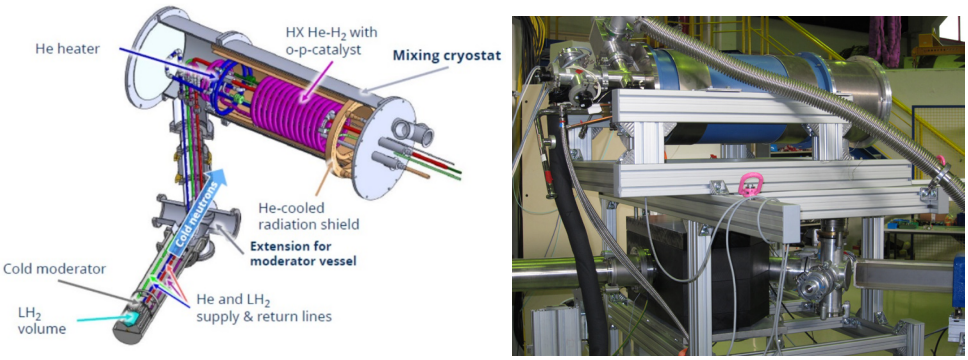

Figure II.42: *Cryogenic ortho/para hydrogen mixing cryostat together with the vacuum extension containing the 1-dimensional moderator volume. Left: CAD rendering, Right: Experimental test setup at the JULIC accelerator.*

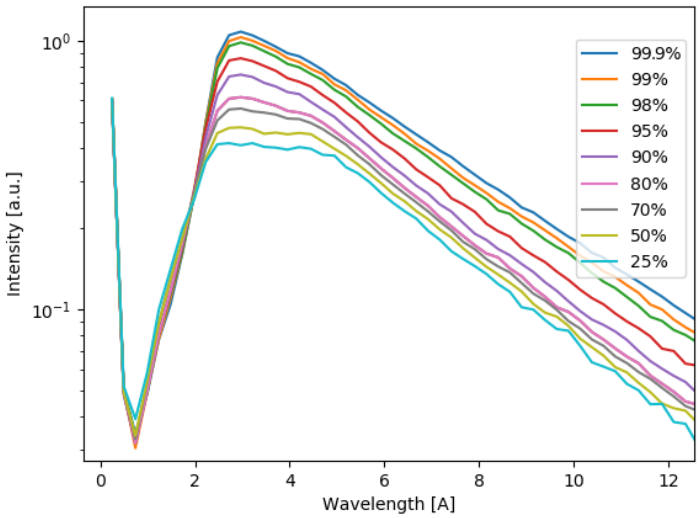

Figure II.43: *Neutron spectra emitted at the ortho/para-hydrogen mixing cryostat measured with the TOAD instrument at the end of a 7 4m long neutron guide at 18 K moderator temperature. The legend shows the concentration of para-hydrogen (to be published).*

II.5.2.3 Solid methane cryostat

Methane is a gas at room temperature and needs to be condensed and frozen in two separate temperature steps. Its low thermal conductivity yields an inhomogeneous temperature profile inside the solid which can be resolved by filling the methane vessel inside the moderator cryostat with aluminium foam with 99% porosity to introduce thermal conductivity. To achieve sufficiently low temperatures with sufficient cooling power, liquid helium is used as a coolant.

A one-dimensional solid CH_4 moderator system has been designed and built with a cylindrical CH_4 vessel attached at the front end of a moderator plug to be placed inside a thermal extraction channel in the centre of the target station, as shown in Figures II.44 and II.45 [Sch23]. The solid CH_4 system is operated in discontinuous batch-style with periodic filling and emptying of the moderator vessel, using a separate flow of liquid helium as its coolant to rebuild the structure of the material. A gas management system with PLC control regulates the methane gas flow during condensation, the nitrogen flow for purging and inertization before startup and after evaporation of the methane inventory, and the helium flow for cooling.

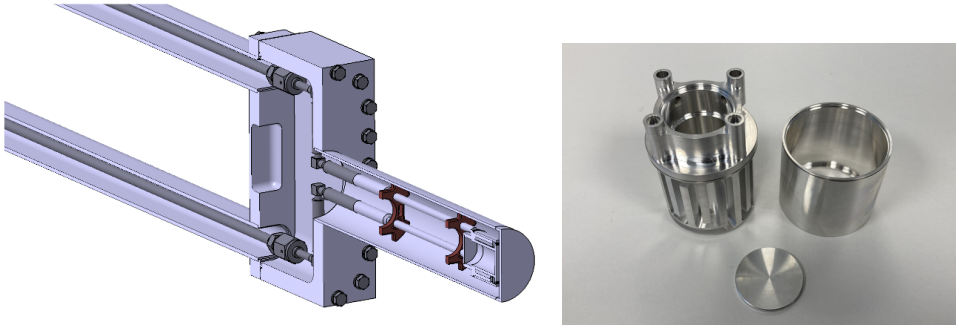

Figure II.44: *Cryogenic finger moderator for solid methane. Left: CAD design of the moderator vessel inside vacuum box including cryogenic supply lines. Right: Moderator vessel with cylindrical methane chamber inside and a labyrinth structure for He gas cooling covering the curved surface shell of the cylinder (courtesy of A. Schwab).*

The cryostat has been assembled together with a neutron guide inside the shielding of an extraction plug (see Section II.6.2) and is now operated as cold source for the TOAD instrument of the JULIC Neutron Platform (see Appendix A.1). Figure II.46 shows the measured cold neutron spectra emitted from liquid and solid methane at various temperatures.

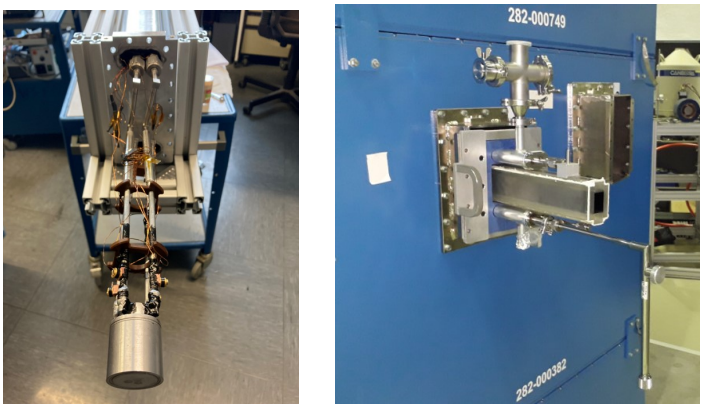

Figure II.45: *Left: Moderator vessel assembled with feeding tubes and sensors (courtesy of A. Schwab). Right: Solid methane cryostat and first neutron guide segment assembled with shielding in the extraction plug and installed in the shielding of the JULIC neutron platform (see Appendix A.1).*

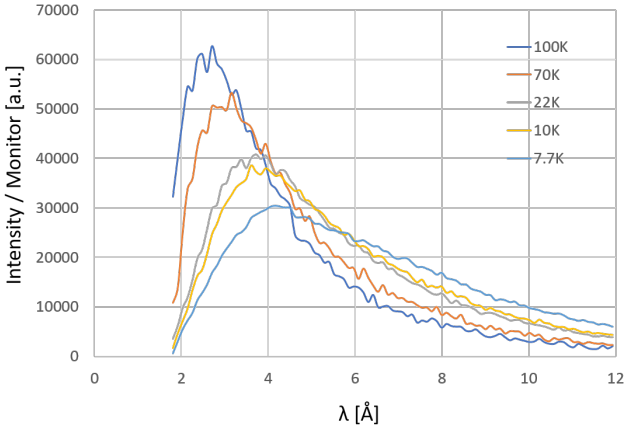

Figure II.46: *Neutron spectrum emitted from liquid (100 K) and solid (70 K and below) methane measured at the TOAD instrument of the JULIC Neutron Platform (see Appendix A.1). The spectra have been corrected from the thermal neutron background and have been normalized to the primary neutron intensity (courtesy of M. El Barbari, to be published).*

II.5.2.4 Mesitylene cryostat

Mesitylene is liquid at room temperature. This makes the handling of the moderator material easy compared to the realizations described before, as no handling of pressurized gases and no condensation at cryogenic temperatures is required. Therefore, as temperature contact between the cooling source (e.g. a cryocooler) and the moderator volume a solid thermal conductor (e.g. copper or pure aluminium) is sufficient.

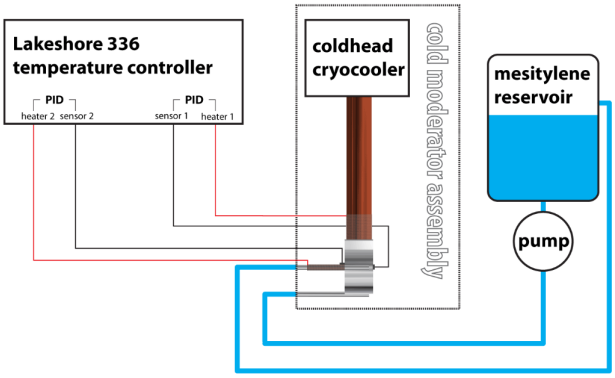

Figure II.47: *Schematics of a cryocooler-based mesitylene cold moderator cryostat. Taken from [Str20]*

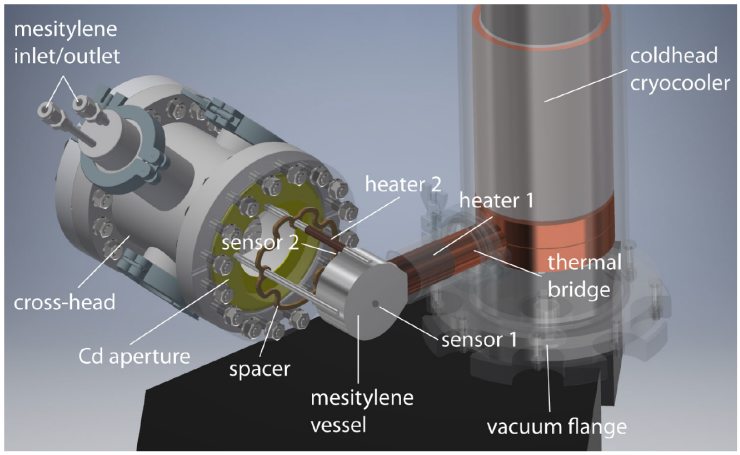

Figure II.48: *CAD rendering of the mesitylene cold moderator cryostat. Taken from [Str20].*

Figure II.47 shows schematically the arrangement of the cryocooler, the heat transfer rod, the moderator volume and the accessories. Typically, mesitylene is frozen while the supply tubes are kept at liquid temperatures, so that the thermal shrinking of the material at the melting temperature can be compensated during the cooling process. Figures II.48 and II.49 show the technical design of the cryostat and the realization, where of course the details are hidden by the vacuum vessel necessary for thermal isolation.

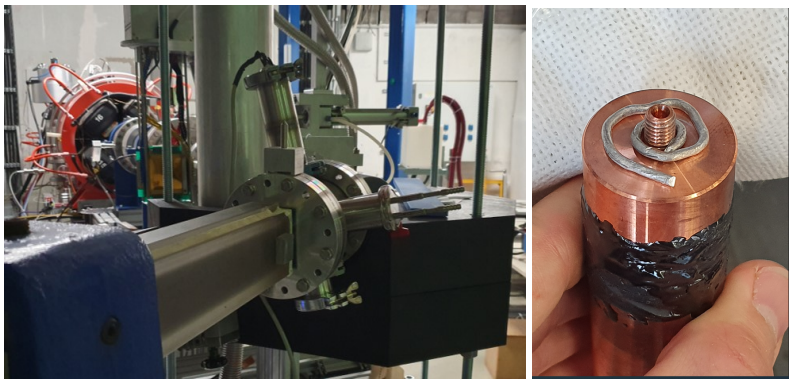

Figure II.49: Mesitylene cryostat installed at the test beamline (left) and copper rod used as thermal conductor before installation (right).

Moderator temperatures below 50 K have been realized with low effort [Str20, Sim19]. Lower temperatures depend on the cooling power of the cryocooler and the quality of the thermal isolation. Figure II.50 shows neutron emission spectra measured at different temperatures between 300 K and 22 K.

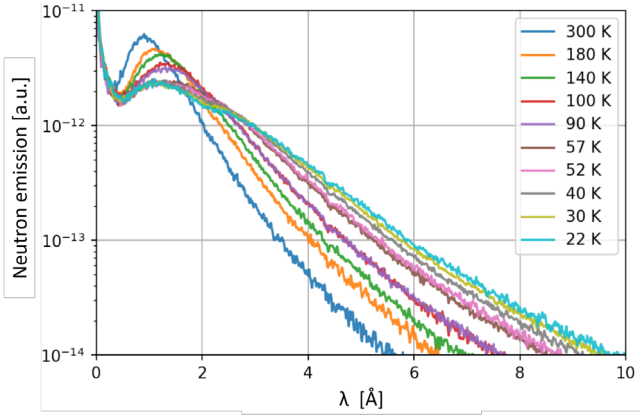

Figure II.50: Neutron emission spectra emitted from the mesitylene cold moderator cryostat at different temperatures. The measured spectra have been corrected from the transmission of the neutron guide, the detector efficiency, and variations of the proton current. Taken from [Str20].

II.5.3 Operation, control, sensors

The cryogenic moderators considered here all use condensed or frozen flammable gases or liquids as moderator materials. They need to be operated under control to avoid the occurrence of explosive gas mixtures between the moderator material and ambient air.

The cryogenic moderators are equipped with temperature and pressure sensors in all relevant sections and with pneumatic valves to enable a complete control and surveillance of every cold moderator fully remote. A PLC is used to ensure that the system is always in a safe state. It enables

automatic operation even of the transient states during initial gas filling, cooldown, condensation, freezing, and warmup of the cryostats.

Each cryostat has its own NICOS based operation GUI where all parameters and actuators are available for manual access, e.g. during troubleshooting. For regular operation, automatic routines are established that bring the cryostat from one operational state into another. These automatic routines can be triggered from a central operation panel in the operator's room, where a status indicator for every cold source informs the operator about the current state of operation.

A safe design together with passive overflow valves ensures that also in the case of a power failure the cryostats can warm up just by the ambient heat intake and release the pressure of the evaporating gas into the ventline without allowing air to enter the cryostat and form an explosive gas mixture there.

II.5.4 Radiative heating, cooling requirements

The cryogenic systems of the moderator cryostats need to remove the heat intake from thermal radiation and conduction, nuclear heating, and heat input from the materials inserted into or circulated through the system.

Table II.8 shows the different contributions to the heat load on the different moderator cryostats. The static heat load has been simulated using ANSYS CFX 2019 for the solid methane cryostat and the values have been extrapolated to the other cryostats based on the differences in the sizes of the moderator vessels and the number of connection tubes to the moderator vessel. The nuclear heat load has been simulated with MCNP6, as well for the solid methane moderator. The values

	liquid para-H_2	ortho/para-H_2	solid CH_4	mesitylene
Operation temperature	18 K	18 K	10 K	40 K
Radiation heat load				
Moderator vessel	0.5 W	0.15 W	0.15 W	0.15 W
Supply tubes	1.3 W	4 W	1.3 W	5 W
Thermal conduction				
Flanges	0 W	0.27 W	0.27 W	0 W
Spacers	1.9 W	3.8 W	1.9 W	1.9 W
Moderator tubes	0 W	0 W	0.1 W	0.1 W
Total static heat load	3.8 W	8.2 W	3.7 W	7.2 W
Nuclear heat load				
Moderator	2.5 W	2 W	2 W	5.5 W
Aluminium vessel	6 W	12 W	6 W	6 W
Total nuclear heat load	8.5 W	14 W	8 W	13.5 W
Gas flow	0 W	34 W	0 W	0 W
Circulation	7 W	0 W	0 W	0 W
Total heat load	**19.5 W**	**55 W**	**12 W**	**21 W**

Table II.8: Heat load on the different types of moderator cryostats

have been extrapolated to mesitylene and hydrogen based on the densities and the fast neutron and gamma photon scattering cross sections of the different materials.

In the case of the ortho/para-hydrogen cryostat the main contribution is the gas flow because in this cryostat the hydrogen inventory needs to be replaced continuously to keep the ortho-hydrogen concentration constant. The supply of ortho-hydrogen is only available by cooling hydrogen gas down from room temperature. For this reason, the ortho/para-hydrogen mixing cryostat can only be operated with an external supply of liquid helium coolant, as the heat load is too high for a cryocooler. The heat load on the mesitylene moderator as well as on the liquid para-hydrogen moderator is well below the limits of a Sumitomo SRDK-500B cryocooler which can deliver about 40 W of cooling power at 20 K temperature. For this reason, these cryostats can be operated without external supply of cryogenic liquids.

The solid methane cryostat is a case at a limit. The frozen methane is immobile, so that the heat transfer must be realized by a helium gas circuit. Together with the energy input of a helium gas circulation pump, the total heat load will be about 20 W, which is above the capabilities of a commercially available cryocooler at 10 K. Here, two options exist: either the operation with external supply of cryogenic liquids, as we did for our experimental tests of the cryostat, or the operation with a closed loop of helium cooling gas at an elevated temperature of 20 K which results in a higher average temperature of the neutron spectrum emitted from the cold neutron source. Condensation and freezing of methane (at 91 K) is no problem with this cooling technique.

II.6 Shielding and neutron extraction

The goal of the shielding is to maintain the gamma and neutron dose rates as low as is reasonably achievable (ALARA principle) to avoid the unnecessary radiation exposure in adjacent areas. Furthermore, the shielding should allow various maintenance work in the target station bunker to be performed after the shut-down of the associated proton beam-line.

The shielding is penetrated by extraction channels that allow to extract neutron beams towards the instruments outside. The dimensions of the shielding should be optimised to be able to position optical elements like neutron guides, choppers or slits of the different instruments as close as possible to the neutron source in order to take maximum advantage of the neutrons produced.

	Side direction	Upwards direction	Downwards direction
0-Layer	Moderator + Reflector	Moderator + Reflector	Moderator + Reflector
Housing	10 mm Steel	20 mm Steel	10 mm Steel
Layer 1	80 mm Pb + 270 mm BPE	80 mm Pb + 270 mm BPE	80 mm Pb + 220 mm BPE
Layer 2	80 mm Pb + 270 mm BPE	80 mm Pb + 270 mm BPE	80 mm Pb + 220 mm BPE
Layer 3	80 mm Pb + 310 mm BPE	80 mm Pb + 288 mm BPE	80 mm Pb + 115 mm BPE
Layer 4	80 mm Pb + 220 mm BPE	80 mm Pb + 270 mm BPE	-
Layer 5	-	80 mm Pb + 250 mm BPE	-
Housing	10 mm Steel	10 mm Steel	20 mm Steel
Total thickness of housing element	1,497 mm	1,775 mm	855 mm

Table II.9: *Shielding configuration listed from inside to outside (total thickness incl. necessary gaps / manufacturing tolerances between different materials)*

The shielding of the target station is made of alternating layers of lead and borated polyethylene. It has different dimensions depending on the viewing direction. The shielding configuration is shown in Table II.9. The side shielding consists of four layers of pure lead (99.5%) and four layers of Borotron (polyethylene blended with B_2O_3 containing 5 weight % elemental boron) placed inside a steel housing. A steel alloy with low cobalt content ($<$ 100 ppm cobalt) has been chosen to minimize activation in the neutron field. The total thickness is below 1.5 m including necessary gaps to compensate production tolerances. The upper shielding needs to be stronger because the highest energy neutrons are emitted along the direction of the proton beam. It is composed of five layers of lead and five layers of Borotron. The bottom shielding consists of three layers of lead and three layers of Borotron. The target station is placed in a bunker with wall, floor and roof thickness of 140 cm each acting as an additional shielding. Bunker walls, floor and roof are made of heavy concrete (normal concrete doped with 50 weight % iron).

II.6.1 Construction and Manufacturing

Shielding structure. The shielding of the target station is designed in an octagonal shape. The shielding consists of 30 elements each made of a steel housing filled with the layers of shielding materials as described in Table II.9. The steel housings are coated with decontaminable paint. Each element has a weight of less than 10 t, so that all of them can be moved by crane. In this way, the entire shielding can be assembled or disassembled in a short time ($<$ 1 week), e.g. for maintenance or repairs inside the target station if the strongly activated content has been removed in advance. A direct view through the gaps between the individual elements is prevented by overlapping of all neighbouring elements with a gap to step ratio of at least 7:1. This configuration efficiently prevents leakage of radiation through the gaps. A vertical cut through the shielding of the target station is shown in Figure II.51.

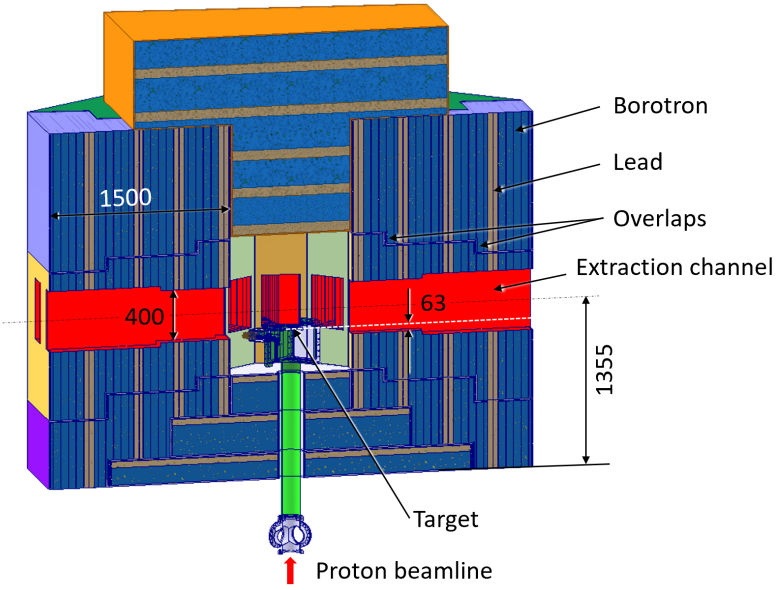

Figure II.51: *Shielding of the target station composed of lead and Borotron layers. The dashed white line indicates the centre of the target. The extraction channels allow the direct view to the target.*

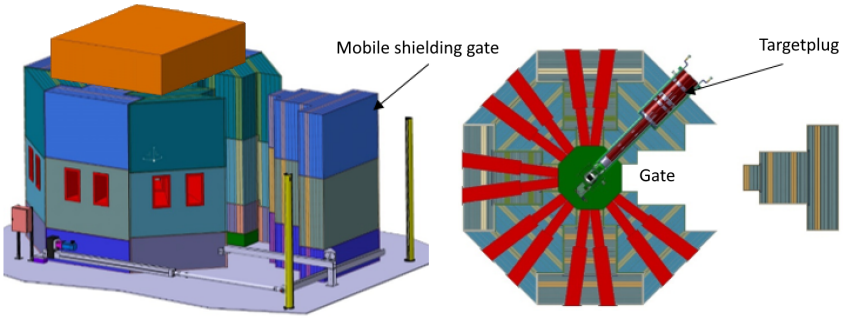

Figure II.52: *Side and top views of the open position of the mobile shielding gate*

One of the eight segments of the shielding acts as a gate that can be moved on wheels as shown in Figure II.52. The gate can be opened automatically by 1.5 m to allow maintenance work inside the target station without the necessity to disassemble the shielding. For the safe operation of the gate motion, safety measures such as light curtains or safety-relevant switches are provided. In the centre of the shielding is an octagonal cave with a width of 1 m in which the target (Section II.1), the L-tube (Section II.2.1), the thermal moderator, and the reflector (Section II.4) are placed.

Extraction Channels. The target station accommodates 12 extraction channels (Figure II.53), which are designed to carry extraction plugs, cold moderator plugs, or shielding plugs. The extraction channels have an angle of at least 16° between each other, an inner height of 400 mm and a width of 150 mm. All extraction channels intersect in the centre of the target station.

If a channel is unused, a shielding plug will be mounted that contains the same shielding material layer structure as the shielding block itself. A streaming of neutrons through the gaps between the plugs and the shielding blocks of the target station is prevented by an overlap with a gap to step ratio of 1:7.

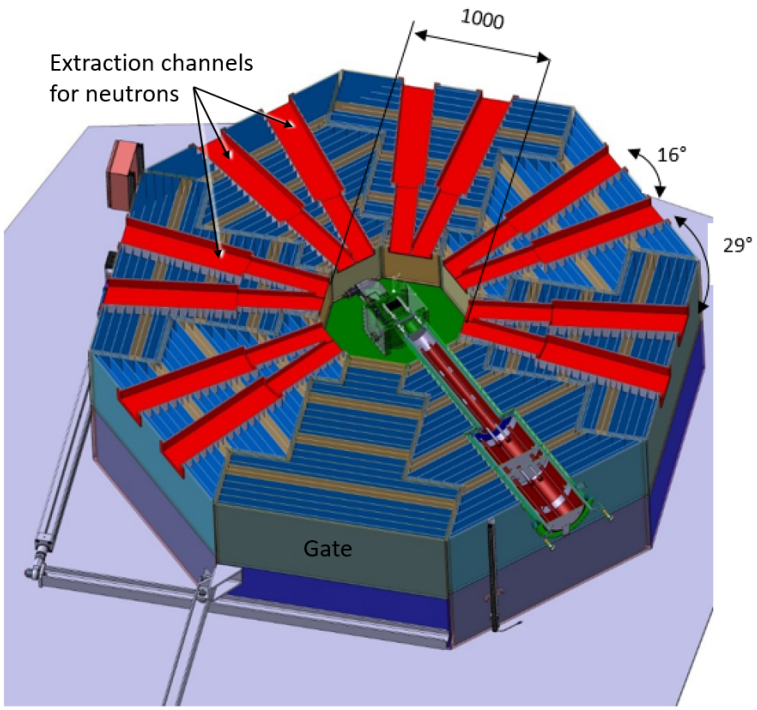

Figure II.53: Extraction channels

II.6.2 Neutron extraction plugs

As shown in Figure II.35, the cross sections of the extraction channels in the shielding are way larger than the cross section of any channel in the moderator / reflector assembly. Each channel in the thermal moderator is the origin of a neutron beam towards a specific instrument that is fed through its individual neutron extraction plug.

The neutron extraction plug may contain a cold moderator to modify the neutron spectrum towards lower energies. In addition, it will either contain a neutron guide to transport a larger beam divergence or the beginning of a collimation setup for a highly collimated beam or other optical elements such as neutron lences.

This neutron extraction setup will then be surrounded by a shielding structure shielding the unused part of solid angle around the neutron transport cross section.

Thermal, epithermal or fast neutron extraction plugs. A collimating extraction plug for thermal, epithermal, or fast neutrons begins immediately after the reflector. Figure II.54 shows an example of a collimating thermal extraction plug for a thermal imaging instrument. Here, a wheel with pinholes

at the surface towards the neutron source allows to choose the size of the virtual neutron beam source, and the collimation is realized just by the distance from the pinhole. The flight path of the neutron beam is fully evacuated and all the volume around the desired beam paths is shielded.

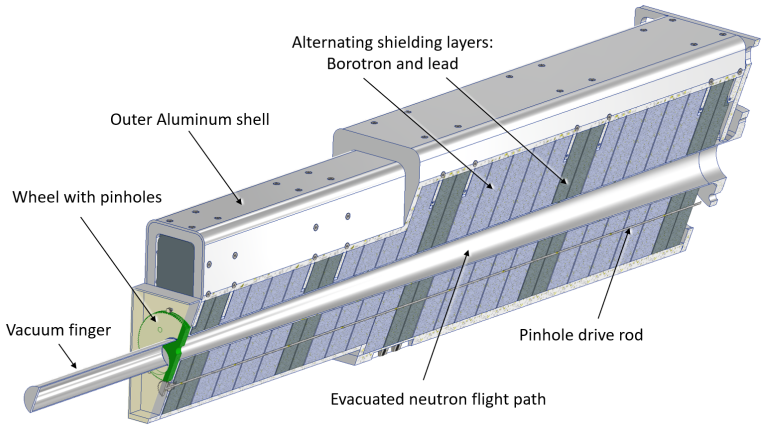

Figure II.54: *Technical design (cut) of a thermal extraction plug*

In the case of epithermal or fast beams, a comparable collimation structure will not face the thermal moderator, but a strongly undermoderated volume (for epithermal neutrons) or immediately the target (to extract fast neutrons towards the instrument).

In the case of extracting thermal beams towards e.g. a diffractometer, an evacuated neutron guide will replace the collimating structure to be able to transport a reasonable divergence of thermal neutrons towards the instrument. The beginning of the neutron guide then can be located at the surface of the reflector, i.e. at about 40 cm distance from the neutron source.

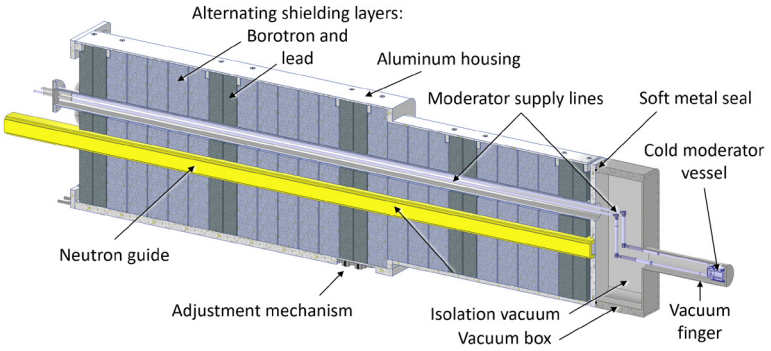

Figure II.55: *Technical design (cut) of a para-hydrogen moderator plug with moderator cryostat attached and built-in neutron optics and supply lines*

Cold moderator plugs. The cold moderator plug hosts the cryogenic moderator vessel, the supply lines required for the operation of the moderator cryostat, diagnostic lines and the first part of the

neutron optics together with some adjustment equipment as well as an adjusting mechanism for the moderator plug itself. A design for a para-hydrogen moderator plug is shown in Figure II.55.

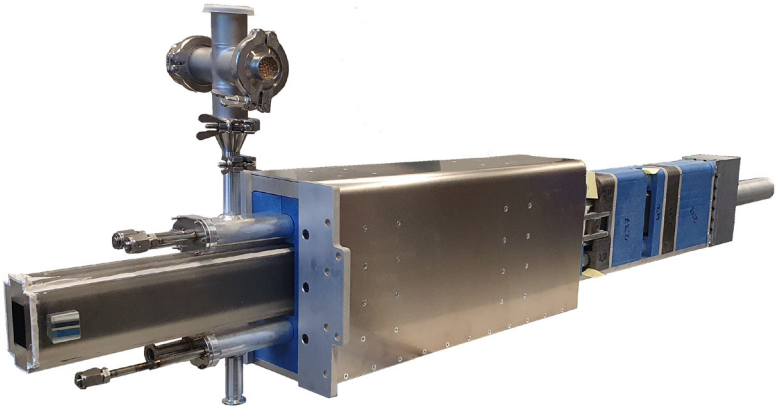

Figure II.56: Solid methane moderator plug from the HBS prototype, partially disassembled for better visibility

In Figure II.56 the solid methane moderator plug constructed for the HBS prototype is shown which has been built on the basis of the same design concept, but with different physical dimensions.

These plugs have an outer shell made of aluminum. This shell contains the adjustment mechanisms for fine alignment in the built-in state. Vacuum tightness of the outer shell is not required except for the vacuum box and the vacuum finger attached on the front side which requires a thermal isolation vacuum. The cold moderator vessel is placed inside the vacuum finger. There, the supply lines run parallel to the neutron flight path close to the outer cylindrical wall towards the vacuum box. There, the supply lines bend to leave the line of sight of the neutron beam. The vacuum box is connected to the aluminum back plate via a soft metal seal. This detachable connection was successfully tested as part of the prototype moderator, it enables comfortable assembly of the cold vacuum components. The entire vacuum box is screwed to the main body of the plug. The neutron guide and a vacuum tube welded to the vacuum box run in parallel through the main body. The supply lines and the signal lines of the cold moderator run through the vacuum tube.

All remaining space is filled with lead and Borotron to reduce the radiation load that can escape through this channel using the same shielding configuration as the target station. The plug has one step matching the step in the extraction channel to counteract beam leakage through the gap between plug and channel.

II.6.3 Beam shutters

Gamma Shutter. The task of the gamma shutter is to maintain the gamma dose rate at an acceptable level to allow maintenance work within the target station bunker when the accelerator is not in operation. The major source of gamma radiation is the tantalum target which is shielded in the direction of an extraction channel exit by 40 cm lead and 60 cm Borotron as the extraction channels have no direct line of slight to the target. Considering 360 days operation the activity of ^{182}Ta is about 10^{15} Bq and leads to gamma dose rate of about 10μSv/h at channel exit. In order to further

reduce the gamma dose rate a simple and compact gamma shutter design has been developed for the HBS that can be mounted at each extraction channel exit. Figure II.57 shows a possible design of this gamma shutter. It consists of a vacuum box with two neutron beam windows made of aluminium. Inside the vacuum box, a 10 cm thick lead block as gamma shielding and optionally a neutron guide are mounted on a driven slide. The air inside the gamma shutter can be evacuated via a vacuum port. The gamma dose rate is reduced to about 40 nSv/h at the outer surface of lead block. It should be noted that the here presented gamma shutter is designed for the extraction channels described in this TDR for thermal and cold neutrons. This channel has no direct sight to the activated target, the main source of gamma radiation. If extraction channels for epithermal or fast neutrons coming directly from the target are planned, the shutter needs to be modified as no absorption due to the target station shielding is present anymore.

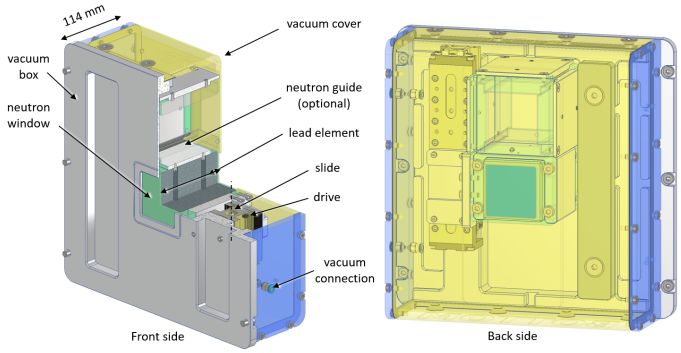

Figure II.57: Design of an evacuated gamma shutter to provide on-demand shielding for the neutron extraction channels of the target station shielding

Neutron Shutter. The function of the neutron shutter is to reliably shield the cold/thermal neutron beam at each neutron guide to enable work on the related instrument during ongoing experiments at other instruments. It consists of a vacuum housing with two neutron beam windows able to fit different neutron guide geometries. The neutron shutter requires a structural gap of 380 mm between two separated neutron guides. This gap will be closed with a 243 mm thick Borotron block facing

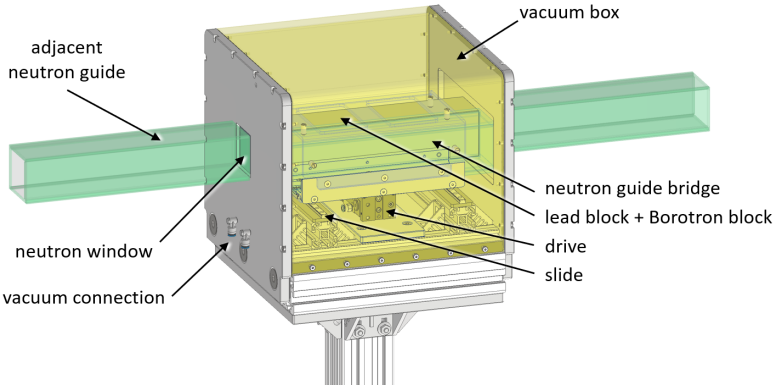

Figure II.58: Technical design of a compact neutron beam shutter realisation

the target station and a 100 mm thick block of lead downstream for neutron and gamma shielding, respectively. To minimize divergence losses, a neutron guide placed adjacent to the shielding block can be driven into the gap. The technical solution of a simple and cost-effective neutron shutter is shown in Figure II.58. As shown in Figure II.62 the beam dose rate is about 5 Sv/h which corresponds to a thermal neutron flux of 1.3 10^{8} cm^{-2} s^{-1}. The thermal neutrons are fully absorbed in the first 1 cm of the Borotron block generating a ^{10}B equivalent prompt gamma source (E_{γ} = 477 keV) of 10^{9} Bq. The resulting gamma dose rate at the output surface of the lead block is determined with the software for radiation protection SISy (version 2.6.0) using as reference radionuclide ^{198}Au which decays by emission of 411-keV gamma rays. Taking into account the difference in the absorption of 441-keV and 477-keV gamma rays in both materials for Borotron and lead, respectively, a ^{198}Au-activity of $3{\cdot}10^{9}$ Bq is used to calculate the dose rate. The gamma dose rate in the first 1 cm layer of the Borotron block is 2.1 Sv/h and reduces to 2.5 μSv/h at the outer surface of the lead block. It is worth to mention that according to [XJZ13] the 243-mm thick Borotron block will shield effectively the small fraction of fast neutrons contained in the neutron beam.

II.6.4 Target station bunker

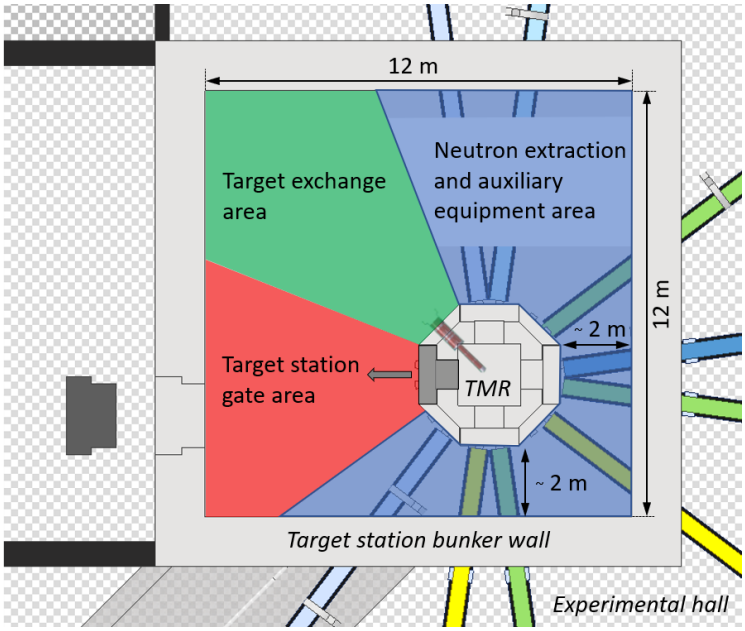

Figure II.59: *Intended areas of the target station bunker*

The target station is placed in a bunker named target station bunker. The bunker has total effective area of 12 m x 12 m, a height of 10 m and 1.4 m thick heavy concrete walls acting as biological shielding. The room is equipped with a crane with a bearing capacity of 10 t with a lifting height of 7 m which is sufficient to fully assemble and disassemble the target station. For radiation purposes, the air in the room is exchanged 8 to 12 times per hour in accordance with the requirements of the responsible licensing authority. The only entrance is the 1.8 m wide gate that connects each target station bunker with the transportation corridor.

The target station is placed inside the target station bunker in accordance with the instrument requirements maintaining a minimal distance to the wall of 2 m. The intended areas of the target

station bunker area are shown in Figure II.59. Around the target station, an angle of about 260° is reserved for neutron extraction (e.g. neutron guides, choppers) and its auxiliary equipment like the cryogenic moderator support. The gases necessary to operate the cold moderators are stored outside the target station bunker in one of the central gas storage facilities. The remaining 100° of the bunker area are occupied with the primary coolant circuit and its auxiliary equipment as well as restricted space for the target exchange process and a reserved space to open the gate of the target station for minor rebuilds. It offers additionally temporary storage space for shielding elements in case of major rebuilds. The target cooling system is divided into two circuits. The primary circuit with approx. 70 l - 120 l of water is located entirely in the target station bunker. The heat of the primary circuit is transferred to the secondary circuit via a water-water heat exchanger. The pipes of the secondary circuit lead out of the bunker and the heat is released into the environment via surface coolers outside the building. The floor of the target station is equipped with a sump that collects the water in the event of a leak in the primary circuit.

II.6.5 Target station prototyping

A prototype of the target station was built at the pre-accelerator of the COSY facility [SBD+97] as shown in Figure II.60 with slightly reduced dimensions to test all components ranging from target, moderators / reflector assemblies, shielding up to the extraction channels. It allows operation up to a power level of 10 kW at the target position but is currently just tested with a proton beam of 45 MeV and a peak current of 10 μA. First beam on target has been realised on the 12$^{\text{th}}$ of December 2022 with three experiments (diffraction, reflectometry and detector tests) performed.

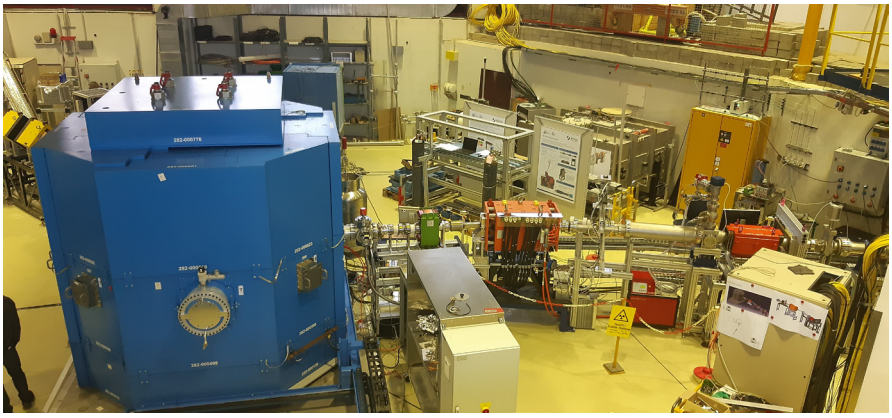

Figure II.60: *Target station prototype at the COSY facility*

The technical details of the target station prototype are shown in more detail in the Appendix A.1.

II.6.6 Shielding activation

Knowledge on the specific activity of the radionuclides formed by neutron activation of the shielding including the lead reflector is required in view of the future decommissioning of the target stations. It is calculated using the cross-section database JENDL-4.0 and the Neutron Activation Tables. The average neutron (thermal, epithermal, and fast) fluxes in the lead reflector and the various materials composing the shielding, lead, borated polyethylene and steel are determined by the Monte Carlo transport code PHITS (Version 3.24). With increasing distance from the moderator the average neutron fluxes decrease and therefore the specific activity too as shown as an example in Figure II.61. The

specific activities of the main radionuclides obtained for 1, 5, 10 and 30 years irradiation and after a decay time of 1 year from the end of the irradiation are given together with the limiting values for unrestricted release in Table II.10. In the following discussion, we consider an irradiation time of 30 years, which corresponds to a possible operation period of the HBS facility. Due to the high specific activity of ^{204}Tl ($T_{1/2}$= 3.78 y) the lead reflector will be declared as radioactive waste. An unrestricted release could be envisaged only after a waiting period of about 17 years. For the lead of the shielding about 90 % of its mass could be unrestricted released. The remaining 10 % will be declared as radioactive waste due to the high specific activity of ^{204}Tl ($T_{1/2}$= 3.78 y) and a unrestricted release only possible after a waiting period of about 8 years. About 96 % of the mass of borated polyethylene could be unrestricted released. The remaining 4 % will be declared as radioactive waste due to the high specific activity of ^{3}H ($T_{1/2}$= 12.33 y) and ^{14}C ($T_{1/2}$= 5730 y) without any possible future unrestricted release. Concerning the steel cladding about 40 % of its mass could be released. The remaining 60 % will be declared as radioactive waste due to the high specific activity of ^{55}Fe ($T_{1/2}$= 2.73 y), ^{60}Co ($T_{1/2}$= 5.27 y), ^{93m}Nb ($T_{1/2}$= 16.13 y), ^{61}Ni ($T_{1/2}$= 100.1 y) and ^{14}C ($T_{1/2}$= 5730 y) without any possible future unrestricted release.

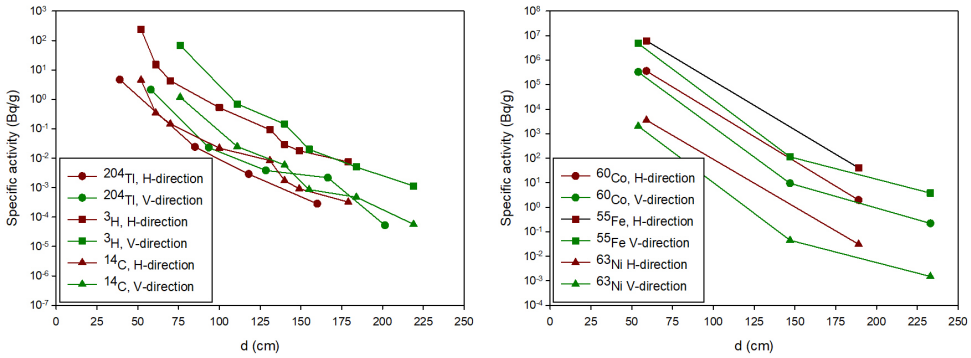

Figure II.61: *Specific activity of some relevant radionuclides for an irradiation time of 30 years and a decay time of 1 year from the end of the irradiation. H-direction: horizontal direction, V-direction: vertical direction*

II.6.7 Shielding dose rates

The goal of the shielding is to maintain the gamma and neutron dose rates as low as is reasonably achievable (ALARA principle) to avoid unnecessary radiation exposure of those working in the adjacent rooms (in the instrument halls and the technical hall) during neutron source operation. Furthermore, the shielding should allow various maintenance works in a neutron source area. The neutron source with shielding is positioned in the middle of a room with an area of 12 $\times$ 12 m^2. The distance between the outer surface of the shielding and the inner surface of the room wall is 4 m. The room wall is made of ordinary concrete wit 50 wt.% iron aggregate to moderate fast neutrons escaping from the shielding and has a thickness of 140 cm. the total (neutrons plus gamma) dose rates generated during accelerator operation with 70 MeV and an average current of 1.44 mA are determined with the transport code PHITS (version 3.24). The total dose rate map is shown in Figure II.62. The average dose rate at the outer surface of the wall is 2.2 μSv/h and at the outer surface of the root 1.9 μSv/h.

The dose rate after the shut-down of the proton beam line is calculated using the software for radiation protection SISy (version 2.6.0) based on the activity of the tantalum target and the activity

Irradiation parameters						
Isotope	Half life	1 y	5 yr	10 y	30 y	UR
Lead Reflector						
^{203}Hg	46.6 d	1.34	1.35	1.35	1.35	10
^{204}Tl	3.78 yr	3.59	12.9	18.0	21.3	1
^{202}Pb	52.5 My	5.35E-05	2.67E-04	5.35E-04	1.60E-03	0.1
^{205}Pb	15.3 My	0.15	0.76	1.52	4.59	10
Lead shielding						
^{203}Hg	46.6 d	$\leq$0.37	$\leq$0.37	$\leq$0.37	$\leq$0.37	10
^{204}Tl	3.78 yr	$\leq$0.78	$\leq$2.81	$\leq$3.93	$\leq$4.66	1
^{202}Pb	52.5 My	$\leq$1.17E-05	$\leq$5.84E-04	$\leq$1.17E-04	$\leq$3.50E-04	0.1
^{205}Pb	15.3 My	$\leq$2.93E-02	$\leq$0.15	$\leq$0.29	$\leq$0.88	10
Borated polyethylene shielding						
^{3}H	12.33 y	$\leq$16.2	$\leq$72.8	$\leq$127.8	$\leq$242.3	100
^{14}C	5730 y	$\leq$0.15	$\leq$0.75	$\leq$1.51	$\leq$4.52	1
^{10}Be	1.51 My	$\leq$2.8E-02	$\leq$0.14	$\leq$0.28	$\leq$0.85	100
Steel cladding						
^{14}C	5730 y	$\leq$1.80	$\leq$8.94	$\leq$18.0	$\leq$53.9	1
^{46}Sc	83.79 d	$\leq$0.71	$\leq$0.75	$\leq$0.75	$\leq$0.75	0.1
^{51}Cr	27.70 d	$\leq$4.97	$\leq$4.97	$\leq$4.97	$\leq$4.97	100
^{54}Mn	312.3 d	$\leq$6.89E+05	$\leq$1.22E+06	$\leq$1.24E+06	$\leq$1.24E+06	1000
^{55}Fe	2.73 y	$\leq$1.36E+06	$\leq$4.38E+06	$\leq$5.61E+06	$\leq$6.10E+06	1000
^{59}Fe	40.50 d	$\leq$1.03E+03	$\leq$1.03E+03	$\leq$1.03E+03	$\leq$1.03E+03	1
^{46}Sc	83.79 d	$\leq$0.71	$\leq$0.75	$\leq$0.75	$\leq$0.75	0.1
^{58}Co	70.86 d	$\leq$547	$\leq$563	$\leq$563	$\leq$563	1
^{60}Co	5.27 y	$\leq$4.50E+04	$\leq$1.76E+05	$\leq$2.67E+05	$\leq$3.58E+05	0.1
^{59}Ni	76 ky	$\leq$0.79	$\leq$3.96	$\leq$7.92	$\leq$23.8	100
^{63}Ni	100.1	$\leq$130.5	$\leq$643.7	$\leq$1.26E+03	$\leq$3.55E+03	100
^{93m}Nb	16.13 y	$\leq$12.8	$\leq$58.8	$\leq$106.2	$\leq$220.3	10
^{94}Nb	20.3 ky	$\leq$0.19	$\leq$0.97	$\leq$1.95	$\leq$5.83	0.1
^{93}Mo	4.0 ky	$\leq$8.36E-02	$\leq$0.48	$\leq$0.83	$\leq$2.50	10

Table II.10: *Specific activity (Bq/g) of main radionuclides produced in the reflector and shielding materials after 1 year decay from the end of the irradiation. The proton energy is 70 MeV and the average current 1.44 mA. UR is the limiting value for unrestricted release (Bq/g).*

of the outer steel cladding of the shielding. After one year irradiation and one week decay time from the end of the irradiation the dose rate at the surface of the shielding is 1.2 μSv/h (0.8 μSv/h from the target and 0.4 μSv/h from the steel cladding). Considering an operation time of 30 years the dose rate increases to 1.5 μSv/h due to a slight increase of the activity of the steel cladding.

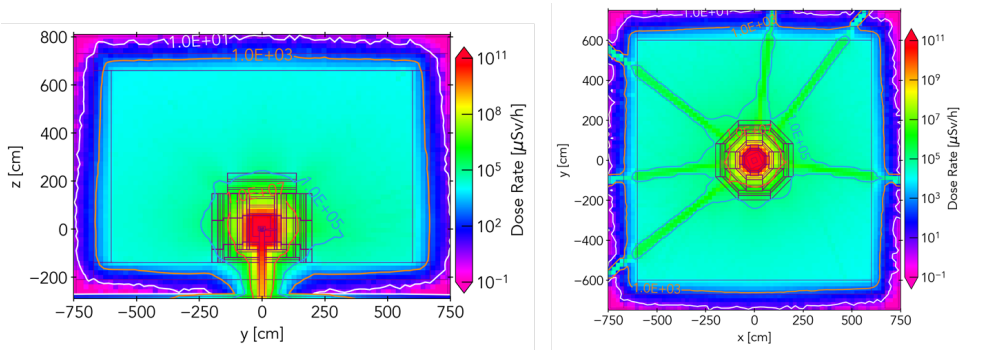

Figure II.62: Total dose rate distribution during operation of the proton beam line. Left: cut in the plane of the proton beam line. Right: cut in the plane of the neutron channels close to the target

II.7 Target station control and operation

The target stations will not have individual control systems. Instead, there will be one integrated control system for the accelerator and the target stations that has been described in the accelerator volume of the TDR. This implementation approach will reduce the development and maintenance efforts and lead to a homogeneous and ergonomic interface for operators. Target station control will be executed from the same control room as accelerator control by adding further engineering screens to the operator consoles, sharing all the common central services like alarm, archiving or logging. As a consequence, target station control follows the identical three-tier architecture as the accelerator control system and will be based on the same technologies that have been selected for the accelerator control:

- EPICS will be used as framework for the control system core, providing device abstraction and location transparency.
- Control System Studio (CSS) will be used as framework for the HMI software. BEAUTY will be used as common archiving system and BEAST will be used as common alarm system for both target and accelerator control. Also, logging system and electronic logbook will be shared by target and accelerator control.
- Timing clients in target stations will use MRF timing receivers connected to the accelerator timing system.
- The implementation of the front-ends of most subsystems like vacuum systems, cooling systems, cold moderators or the personnel protection system (PPS) will be based on Siemens PLC technology, using the most recent product families like Siemens S7-1500 PLCs and ET200SP, ET200MP, ET200eco and ET200pro decentral periphery systems as well as Profinet, Profibus and IO-link for the communication with these devices.
- The target station will share a common machine protection system (MPS) with the accelerator that is based on FPGA technology. Due to the independent operation of the target stations in in the states FAULT, IDLE, MAINTENANCE and BEAM-ON, shutdown interlocks in the MPS as well as the HBS components affected by a shutdown must be dynamically changed according to the state of the targets.

- The target stations will share a common PPS with the accelerator that is based on Siemens PLC technology.

In addition to the common subsystems that are shared between target station and accelerator control, the target station control systems add the following subsystems to the overall HBS control systems with subsystem-specific automation (e.g. based on scripts) in each subsystem domain at the middle tier of the control system:

Target cooling: A water cooling system is foreseen for each target, including redundant pumps, a heat ex-changer and water quality monitoring. All automatic procedures, including operation of pumps and valves, as well as all monitoring of physical values (e.g. pressures and flows) will be implemented with Siemens PLC technology.

Target vacuum: Each target vacuum vessel will be separated with a vacuum window from the accelerator beam tube and a vacuum system will be implemented to provide the required vacuum. Control and monitoring of the vacuum equipment like pumps, valves, or pressure gauges will be implemented with Siemens PLC technology. The target vacuum systems interact with the accelerator machine protection system in order to shut down the accelerator when the pressure exceeds a threshold.

Target diagnostics: To guarantee a stable operation of the target, several parameters (e.g. target surface temperature distribution) have to be monitored. The required front-end electronics depend on the selected parameter types and have not yet been decided. A coupling of the target diagnostics with the machine protection system is foreseen.

Target handling: The target is mounted on a target plug in a beam port of the target shielding, which has to be extracted for the target exchange. For the target extraction a complex mechanical system based on several servo motors is foreseen. Control of the extraction and insertion procedure will be based on a Simatic PLC technology in combination with Sinamics servo drives.

Target area access mechanism: A mechanism for the automatic, motor-driven opening of the target shielding will be implemented. This will require a complex safety system coupled with the PPS, not only because of radiation safety but also to avoid human injuries by crushing or damages by collision with equipment left in the target area.

Cryogenic moderators: There will be several different cryogenic moderators for the three target stations. From the controls point of view, the main subsystems of the cryogenic moderator are a cryostat, a vacuum system and a gas management system. Equipment to be controlled includes temperature controllers, flow controllers, valves, pumps and pressure gauges.

Compared to the tight coupling between accelerator and target station control, the neutron instruments control systems are only loosely coupled with the target control:

- For the synchronization of detectors and choppers, the timing system has to provide the trigger information corresponding to the pulse-on-target event to the instruments. It is intended that there will be a timing client equipped with an MRF timing receiver in each instrument.
- The beam current and potentially other diagnostic information of the target must be made available to the instruments. The time resolution can be lower than the detector resolution and should be in the order of milliseconds.
- The personal protection system of each target station has to provide safe signals to the related instruments indicating beam at the target station to prohibit opening of the beam shutters when humans are present in the instrument area. In the other direction, these instruments have to provide safe signals which permit switching on the beam to the corresponding target station. The implementation of these signals can be based on potential-free electrical contacts or on PROFIsafe communication links.

- It is intended to use vacuum windows to decouple the vacuum systems of the target stations from the instrument vacuum systems.

A prototype of an HBS target station has been implemented for the HBS demonstrator at the JULIC accelerator of the Institute for Nuclear Physics, Forschungszentrum Jülich. The following sections discuss the subsystems cold moderators, target cooling, vacuum, handling and area access in more detail. The corresponding implementation for the target station demonstrator at the JULIC neutron platform will be presented as a possible implementation option for the final HBS target stations. The control system implementation at the target station demonstrator illustrates how technology and approach for the control system hardware and software of the final HBS target stations could look like.

II.7.1 Target area access mechanism

For service reasons, the target area inside the target shielding should be accessible, which will be achieved by a fully automatic, motor-driven mechanism. Special attention has to be paid to the personnel protection system, which has to protect humans against radiation and injuries by crushing. Collisions with equipment left in the target area have to be avoided, too. An extensive risk and hazard analysis will lead to the definition of the PPS safety functions, from which the technical design will be derived. Required safety devices will include light curtains, limit switches, pressure switches and emergency stop buttons.

As an option for the final solution in the HBS target stations, the shielding of the prototype target station at the JULIC neutron platform is equipped with a gate that can be moved on air cushion feet by a high force electric cylinder. Control of this movement will be done by a fail-safe Simatic S7-1500 PLC in combination with a servo drive, which demonstrates how the implementation of the control electronics and the safety system for a final HBS target station may look like.

Figure II.63: *Main PLC cabinet, satellite servo drive cabinet and electric cylinder with servo motor.*

Fig. II.63 shows the selected electric cylinder together with the main PLC cabinet and a satellite cabinet with the frequency converter on photos taken in the electronics lab during pre-commissioning. Most of the safety equipment, which is distributed over the target station area, is directly connected to local ET 200eco digital or analog IO modules in protection class IP67. The ET200eco modules are connected to the main PLC via PROFINET, leading to a major cabling reduction. The same main PLC

will be used also for other target station subsystems like target cooling, vacuum, diagnostics and handling.

Figure II.64: *Safety sensors at the shielding gate.*

As shown in Fig. II.64, light curtains will protect the area in front of the movable shielding door. The safety is further increased by tactile safety edge sensors mounted at the door. Several emergency stop buttons, a light signal and an acoustic signal are foreseen, too.

II.7.2 Target handling system

As described in section II.3, a prototype for a target handling tool has been implemented that can extract or insert the target plug with the attached target at the target stations. The extraction process relies on six servo motors operating linear actuators for the main extraction axis, auxiliary support axes for the target plug and additional axes moving shielding segments in proper positions to completely shield the target. The extraction and insertion processes of the target are fully automatic with all axes moving in a coordinated way guaranteeing that the target plug is always properly supported and the target is always properly shielded. Due to the obvious personal safety issues, an extensive risk and hazard analysis has been executed and a personnel protection system has been designed that will be implemented on the fail-safe Siemens S7-1500 PLC in the main cabinet shown in Fig. II.63. Fig. II.65 shows one of the additional control racks with an ET200SP decentral periphery system.

II.7.3 Target cooling system

At the target station prototype of the JULIC neutron platform a simplified prototype for the final HBS target station cooling system has been implemented, whose structure is shown in Fig. II.66

Central components are a reservoir tank, a heat ex-changer and a pump, with a variety of valves, pressure and temperature sensors. The water quality is observed with additional sensors for parameters like conductivity or pH value. The cooling system setup has been integrated with the electronics into one single movable system, as shown in Fig. II.67. The electronics consists mainly of a decentral ET200MP system with digital and analog IOs that are connected to the sensors and actuators of the vacuum system. The ET200MP system is connected via PROFINET to the Siemens S7-1500 PLC in the main PLC rack. The S7-1500 is responsible for the fully automatic operation of the cooling system,

Figure II.65: One of the decentral control racks for the target handling tool.

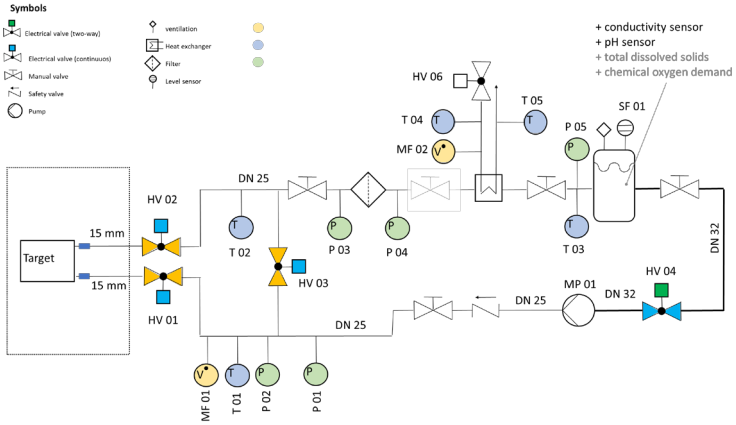

Figure II.66: Structure of the cooling system of the target at the JULIC neutron platform.

including startup and shutdown procedures. An interface to the MPS is implemented that enables an accelerator shutdown, when the target cooling fails.

The cooling systems for the final HBS target stations will be slightly more complex, e.g. by adding a second redundant pump.

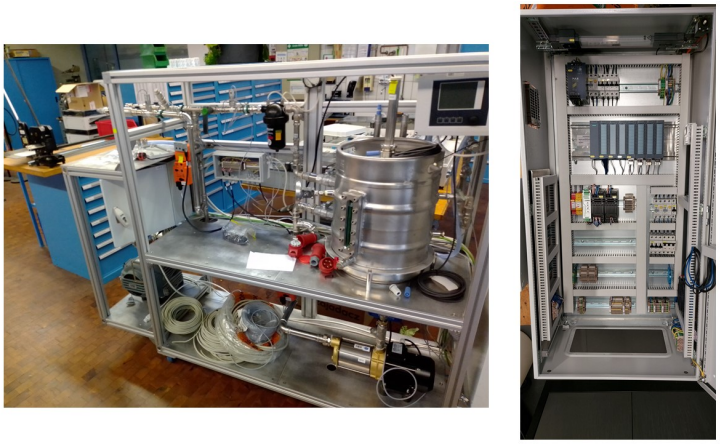

Figure II.67: Cooling system with integrated electronics.

II.7.4 Target vacuum system

For the target vacuum vessel at the target station prototype of the JULIC neutron platform, a differential pumping system consisting of a scroll pump and a turbo-molecular pump has been implemented, including several pressure gauges and valves. The vacuum equipment is controlled by the Siemens S7-1500 PLC in the main PLC cabinet that is responsible for automatic startup and shutdown procedures as well as for the readout of relevant state information like pressure values.

Due to the moderate complexity of the prototype vacuum system, some of the vacuum components and most of the vacuum electronics have been physically integrated into the cooling systems setup shown in Fig. II.67.

Pressure readings are available also to the accelerator vacuum system, enabling interlocks of the MPS when the vacuum quality deteriorates. The final HBS target station vacuum system will have a similar architecture, most likely with a higher number and different type of vacuum components. In the final vacuum system fast closing shutters will protect the beam-line vacuum from any air inrush, e.g. due to vacuum window defects.

II.7.5 Cryogenic moderators

As a typical example for cryogenic moderator control, the control sub-system of the solid methane moderator (refer to section II.5) has been implemented with Siemens PLC technology. Due to delivery problems of PLC components, this control sub-system is still an intermediate prototype system. As shown in Fig. II.68, sensors and actuators like mass flow controllers, valves or pressure gauges are directly attached to PROFIBUS and PROFINET networks or connected to ET200pro decentral periphery modules in protection class IP67 without cabinet. The overall control is executed by a Siemens S7-1500 PLC, which is responsible for automatic operation, state changes like startup and shutdown as well as machine safety related interlocks. As soon as the component delivery problems are solved, a cabinet for the PLC system will be integrated into the gas management panel and a valve manifold with Profinet interface will replace the individual valves, leading to a major cabling reduction.

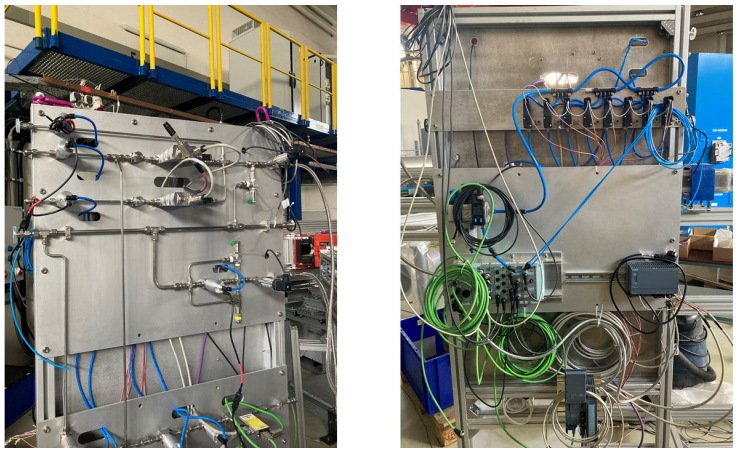

Figure II.68: Front and backside of the solid methane moderator gas management panel.

II.7.6 Target station integration into the MPS

The independent operation of the target station in the states IDLE, MAINTENANCE, BEAM-ON or FAULT requires a flexible reaction of the MPS when a target station does a state change. If a target station goes to one of the states IDLE, MAINTENANCE or FAULT, the beam into that station has to be blocked and the pulse structure has to be changed accordingly. To avoid unnecessary shutdowns, the accelerator has to continue its operation and the beam has to be delivered to the other target stations. In order to achieve this, the MPS interlocks have to be dynamically adapted to this situation by masking the corresponding MIDs (MPS Input Devices) and potentially also some MODs (MPS Output Devices). The MPS protection system will be connected to the cooling, vacuum and diagnostic systems of the target stations, enabling an accelerator shutdown in the case of a severe fault detected by one of these subsystems.

II.8 Commissioning and decommissioning of TMR and targets

Following procedures established at accelerator-based large scale facilities, the commissioning of the facility will be a stepwise effort following the timeline of the construction of the different compartments. After the construction of the accelerator, the commissioning of the ion source, LEBT, RFQ, MEBT and DTLs will be established step by step. By this stepwise procedure the full commissioning of the accelerator up to its final energy and the full proton beam transport system to all three target stations will take about 3.5 years. Each target station will be commissioned within three months after construction. The instruments will be commissioned step by step following the construction of the individual instruments. This may take up to one year for all instruments at an individual target station.

The HBS facility is designed and constructed to minimize the amount of radioactive and hazardous materials and to facilitate the management of activated materials used by using modular shielding and technical components (see section II.6.6). An initial decommissioning plan including risk analysis, will be developed to demonstrate the feasibility of decommissioning and to define the strategy decommissioning strategy and to estimate costs. The amounts of radioactive waste and classifications will be derived using: i) precise calculations performed by means MCNPX2.6.0 computer codes

ii) scaling the activity from the operation experience of existing accelerator based neutron source installations. Additional information to improve and update the initial decommissioning plan will be gained continuously during the commissioning and operation of the facility.

With respect to the TMR unit, target components and the target bunker the main radiological challenge will be the dismantling of the TMR shielding blocks being irradiated within the total operational time of the facility. The procedure for dismantling and storage of these elements will be developed carefully along the requirements of radiation safety and storage of activated materials. The dismantling of the concrete walls, ceiling and ground floor of the target bunker will also require a stepwise approach and separating contaminated wall surfaces from the remaining low or not activated parts of the construction. The dismantling of used targets, transport and storage is a continuous process during operation and has been described in Section II.6.

III.
NUCLEONICS

The design of a HiCANS like HBS allows to develop and operate different target stations with dedicated TMR assemblies specialized for different applications. The nucleonic performance can be tailored to the needs of the individual instrument by a dedicated moderator insert. The variability of configurations of the target stations and their performance is thus large.

Various configurations have been investigated. In the conceptual design report published [BBD$^+$20] a single extraction channel inside the TMR assembly was investigated showing the highest achievable brightness. In this TDR we now present two different configurations which have slightly different neutronic and functional features. One is aiming to maximize the brightness for up to 6 instruments using cold and thermal instruments [1]. A second configuration increases the number of extraction channels with a similar performance for all instruments on the cost of a reduced brightness for all instruments. The optimization of the TMR assembly presented here follows this guiding principle.

The geometry presented in sections II.4 & II.5 has been simulated with MCNP6.1 with the evaluated data library ENDF/B-VII.1. The neutrons are recorded at the respective moderator surfaces with their energy, time after the proton pulse, and their momentum.

III.1 Neutron yield

The neutron yield depends on the target material, the primary particle type and its energy. A detailed comparison of the neutron yield for different materials can be found in [ZDB$^+$20]. Tantalum was chosen as a target material because it releases many neutrons at a proton beam energy of 70 MeV with the benefits of a high blistering threshold as described in the HBS conceptual design report [BBD$^+$20] and in Section 1.1.1 of this volume. The total neutron yield for a power of 100 kW is $\sim 10^{15}\mathrm{s}^{-1}$ as calculated with MCNP6.1 and the ENDF/B-VII database. As such, the primary source strength (time-averaged) is two to three decades below the source strength of research reactors. Also the energy spectrum is softer in comparison to fission or spallation neutron sources with a peak neutron energy of around 0.5 MeV. Both effects make it easier to meet the radiation protection requirements and to lower instrumental background and hence to optimize the instrumentation for signal-to-noise ratio. Furthermore, it allows to place optical components like neutron guides and chopper systems close to the moderator surface and thus realize an efficient neutron extraction. This results in competitive neutron fluxes at the sample position as described in the TDR volume 4 "Instrumentation".

The primary neutron spectrum is shown in Figure III.1 for a bare tantalum target at HBS parameters. It has a peak at ~ 0.8 MeV and is thus much softer than the neutron spectrum emitted by other

[1] The Volume "Instrumentation" uses the calculations featuring this model with 6 extraction channels.

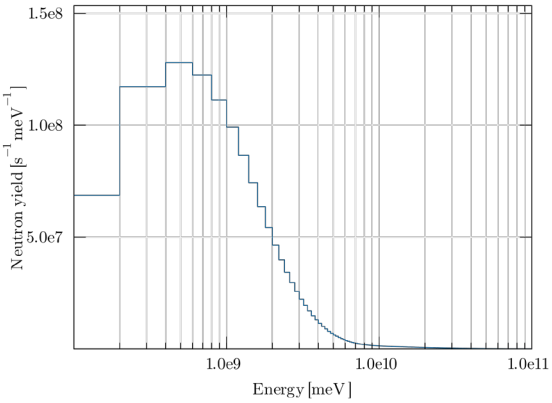

Figure III.1: *Primary neutron spectrum for a bare tantalum target at HBS parameters.*

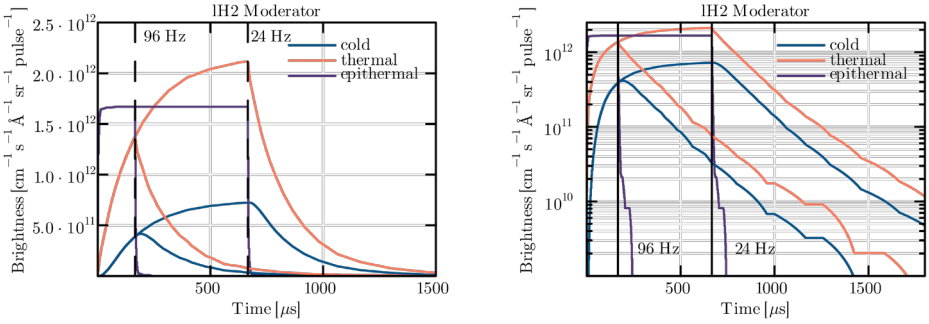

Figure III.2: *Neutron time structure at the exit of the lH_2 moderator in the top extraction plane.*

well-known target materials for low energy accelerator-driven neutron sources like beryllium.

III.2 Neutron time structure

The time structure of the neutron pulse depends on the proton pulse length, the TMR geometry, the moderation properties of the materials inside the TMR assembly as well as their absorption properties. A detailed description is presented in [ZLB+21].

In Figure III.2 the time structures for three different neutron populations (epithermal, thermal and cold) of the liquid para-hydrogen moderator in the top layer are shown which are relevant for neutron scattering and analytical experiments. The vertical dotted lines marked with 24 Hz and 96 Hz indicate the two proton pulse lengths considered. The epithermal neutrons with wavelengths between 0.2 and 0.4 Å follow the proton pulse structure with a similar peak brightness for 24 Hz and 96 Hz. This energy range is populated only during the moderation process. As the neutrons reach thermal equilibrium in less than 10 μs, much shorter than the proton pulse, the time structure is defined by the proton pulse length and the brightness depends on the proton peak current.

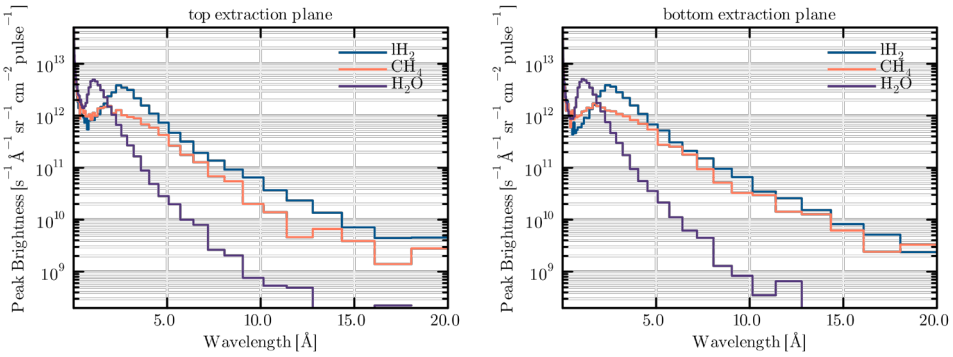

Figure III.3: *Neutron energy spectrum for the top extraction layer (left) and the bottom extraction layer (right) for all moderator types for the 24 Hz target station.*

The slow neutron populations build up according to the neutron life-time within the extraction volume of the moderator. Hence they depend on the moderator geometry and the absorption cross sections. The thermal ($\lambda = 0.4 - 3$Å) and cold ($\lambda = 3 - 9$Å) neutron populations have similar shapes as water with an absorption time of 190 μs has the strongest effect. Matching the proton pulse length to the life-time optimizes the peak-to-width ratio like for the 96 Hz target station with a proton pulse length of 166 μs. For many applications it provides the required resolution and a high sample flux as the full pulse can be used. The longer proton pulse provides a higher peak brightness but less pulses per second like for the 24 Hz target station with a proton pulse length of 667 μs. This pulse structure serves therefore perfectly broad band applications like SANS. It should be noted that the time averaged brightness is independent of the pulse time structure. The instruments can therefore chose what pulse structure is the most suited.

The other moderator materials show similar neutron time structures but with different peak intensities. In Appendix A.5 the time spectra for the water moderator as well as the methane moderator are presented.

III.3 Neutron spectra

The neutron energy spectra for the different moderators used in the TMR assembly for up to 12 extraction channels are shown in Fig. III.3 for the 24 Hz target station. The 96 Hz target station shows similar spectra but with reduced peak brightness as indicated in Fig. III.2.

The moderators can be distinguished by their purpose to moderate the neutrons to the required energies as described in sections II.4.2 and II.5.1. The water moderator has the peak brightness at 1Å with a fast decaying tail for larger wavelengths. The liquid para-hydrogen moderator has a cold spectrum with its maximum at 2.5 Å. The methane moderator, a very good cold moderator, requires small moderation volumes to produce cold energy spectra due to the higher density in comparison to hydrogen and due to the higher cross section compared to para-hydrogen. In a spallation neutron source this can be used in a flat rectangular geometry to extract very cold neutrons from the large surface while still maintaining a moderate absorption due to a small width. Such a moderator geometry is not suitable for the TMR geometry presented here, thus a small moderator volume in all dimensions was used. This allows the extraction of a bi-spectral energy spectrum as neutrons can be extracted from the methane moderator volume and the surrounding water volume simultaneously. This creates a broad energy spectrum with a peak at ~1.8 Åwhich is higher in energy than such a moderator at other sources.

It was chosen to leave an empty volume in the center of the first extraction layer to allow a better neutron feeding into the second extraction plane. This results in a reduced brightness in the first layer and an enhancement in the second layer. This can especially be seen in the spectrum emitted from the methane moderator due to the imperfect feeding into the moderation volume.

Instruments as described in the TDR Instrumentation can choose a moderator and further optimize it to their needs.

III.4 Neutron source comparison

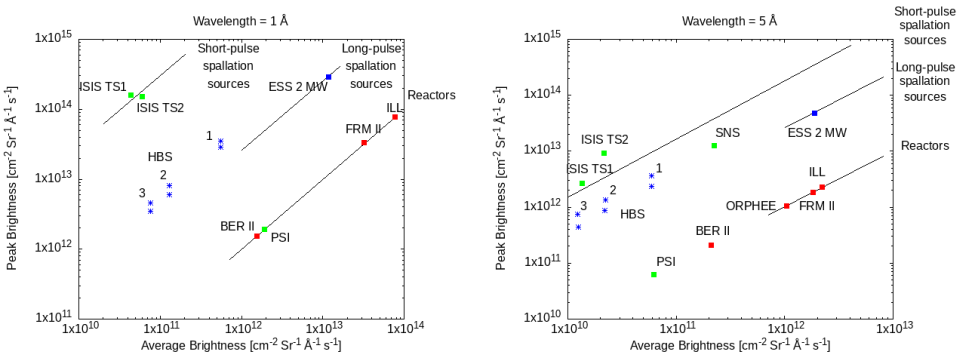

Figure III.4: *Comparison of different national and international neutron sources for neutron experiments for 1 Å and 5 Å neutrons. Reactor neutron sources are plotted in red, long-pulse spallation sources in blue and short pulse spallation sources in green. The stars indicate the HBS performance parameters for different configurations studied. 1: Optimized and ideal 1 channel geometry [BBD^{+}20]; 2: 1 extraction layer geometry as presented in the TDR Instrumentation; 3: 2 extraction layer geometry as presented here. Image is adapted from [Lan] with brightness values calculated using McStas with the corresponding source component [McS].*

The performance of an HBS source depends strongly on the exact realization of the TMR station and the chosen proton pulse structure as the peak brightness and the time-averaged brightness change. The performance will be different for a epithermal, thermal or cold neutron producing target station. As the facility is developed mostly for neutron scattering and analytical experiments in the thermal and cold energy range, we will compare HBS with other national neutron sources for a wavelength of 1 Å and 5 Å for thermal and cold neutrons, respectively. In Figure III.4 the peak versus the time-averaged brightness is shown for a selection of important neutron sources.

Reactor based neutron sources and continuously operating spallation sources like PSI have the peak brightness equal to the time-averaged brightness indicated by the drawn line. All pulsed spallation neutron sources are above this line regarding the ratio between peak brightness and time-averaged brightness. For pulsed spallation neutron sources, two different types can be distinguished namely a short-pulse spallation source and a long-pulse spallation source. A short-pulsed spallation realised by a compressor ring has a very high peak brightness whereas long-pulsed spallation sources have a higher time-averaged brightness. HBS has a pulse structure which is between both spallation source types and thus lies in-between regarding the ratio between peak brightness to time-averaged brightness.

Other sources like e.g. LENS, RANS I, RANS II are not included in this comparison as the source characteristic has not been available. Due to the low power of such Compact Accelerator-driven

Neutron Sources (CANS), their performance is on the lower end if brightness is used as criterion. International neutron sources like J-PARC, ESS and SNS have a better performance than HBS regarding peak brightness and time-averaged brightness. This is expected as HBS is planned as an affordable national neutron source.

When comparing neutron sources, it has to be kept in mind that the brightness values shown for the HBS and the ESS are based on simulations only, while the other facilities exist (or have existed). But it must also be emphasized that the technical design of the HBS is for a first of its kind HiCANS, while research reactors and spallation sources have a history of more than 60 and 40 years of development and optimization, respectively. This becomes evident from Figure III.4. The figure clearly shows that, depending on the optimization criteria, a HiCANS can have very different performance levels in terms of beam brightness. The reason for this is the compactness of the target, which results in a more localized thermal neutron cloud. The HBS TMR described in this TDR volume is designed to supply a large number (12) of instruments with thermal and cold neutrons. Other design criteria result in much higher peak and average brightness values. Also, the design of the target itself for a power denisty of 1 kW/cm^2 seems rather conservative in view of the successful experimental tests performed. Thus, it can be safely assumed that HiCANS have a huge potential for further improvement in the future. To give some examples of possible design choices:

1. High brightness option: An HBS TMR station, including the necessary beam multiplexer, has an investment cost comparable to a neutron instrument. Thus, one could decide to increase the number of TMR stations, while each TMR station deserves only a few instruments. Such a choice significantly increases both the average and the peak brightness of the beams.

2. High source strength option: The current HBS design uses only a fraction of the duty cycle of the accelerator. Up to 14 mA average current is still available for other uses. This exceptional power (14 mA proton current at 70 MeV) could be used for a dedicated high source strength target station if the target area is increased accordingly. This additional station could be used for radionuclide production, for example, and could run in parallel without interfering with the other uses described in this TDR.

Finally, depending on the desired instruments, brightness is not the only criterion. Advantages of HiCANS for neutron beam instrumentation are e.g. (i) that the compactness of the TMR unit allows to extract a large phase space volume for instruments that can digest it; (ii) that HBS can provide a

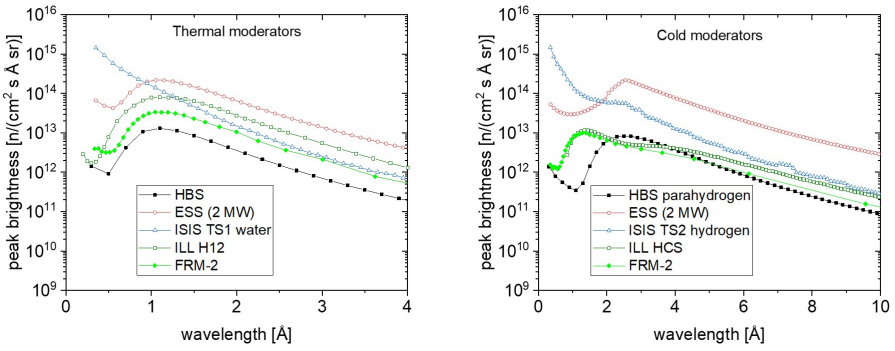

Figure III.5: *Simulated brightness as a function of wavelength of the 24 Hz HBS target station for the thermal (left) and a cold moderator (right) arranged in the triangular moderator geometry in comparison with simulated brightness values of neutron facilities that exist or are under construction.*

wide range of neutron spectra from cold via thermal to epithermal; and (iii) that the pulse structure for each TMR unit can be freely chosen within a wide range of frequencies and pulse widths.

In summary, the HBS has a higher peak brightness compared to continuous national neutron sources like BER II, ORPHEE and PSI and a comparable time average brightness compared to national spallation neutron sources, which are mostly of the short pulse type. It is therefore a link between the two types. The great strength of the HBS is its enormous flexibility. It offers the possibility to easily tune the source parameters by using different target stations. Considering the fact that the HBS is the first HiCANS of its kind, it is safe to assume that these types of sources offer a huge potential for further improvements.

IV.
INFRASTRUCTURE AND BUILDINGS

IV.1 General layout

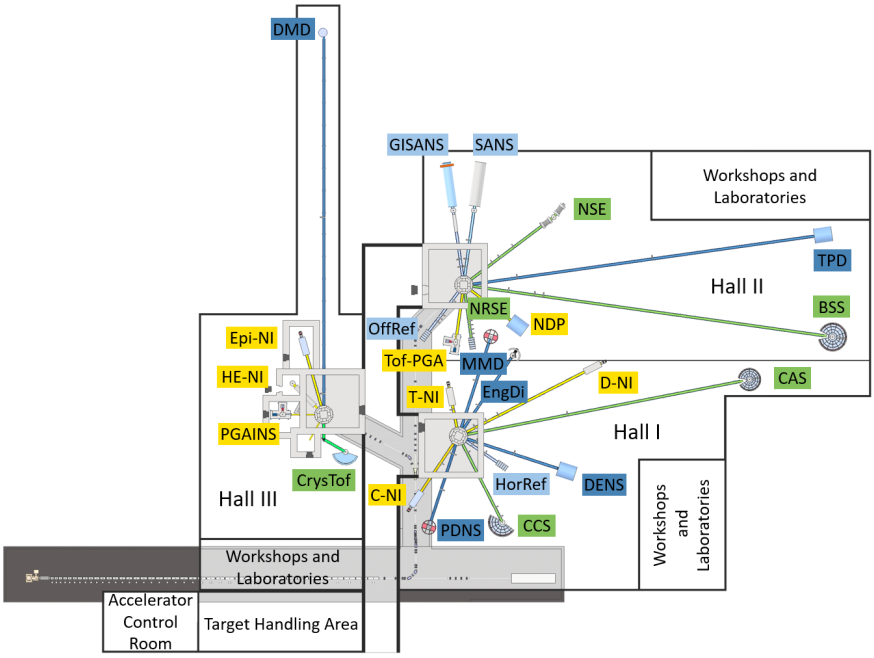

Figure IV.1: *General layout HBS. The following instruments are indicated: SANS, SANS with GISANS option (GISANS), Offspecular Reflectometer (OffRef), NSE, NSRE, Backscattering Spectrometer (BSS), Tof-PGNAA (T-PGA), Neutron Depth Profiling (NDP), Horizontal Reflectometer (HorRef), Engineerting Diffractometer (EngDi), Diffuse Elastic Neutron Scattering (DENS), Polarized Diffuse Neutron Scattering (PDNS), Single Crystall Diffractometer (MMD), Cold Chopper Spectrometer (CCS), Indirect Geometry Spectrometer (CAS), Cold Neutron Imaging (C-NI), Thermal Neutron Imaging (T-NI), Diffractive Neutron Imaging (D-NI), Disordered Material Diffractometer (DMD), PGAINS, Epithermal Neutron Imaging (Epi-NI), High Energy Neutron Imaging (HE-NI), CRYSTOF.*

In its final configuration the HBS will have three target stations which are placed at the individual instrument halls. These target station contain the target-moderator-reflector unit (TMR) and are radiation-controlled areas.

The HBS will operate these target stations in parallel using a dedicated proton beam pulsing and distribution scheme. Based on a proton beam multiplexer, described in TDR Accelerator, the high energy beam transfer (HEBT) structure will guide the pulsed proton beams with the required frequency to the individual target station. The proton beam impinges on the target from the bottom. The TMR unit and the target station bunker are positioned in the experimental hall to allow sufficient space to accommodate the various instruments placed around (see Fig. IV.1).

At each target station infrastructure and equipment for an independent individual target operation is implemented. Central supply units e.g. for liq. helium or secondary water cooling systems are arranged outside of the target station bunkers (detailed description in Chapter II.6.4). Support lines for cryogenic gases in particular liq. helium is installed connected with the central liq. helium supply outside of the target bunker. Remote gas management control systems are added to the corresponding cold moderator systems around the TMR. Pulse shaping choppers are installed along the neutron beam guides at the instruments, which need such choppers to be positioned close to the neutron source within the target station bunker. Primary water cooling and support is paced within the target station bunker and connected to secondary water cooling systems outside of the bunker to separate potentially activated cooling cycles. IT connections and components for operation and control are if possible outside of the bunker as well as any electricity support. Only indispensable components for control and support are installed within the target station bunker.

Each target station bunker is located in one experimental hall. One wall of each target station bunker is equipped with a radiation-protection gates which connects each bunker to the adjacent handling zone. The handling zone is the transport corridor which connects each target station bunker with the target handling area and a truck bay. The transport of all equipment and components for the target station bunker as well as the removal of activated targets is carried out through the handling zone. The proton beam passes from the basement through the floor slab of the bunker towards the target station. Ventilation and media are supplied via supply shafts in the level above the bunkers.

IV.2 Buildings and construction

The main building and construction part considering the target stations is located within the experimental halls. There the area of the target stations covers an outer size of 12 x 12 m^2 and a height of 10 m including a 1.4 m shielding (wall thickness). It will have a soil bearing capacity of 5 t/m^2 and will be equipped with a crane. This construction is also termed as target bunker.

Target-moderator-reflector unit (TMR). The TMR as described in Chapter II does have a diameter of max. 4 m and a height of about 4 m. The technical details of the TMR unit, its detailed construction and composition were described above. The TMR station resembles an octagon. The 8-cornered monolith will have 12 extraction channels. It will have a total weight of about 90 tons. The shielding blocks within the TMR have a similar size and a maximum weight less than 5 t to be handled with the installed crane in the target bunker. A movable gate within the TMR unit allows to open the system for repair or maintenance of the target and moderator systems. The proton beam and vacuum tube reaches the TMR unit from below. The TMR units are placed acentric inside the bunker depending on instrument requirements. The operation of each TMR unit requires a closed cooling circuit with 120 kW cooling capacity. The ground will be equipped with a collection tray to catch possible coolant leakage.

Target bunker. The TMR unit is surrounded by 1.4 m thick concrete walls and ceiling for radiation protection reasons as described in Section II.5.3. Elements belonging to the instruments like neutron guides are placed along the extraction ducts penetrating the outer target bunker wall going into the instrument halls. Support infrastructure to operate the TMR units, installed instrument equipment as choppers and cryogenic moderator systems are installed close in the vicinity of the target bunker to minimize connection distance and piping.

All three target bunkers will be connected at the ground floor for maintenance access and transport of used targets to the central target storage and handling area. A gate with a size of 3.5 m width and 3.5 m height connects the target bunkers with the transport area. The gate is of the same material as the walls of the target area. The target area will be equipped with a separate ventilation and air conditioning system following the requirements for a radiation controlled area.

Target transport and handling areas. A connection hall for handling of the activated target is placed between the three target bunkers. The regular exchange of targets at each TMR unit will happen at least once per year. This connection hall is treated as a radiation-controlled environment during the changing of the targets (e.g. with interlocks to prevent people from accessing it). The targets are removed with the target handling tool and moved together with the shielding plug to the storage area where it will be stored for a period of 5 years. The target handling tools will be stored in the target handling area.

For the safe handling and storage of the activated targets two hot cell systems are required for redundancy. The hot cells will be installed as part of the target storage area directly connected with the target transportation zone connecting the individual target zones and separated from the experimental halls and the accelerator systems.

IV.3 Costing and Timeline

The basic costs for installation of a TMR unit is given in Table IV.1. The construction costs for the target bunker, support systems, ventilation and auxiliary equipment are given in the HBS TDR Infrastructiure and Sustainability as this is part of the building construction.

The manufacturing and construction of the full TMR unit can be done within one year after contracting based on the developed and realized design as shown in the Appendix. The construction of the TMR bunker and corresponding buildings for transport and storage of targets have to be done upfront.

Component	Investment [kEUR]
Shielding	1400
Target system	700
Target handling system	700
Support systems	200
Total	3000

Table IV.1: *Investment costs of the TMR unit in 2021 costs.*

V.
AUTHOR LIST AND ACKNOWLEDGEMENTS

V.1 Volume author list

J. Baggemann, Q. Ding, M. El Barbari, H. Kleines, J. Li, K. Lieutenant, E. Mauerhofer, I. Pechenitzky, U. Rücker, A. Schwab, J. Voigt, P. Zakalek
Forschungszentrum Jülich GmbH, Jülich Centre for Neutron Science, JCNS, Jülich, Germany

E. Vezhlev
Forschungszentrum Jülich GmbH, Jülich Centre for Neutron Science at Heinz Maier-Leibnitz Zentrum MLZ, Garching, Germany

R. Achten, Y. Beßler, R. Hanslik, F. Löchte, J.Wolters
Forschungszentrum Jülich GmbH, Central Institute of Engineering, Electronics and Analytics, ZEA-1, Jülich, Germany

S. Eisenhut
Technische Universität Dresden, Bitzer-Chair of Refrigeration, Cryogenics and Compressor Technology, Dresden, Germany

V.2 Acknowledgments

This Technical Design Report has been compiled with the kind support of a large number of colleagues at the Jülich Centre for Neutron Science and other collaborating institutes and universities. The editors would like to thank in particular:

J. Baggemann, Th. Brückel, J. Chen, T. Claudio Weber, T. Cronert (†), Q. Ding, P.-E. Doege, M. El Barbari, T. Gutberlet, J. Li, Z. Ma, E. Mauerhofer, N. Ophoven, I. Pechenitzky, T. Randriamalala, U. Rücker, N. Schmidt, A. Schwab, E. Vezhlev, P. Zakalek
Forschungszentrum Jülich GmbH, Jülich Centre for Neutron Science, JCNS-HBS, Jülich, Germany

F. Beule, P. Kämmerling, H. Kleines, K. Lieutenant, F. Suxdorf, J. Voigt
Forschungszentrum Jülich GmbH, Jülich Centre for Neutron Science, JCNS-IT, Jülich, Germany

B. Daegener, F. Gossen
Forschungszentrum Jülich GmbH, Jülich Centre for Neutron Science, JCNS-2, Jülich, Germany

N. Bernard, H. Feilbach, J. Lipperts, J. Peetz, S. Pistel, J. Schnitzler
Forschungszentrum Jülich GmbH, Jülich Centre for Neutron Science, PGI/JCNS-TA, Jülich, Germany

R. Achten, Y. Bessler, R. Hanslik, F. Löchte, M. Strothmann, J. Wolters
Forschungszentrum Jülich GmbH, Central Institute of Engineering, Electronics and Analytics, ZEA-1,

Jülich, Germany

O. Felden, R. Gebel, A. Lehrach, M. Marzen, M. Rimmler, R. Similon
Forschungszentrum Jülich GmbH, Nuclear Physics Institute, IKP-4, Jülich, Germany

B. Neumaier
Forschungszentrum Jülich GmbH, Institute of Neurosciences and Medicine, INM-5, Jülich, Germany

O. Meusel, H. Podlech
Goethe University Frankfurt, Institute for Applied Physics, Frankfurt, Germany

W. Barth
GSI Helmholtzzentrum für Schwerionenforschung, Darmstadt, Germany / Helmholtz Institute Mainz, Mainz, Germany

J. Fenske, M. Müller, A. Schreyer
Helmholtz-Zentrum Geesthacht, Geesthacht, Germany

S. Böhm, J.-P. Dabruck, R. Nabbi
RWTH Aachen University, Nuclear Engineering and Technology Transfer, Aachen, Germany

S. Eisenhut, Ch. Haberstroh
Technische Universität Dresden, Bitzer-Chair of Refrigeration, Cryogenics and Compressor Technology, Dresden, Germany

C. Lange
Technische Universität Dresden, Institute of Power Engineering - Chair of Hydrogen and Nuclear Energy, Dresden, Germany

A.
APPENDICES

A.1 Shielding for the HBS-type target station of the JULIC Neutron Platform

The JCNS HBS Group developed a concept for the prototype of the target station (HBS JULIC Neutron Platform). This assembly allows scientists to perform tests for target handling development, target cooling systems, and biological shielding. This target-moderator-reflector (TMR) station unit was successfully assembled in the Big Karl experimental area of the Institute of nuclear physics (IKP) of the Forschungszentrum Jülich. (Figure A.1). In partnership with JCNS a special target station was developed by the Engineering and Technology institute (ZEA-1) of Forschungszentrum Jülich. This target station with its shielding meets the requirements for the HBS system but for a reduced power level to 10% (10 kW). In contrast to the HBS target station, the proton beam enters from the side and not from below.

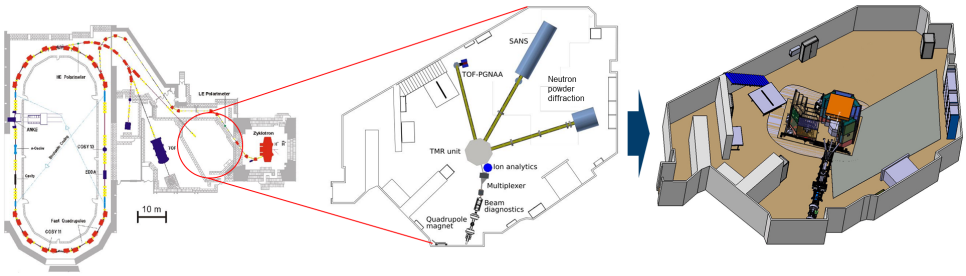

Figure A.1: Big-Karl-Area at IKP

The shielding of the target station was divided into three levels. All shielding blocks are interlocked with chicanes. Special stepped shielding boxes accommodate layers of lead and boron-PE (Fig. A.2 top). The shielding design consists of a 1 m^3 cube in the centre surrounded by an octagonal shield of about 1 m thickness (Fig. A.2 bottom). The inner cube contains the termination of the accelerator vacuum, the target with all supply and monitoring units, the thermal moderator and a reflector. Due to the space conditions in the Big Karl area, the outer diameter of the shielding had been limited to not exceed 3 metres. The whole shielding weights about 78 t and is built on a footprint of 3 m $\times$ 3 m (Fig. A.2 bottom). A special shielding plug (ca. 8 t) shields the radiation emanating upwards. For better weight distribution, the shielding was placed on an adjustable base plate (Fig. A.2 bottom). After adjustment, this plate was grouted with a concrete grout .

The shielding levels are modular assembled to allow for the following scenarios in addition to chang-

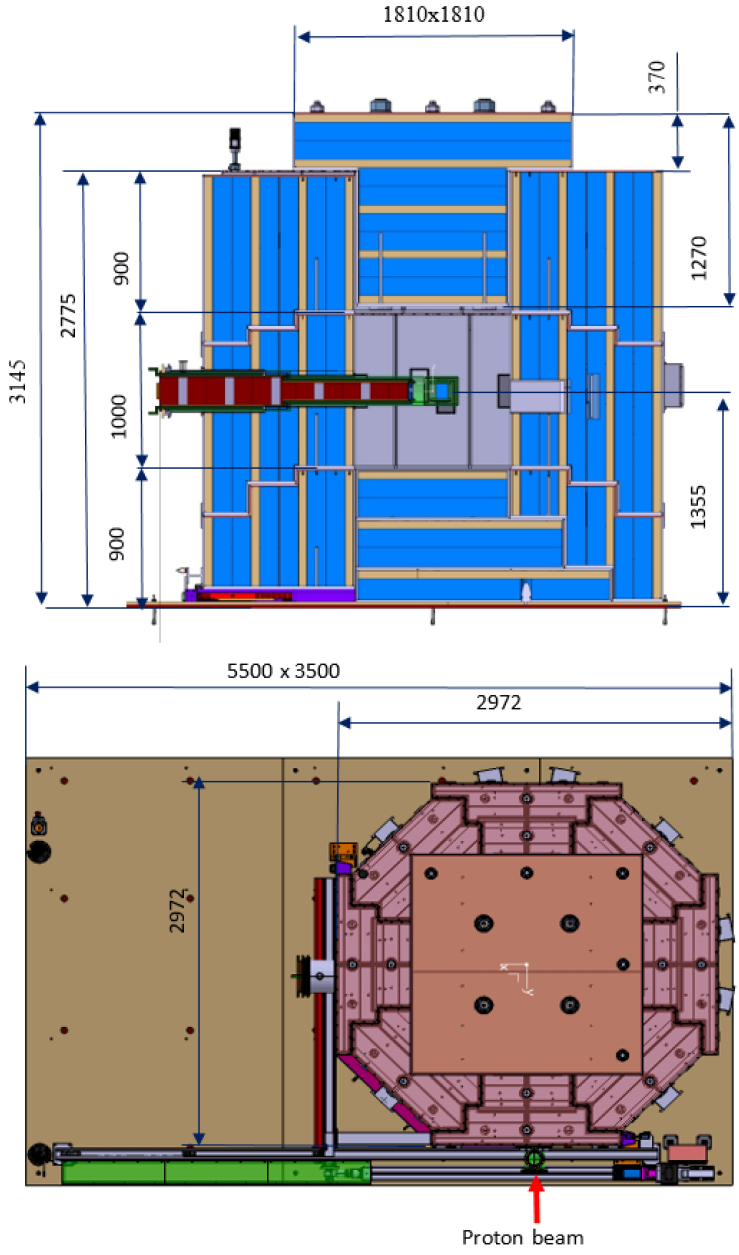

Figure A.2: *Top: Vertical cut through the shielding with plug. Bottom: Top view octagonal HBS shielding with plug.*

ing the target: i) partial disassembly to perform work on an extraction channel in level 2, ii) partial disassembly to move the prototype within the Big Karl area and iii) complete disassembly to free the prototype or for final storage.

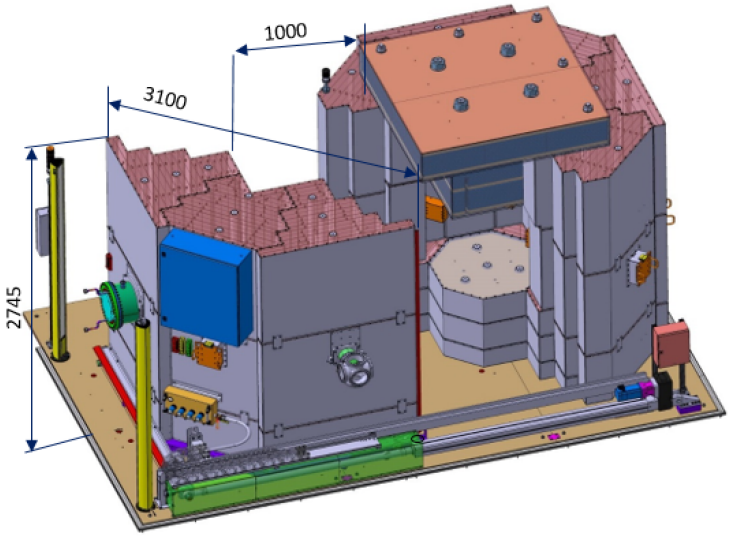

Figure A.3: Mobile shielding gate

Part of the shielding was assembled as a mobile shielding gate (Fig. A.3). The shielding gate is moved on roller carriage so that access to the inner structures (such as moderator, reflector, etc.) of the shielding is possible.

The neutrons obtained from the target are guided to the measuring instruments via individual ex-

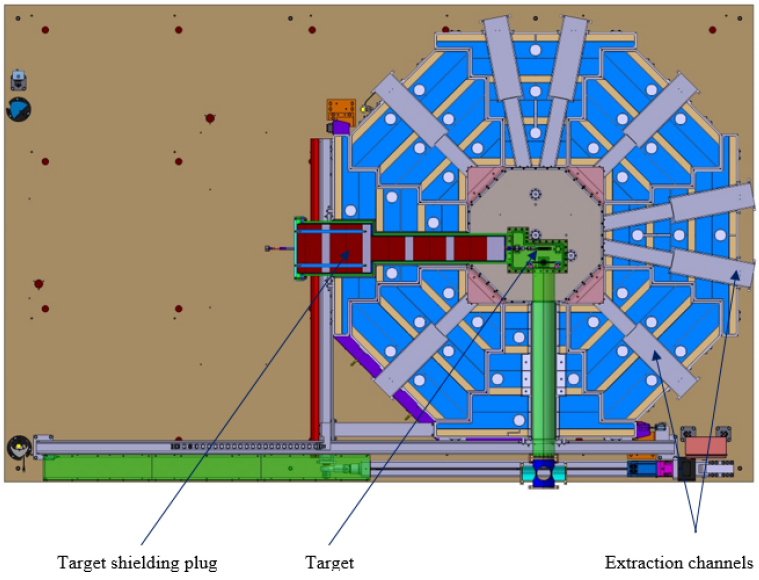

Figure A.4: Horizontal cut through central shielding level with the extraction channels

traction channels. The neutron guides, which are installed in a extraction plug, are mounted in the extraction channels. There are 8 extraction channels designed, which are located in the central shielding layer (Fig. A.4). Channels not used are closed with a shielding plug.

Manufacturing The construction and manufacturing of the steel housings was successfully realized (by Norte Mechanica). All box plates were made of low cobalt steel (<100 ppm) with a plate thickness of 10 mm for the side and top plates and the bottom plate with thickness of 20 mm. The steel housings are welded (Fig. A.5). In order to keep the tolerances, after the first tacking a post-treatment with fine alignment took place. After the actual welding, the alignment was checked again and corrected if necessary.

Figure A.5: *Examples of the finished steel boxes.*

All metallic surfaces on the outside are coated with a decontaminable coating (according to DIN 25415) RAL 5015 sky blue. Boxes interior only primed. According to the shielding calculations, 4 layers of lead plates of 50 mm thickness and 3 layers of borated polyethylene (4x60 mm) of a layer thickness of 240 mm are built up alternately in each shielding box.

L-tube The shielding layer in the middle also houses a so-called L-tube with the tantalum target and a diagnostic box for verifying the proton beam (Fig. A.6). The water-cooled target is located behind a target shielding plug.

TMR assembly The assembly of the TMR unit was carried out in four phases: i) assembly and adjustment of the base plate, ii) assembly of the mobile shielding gate and L-tube with ground middle parts, iii) assembly of the stationary part of the shielding and iv) installation of target with the target plug as shown in the following series of pictures (Fig. A.7-A.10).

Thermal and cold moderator assembly After mounting the target with the diagnostics box within the L-tube, the thermal and cold moderator was mounted within the TMR (Fig. A.11).

The entire facility was completed and commissioned with the proton beam at the beginning of December 2022. The first measurements with neutrons were carried out on the 12th of December.

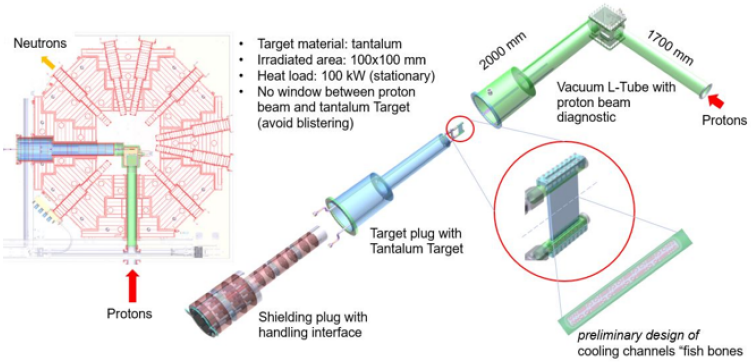

Figure A.6: *Design and assembly of L-Tube*

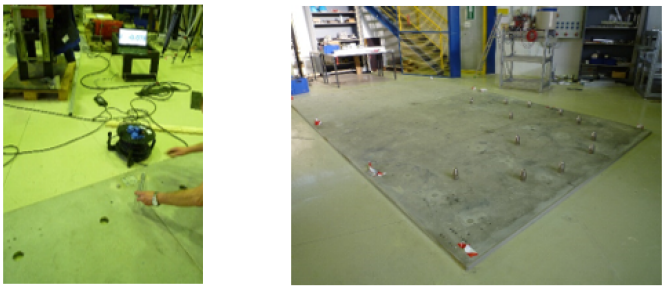

Figure A.7: *i) Assembly and adjustment of the base plate*

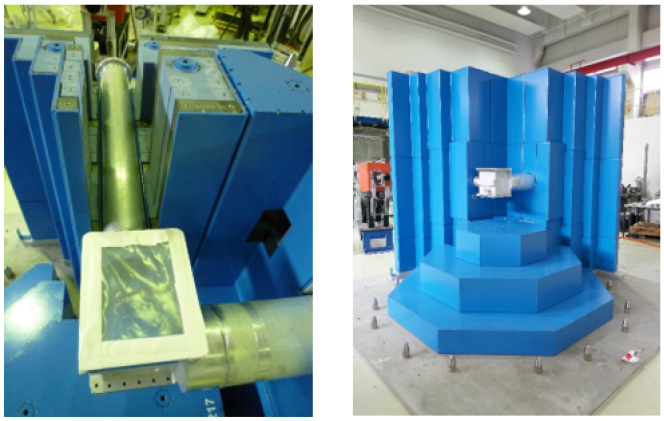

Figure A.8: *ii) Assembly of the mobile shielding gate and L-tube with ground middle parts*

Figure A.9: iii) Assembly of the stationary part of the shielding

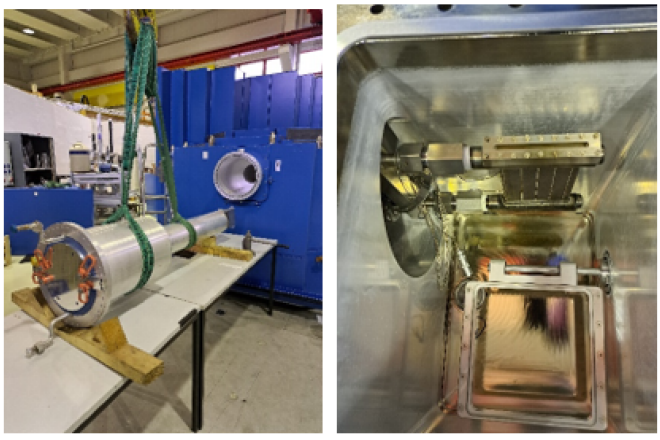

Figure A.10: iv) Installation of target with the target plug

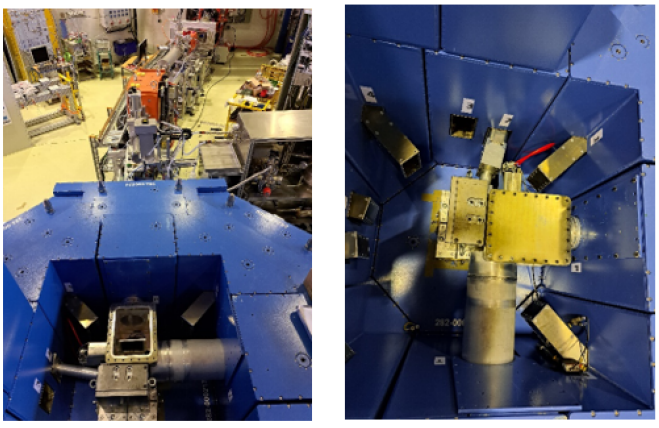

Figure A.11: Thermal and cold moderator installation.

A.2 Technical drawing of the neutron target assembly

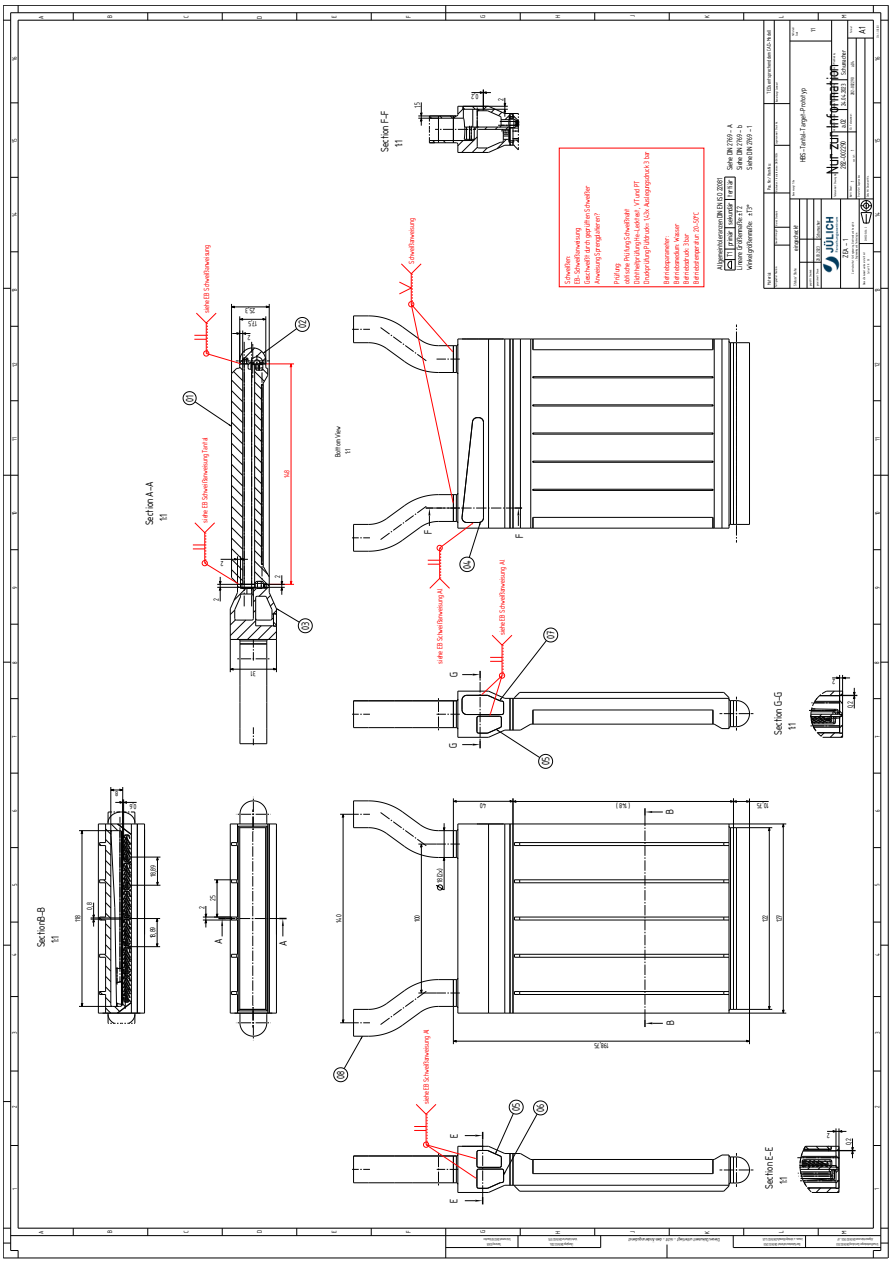

Figure A.12: Technical drawings of the HBS target assembly consisting of the main body, the 180° turnaround adapter for coolant flow and the adapter for inlet and outlet.

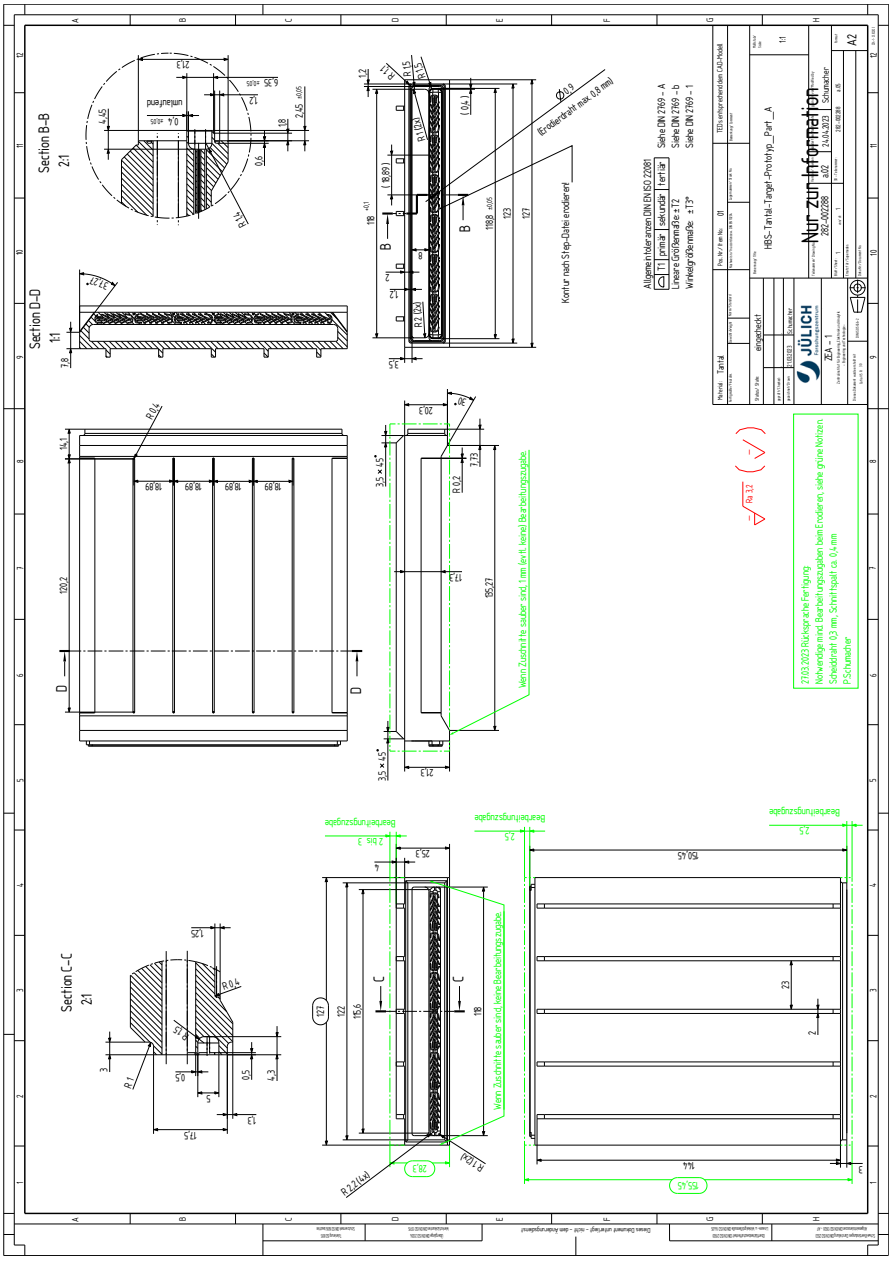

Figure A.13: *Technical drawings of the main body of the HBS target.*

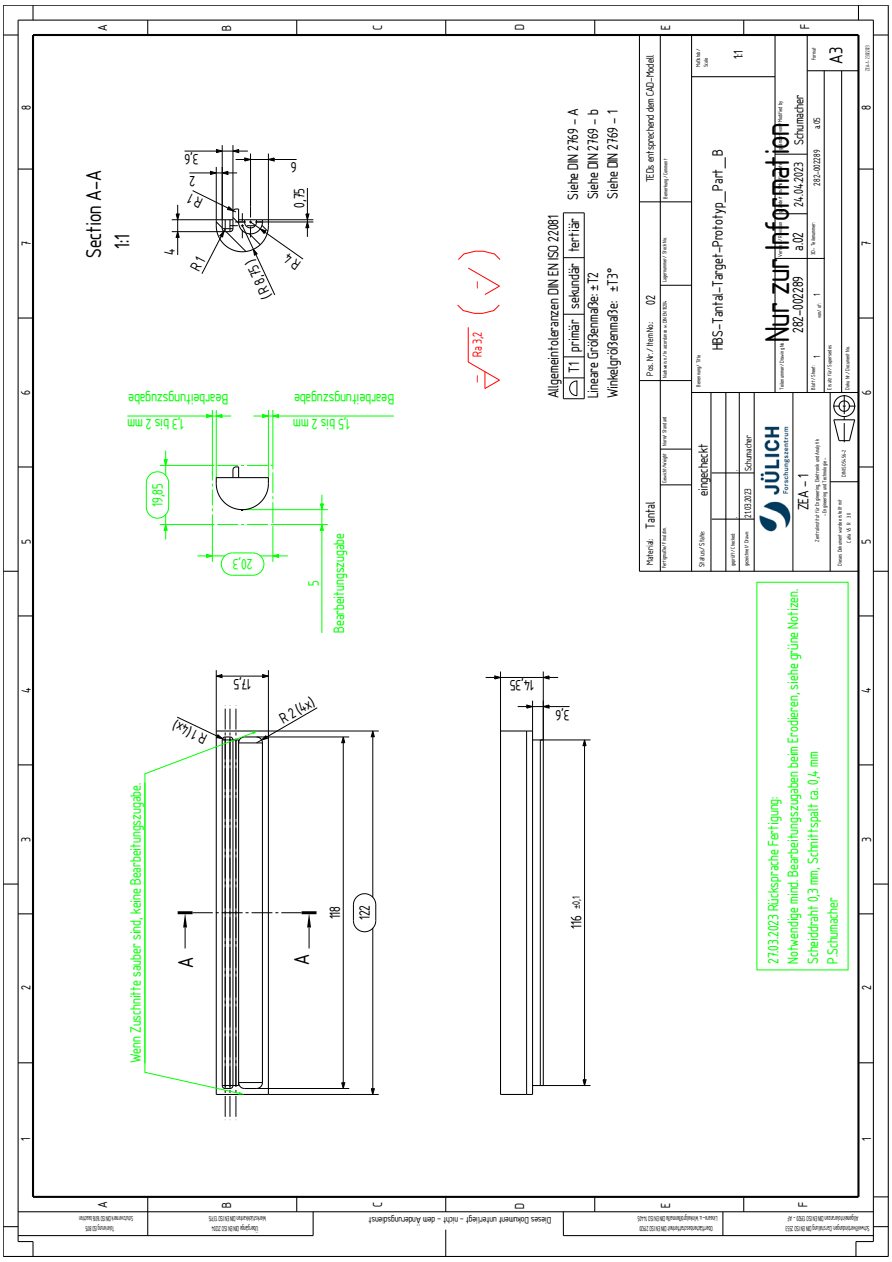

Figure A.14: *Technical drawings of the 180° turnaround adapter for coolant flow of the HBS target.*

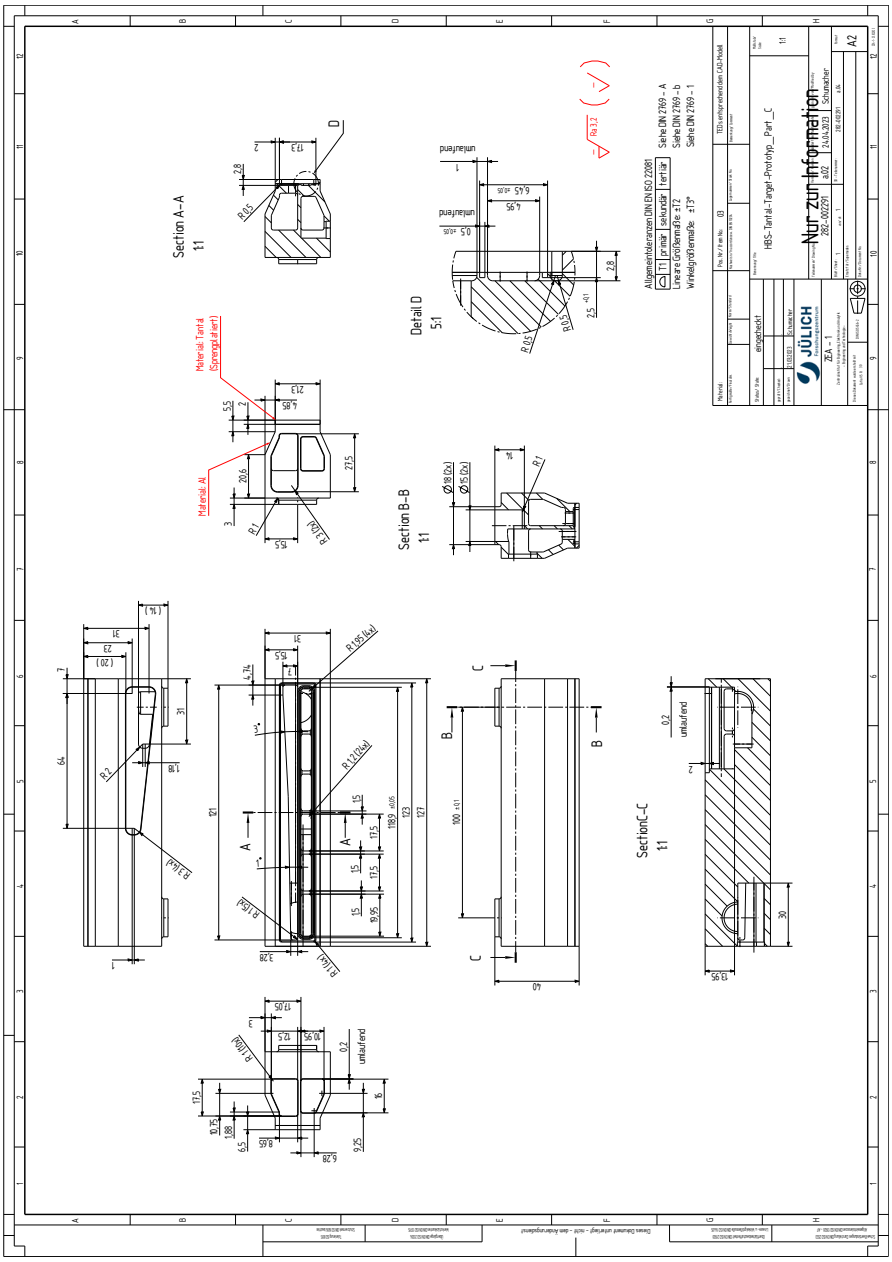

Figure A.15: *Technical drawings of the adapter for inlet and outlet of the HBS target.*

A.3 Schematic of the liquid para-hydrogen moderator cryostat

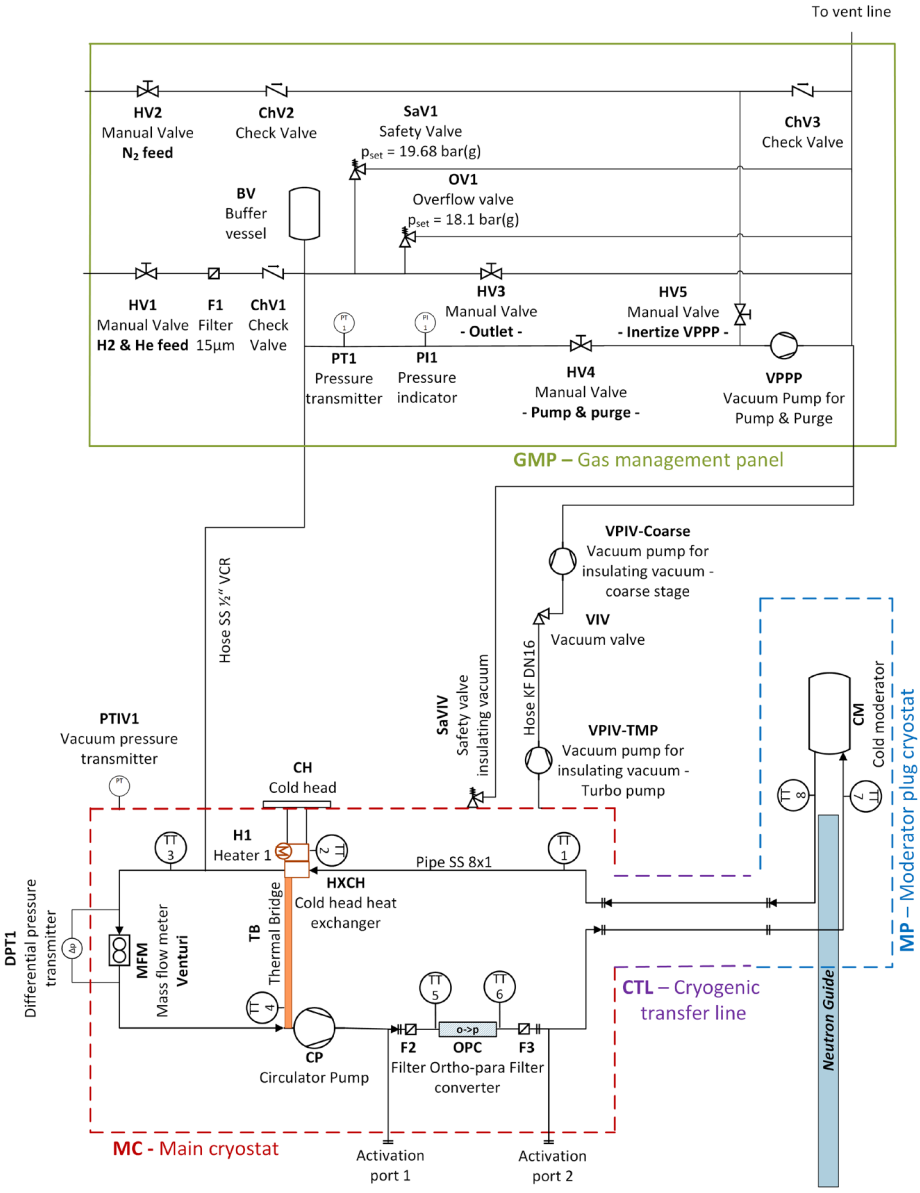

Figure A.16: Schematic of the liquid para-hydrogen cryostat consisting of the main components: Gas management panel (top), Main cryostat (bottom left), and Moderator plug cryostat (bottom right). Figure courtesy of S. Eisenhut.

A.4 Technical drawings of the L-tube from the HBS target station prototype

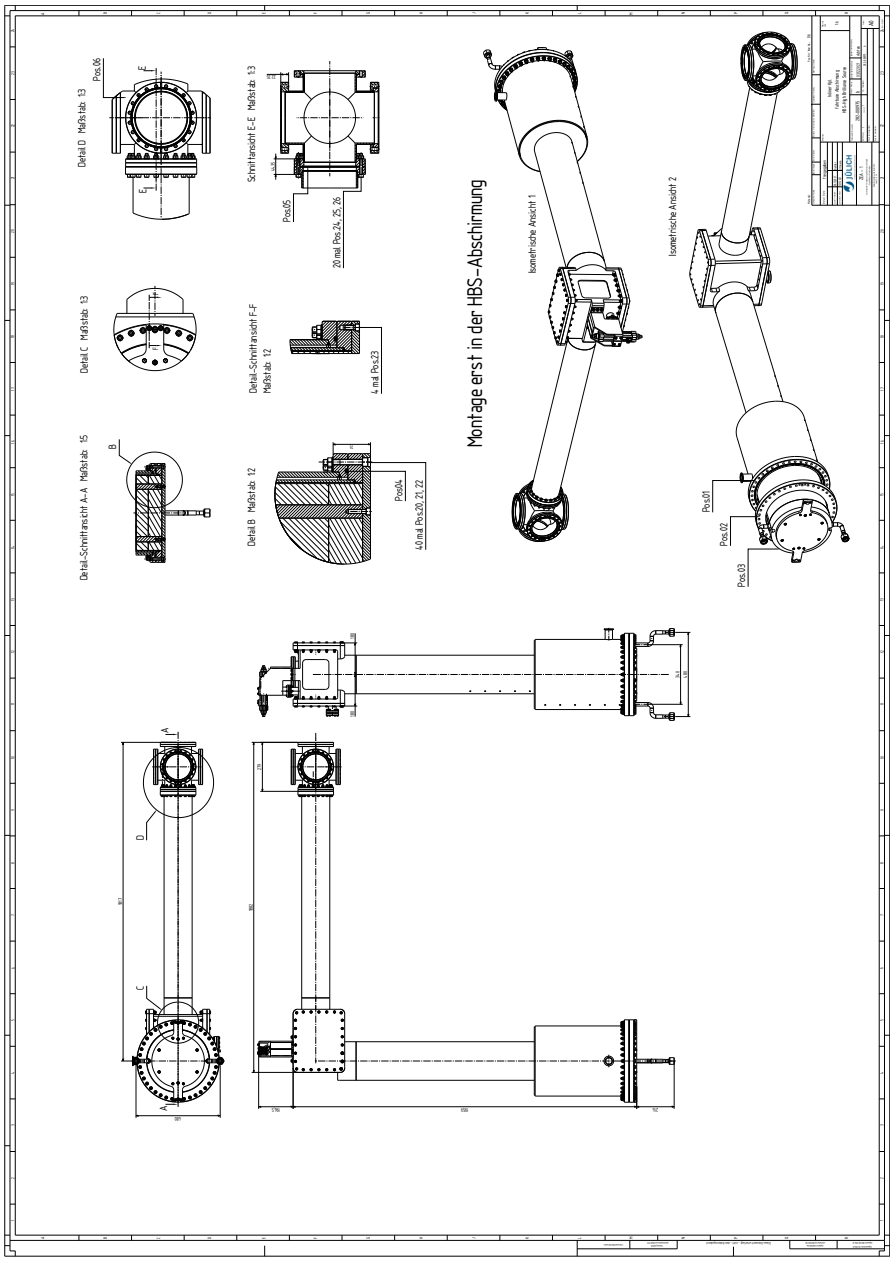

Figure A.17: *Technical drawing: overall view and detailed views of the L-tube from the HBS target station prototype*

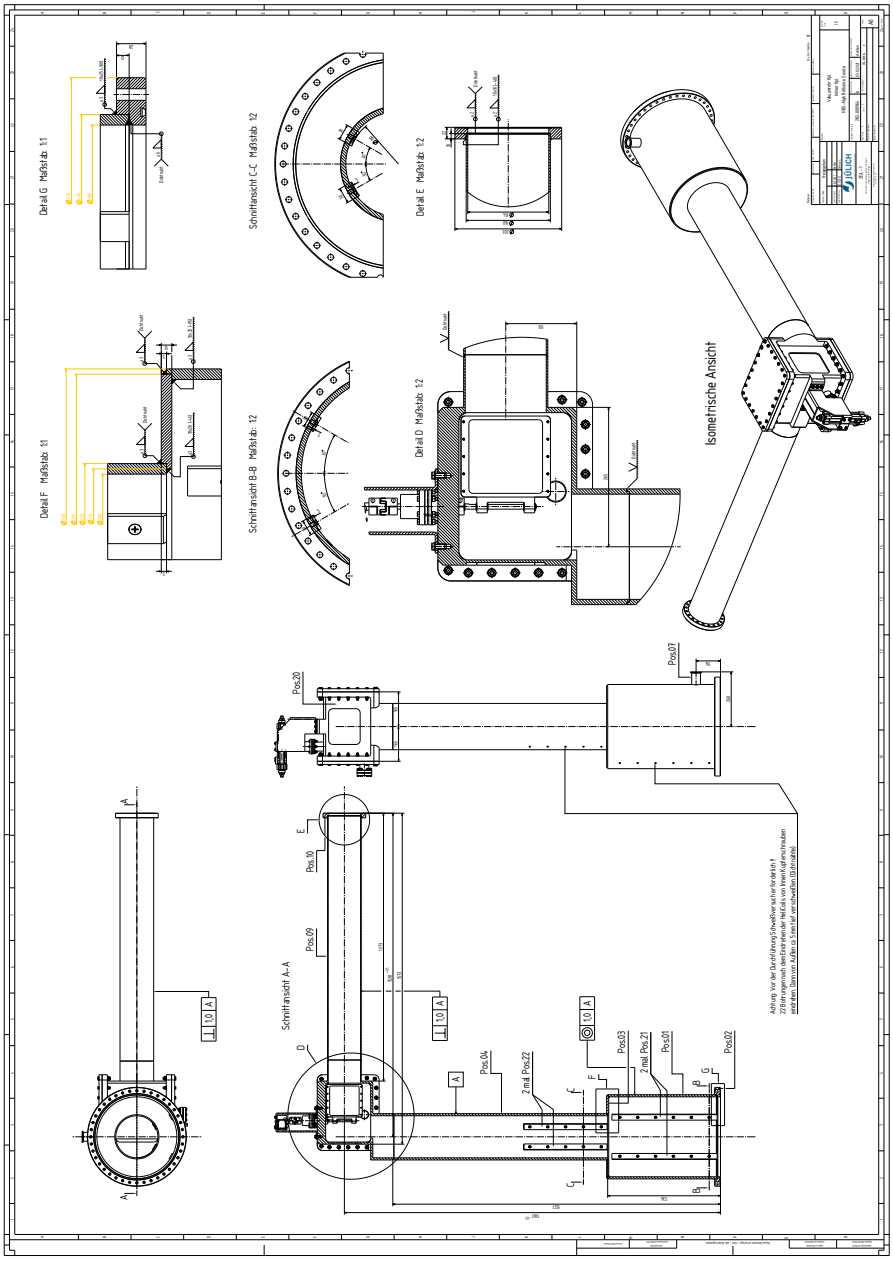

Figure A.18: *Technical drawing: cross sections and detailed views of the L-tube from the HBS target station prototype*

A.5 Neutron time structure

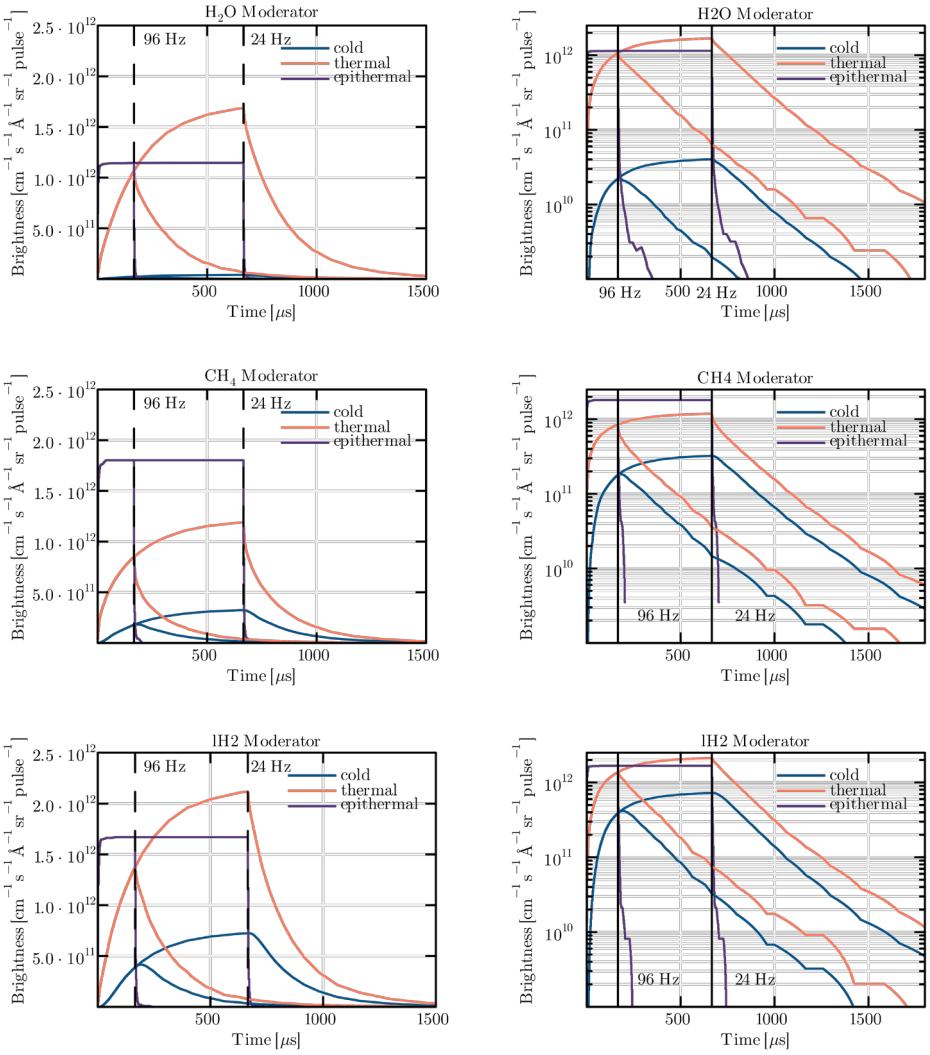

Figure A.19: Neutron time structure at the exit of the thermal and cold moderators in the top extraction plane, top: H_2O moderator, middle: CH_4 moderator, bottom: lH_2 moderator.

Bibliography

[ABB+10] V.T. Astrelin, A.V. Burdakov, P.V. Bykov, I.A. Ivanov, A.A. Ivanov, Y. Jongen, S.G. Konstantinov, A.M. Kudryavtsev, K.N. Kuklin, K.I. Mekler, S.V. Polosatkin, V.V. Postupaev, A.F. Rovenskikh, S.L. Sinitskiy, and E.R. Zubairov. Blistering of the selected materials irradiated by intense 200 kev proton beam. *Journal of Nuclear Materials*, 396(1):43 – 48, 2010.

[Bau10] G.S. Bauer. Overview on spallation target design concepts and related materials issues. *Journal of Nuclear Materials*, 398(1):19 – 27, 2010. Proceedings of the Ninth International Workshop on Spallation Materials Technology.

[BBD+20] J. Baggemann, S. Böhm, P. Doege, J. Fenske, M. Feygenson, A. Glavic, O. Holderer, S. Jaksch, M. Jentschel, S. Kleefisch, H. Kleines, J. Li, K. Lieutenant, P. Mastinu, E. Mauerhofer, O. Meusel, S. Pasini, H. Podlech, M. Rimmler, U. Rücker, T. Schrader, W. Schweika, M. Strobl, E. Vezhlev, J. Voigt, P. Zakalek, and O. Zimmer. *Conceptual Design Report: Jülich High Brilliance Neutron Source (HBS)*, volume 8 of *Schriften des Forschungszentrums Jülich. Reihe Allgemeines*. Forschungszentrum Jülich GmbH, Zentralbibliothek, Jülich, 2020.

[BBR+23] J. Baggemann, Y. Bessler, U. Rücker, J. Wolter, P. Zakalek, and T. Brückel. A scalable solution to develop compact high-performance targets for hicans. *in preparation*, 2023. Platzhalter, Veröffentlichung wird am 22.04.23 an Coauthoren geschickt; Plan: Einreichung vor Druck des Target Station TDR.

[BGB+23] Brückel, T., Gutberlet,T., Baggemann, J., Chen, J., Claudio Weber, T., Ding, Q., El-Barbari, M., Li, J., Lieutenant, K., Mauerhofer, E., Rücker, U., Schmidt, N., Schwab, A., Voigt, J., Zakalek, P., Bessler, Y., Hanslik, R., Achten, R., Löchte, F., Strothmann, M., Felden, O., Gebel, R., Lehrach, A., Rimmler, M., Podlech, H., Meusel, O., Ott, F., Menelle, A., and Paulin, M. A. The high brilliance neutron source (hbs): A project for a next generation neutron research facility. *EPJ Web Conf.*, to be published in 2023.

[BM08] T. Sang Byun and S. A. Maloy. Dose dependence of mechanical properties in tantalum and tantalum alloys after low temperature irradiation. *Journal of Nuclear Materials*, 377(1):72–79, 2008. Spallation Materials Technology.

[Car08] F. Cardarelli. *Materials Handbook*. Springer International Publishing, 2008.

[CBB+03a] J. Chen, G.S. Bauer, T. Broome, F. Carsughi, Y. Dai, S.A. Maloy, M. Roedig, W.F. Sommer, and H. Ullmaier. Summary of the results from post-irradiation examination of spent targets at the FZ-Juelich. *Journal of Nuclear Materials*, 318:56 – 69, 2003. Fifth International Workshop on Spallation Materials Technology.

[CBB+03b] J. Chen, G.S. Bauer, T. Broome, F. Carsughi, Y. Dai, S.A. Maloy, M. Roedig, W.F. Sommer, and H. Ullmaier. Summary of the results from post-irradiation examination of spent

targets at the fz-juelich. *Journal of Nuclear Materials*, 318:56–69, 2003. Fifth International Workshop on Spallation Materials Technology.

[CDD17] O. Caretta, T. Davenne, and C.J. Densham. Water erosion tests on a tantalum sample: A short communication. *Journal of Nuclear Materials*, 492:52–55, 2017.

[Din23] Qi Ding. *Optimization of Microchannel Target for a High-current Accelerator-driven Neutron Source*. Dissertation in preparation, Rheinisch-Westfälische Technische Hochschule Aachen, Aachen, 2023.

[EKB+20] S. Eisenhut, M. Klaus, J. Baggemann, U. Rücker, Y. Beßler, A. Schwab, C. Haberstroh, T. Cronert, T. Gutberlet, T. Brückel, and C. Lange. *Cryostat for the provision of liquid hydrogen with a variable ortho-para ratio for a low-dimensional cold neutron moderator*, volume 231 of *The European physical journal / Web of Conferences*, page 04001. EDP Sciences, 2020.

[FGT14] S. A. H. Feghhi, Z. Gholamzadeh, and C. Tenreiro. Investigation of the optimal material type and dimension for spallation targets using simulation methods. *Journal of Theoretical and Applied Physics*, 8(1):117, 2014.

[KLJ+17] O. Kirichek, C.R. Lawson, D.M. Jenkins, C.J.T. Ridley, and D.J. Haynes. Solid methane in neutron radiation: Cryogenic moderators and cometary cryo volcanism. *Cryogenics*, 88:101–105, 2017.

[KMT+16] M. Komori, K. Matsuda, T. Terakawa, F. Takeoka, H. Nishihara, and H. Ohashi. Active omni wheel capable of active motion in arbitrary direction and omnidirectional vehicle. *Journal of Advanced Mechanical Design, Systems, and Manufacturing*, 10(6):JAMDSM0086–JAMDSM0086, 2016.

[Lan] P. Langan. Proton power upgrade and second target station for the spallation neutron source., organization = Basic Energy Sciences Advisory Committee Meeting year = 2019,.

[McS] McStas. https://www.mcstas.org/download/components/2.7.2/.

[OML+21] N. Ophoven, E. Mauerhofer, J. Li, U. Rücker, P. Zakalek, J. Baggemann, T. Gutberlet, T. Brückel, and C. Langer. Monte carlo simulation of proton- and neutron-induced radiation damage in a tantalum target irradiated by 70 mev protons. *Applied Physics A*, 127(8):576, Jul 2021.

[SBD+97] H. Stockhorst, U. Bechstedt, J. Dietrich, R. Maier, S. Martin, D. Prasuhn, A. Schnase, H. Schneider, and R. Tolle. The cooler synchrotron cosy facility. In *Proceedings of the 1997 Particle Accelerator Conference (Cat. No.97CH36167)*, volume 1, pages 1048–1050 vol.1, 1997.

[Sch23] A. Schwab. *Design and manufacturing of a cryostat for a compact cryogenic neutron moderator for operating at temperatures below 10 K*. Dissertation in preparation, Rheinisch-Westfälische Technische Hochschule Aachen, Aachen, 2023.

[SHK+09] A. Schmidt, T. Hirai, S. Keusemann, M. Rödig, G. Pintsuk, J. Linke, H. Maier, V. Riccardo, G. F. Matthews, M. Hill, and H. Altmann. First demonstration of non-destructive tests on tungsten-coated jet divertor cfc tiles in the electron beam facility judith-2. *Physica Scripta*, 2009(T138):014034, dec 2009.

[Sim19] R. Similon. Thermische Analyse der Wärmeflüsse eines Mesitylen-Neutronen-Moderator-Systems im kryogenen Temperaturbereich. Bachelorarbeit, Fachhochschule Aachen, Campus Jülich, Fachbereich 10: Energietechnik, Jülich, 2019. Bachelorarbeit, Fachhochschule Aachen, Campus Jülich, Fachbereich 10: Energietechnik, 2019.

[SLK+18] N. Simos, H. Ludewig, H. Kirk, E. Dooryhee, S. Ghose, Z. Zhong, H. Zhong, S. Makimura, K. Yoshimura, J. R. J. Bennett, G. Kotsinas, Z. Kotsina, and K. T. McDonald. Multi-MW accelerator target material properties under proton irradiation at Brookhaven National Laboratory linear isotope producer. *Phys. Rev. Accel. Beams*, 21:053001, 2018.

[SMM91] A. San-Martin and F. D. Manchester. The H-Ta (hydrogen-tantalum) system. *Journal of Phase Equilibria*, 12(3):332–343, June 1991.

[Str20] M. Strothmann. Efficiency of a mesitylene based cold moderator system for a compact accelerator driven neutron source. Masterarbeit, RWTH Aachen University, Jülich, 2020. Masterarbeit, RWTH Aachen University, 2020.

[UC95] H. Ullmaier and F. Carsughi. Radiation damage problems in high power spallation neutron sources. *Nuclear Instruments and Methods in Physics Research Section B: Beam Interactions with Materials and Atoms*, 101(4):406 – 421, 1995.

[Ull03] H. Ullamier. Design properties of tantalum or everything you always wanted to know about tantalum but were afraid to ask, 2003.

[XJZ13] P. Xiang, P. Junfeng, and L. Zhikai. Experimental studies and analysis of 5% borated polyethylene shielding fast neutron. *Chinese Journal of Radiological Health*, 22(4):396–397,400, 2013.

[ZAB+23] Zakalek, P., Achten, R., Baggemann, J., Bessler, Y., Beule, F., Brückel, T., Chen, J., Ding, Q., El-Barbari, M., Engels, R., Felden, O., Gebel, R., Grigoryev, K., Gutberlet, T., Hanslik, R., Kamerdzhiev, V., Kämmerling, P., Kleines, H., Li, J., Lieutenant, K., Löchte, F., Mauerhofer, E., Paulin, M. A., Pechenizkiy, I., Rücker, U., Schmidt, N., Schwab, A., Steffens, A., Ott, F., Valdau, Y., Vezhlev, E., and Voigt, J. The high brilliance neutron source target stations. *EPJ Web Conf.*, to be published in 2023.

[ZDB+20] Zakalek, P., Doege, P.-E., Baggemann, J., Mauerhofer, E., and Brückel, T. Energy and target material dependence of the neutron yield induced by proton and deuteron bombardment. *EPJ Web Conf.*, 231:03006, 2020.

[ZKMT20] Zanini, L., Klinkby, E., Mezei, F., and Takibayev, A. Low-dimensional moderators at ESS and compact neutron sources. *EPJ Web Conf.*, 231:04006, 2020.

[ZLB+21] P. Zakalek, J. Li, S. Böhm, U. Rücker, J. Voigt, E. Mauerhofer, T. Gutberlet, and T. Brückel. Tailoring neutron beam properties by target-moderator-reflector optimisation. *Journal of Neutron Research*, 23:185–200, 2021.

List of Figures

Schriften des Forschungszentrums Jülich
Reihe Allgemeines / General

Band / Volume 3
Advances in Nuclear and Radiochemistry
Extended Abstracts of Papers presented at the Sixth International Conference on Nuclear and Radiochemistry (NRC-6), 29 August to 3 September 2004, Aachen, Germany
edited by S. M. Qaim, H. H. Coenen (2004), XXXII, 794 pp
ISBN: 3-89336-362-9

Band / Volume 4
Wissenschaft im Zeichen der Zeit
Preisträger des Leibfried-Preises im Forschungszentrum Jülich 2000 – 2005
herausgegeben von R. Ball (2005), ca. 185 pp
ISBN: 3-89336-411-0

Band / Volume 5
Proceedings of the 1st International Conference on Natural and Biomimetic Mechanosensing
edited by: J. Casas, G. Krijnen, M. Malkoc-Thust, J. Mogdans, A. Offenhäusser, H. Peremans (2009), ca. 80 pp
ISBN: 978-3-89336-583-8

Band / Volume 6
Leo Brandt (1908-1971)
Ingenieur – Wissenschaftsförderer – Visionär
Wissenschaftliche Konferenz zum 100. Geburtstag des nordrhein-westfälischen Forschungspolitikers und Gründers des Forschungszentrums Jülich
herausgegeben von B. Mittermaier, B.-A. Rusinek (2009), I, 121 pp
ISBN: 978-3-89336-602-6

Band / Volume 7
Conceptual Design Report
NOVA ERA
(Neutrons Obtained Via Accelerator for Education and Research Activities)
A Jülich High Brilliance Neutron Source project
E. Mauerhofer, U. Rücker, T. Cronert, P. Zakalek, J. Baggemann, P.-E. Doege, J. Li, S. Böhm, H. Kleines, T. Gutberlet, and T. Brückel (2017), 68 pp
ISBN: 978-3-95806-280-1

Band / Volume 8
Conceptual Design Report
Jülich High Brilliance Neutron Source (HBS)
T. Brückel, T. Gutberlet (Eds.) (2020), 197 pp
ISBN: 978-3-95806-501-7

Schriften des Forschungszentrums Jülich
Reihe Allgemeines / General

Band / Volume 9-01
Technical Design Report HBS
Volume 1 – Accelerator
R. Gebel, A. Lehrach, H. Podlech (Vol. Eds.), T. Brückel, T. Gutberlet (Ser. Eds.)
(2023), 151 pp
ISBN: 978-3-95806-709-7

Band / Volume 9-02
Technical Design Report HBS
Volume 2 – Target Stations and Moderators
J. Baggemann, E. Mauerhofer, U. Rücker, P. Zakalek (Vol. Eds.),
T. Brückel, T. Gutberlet (Ser. Eds.) (2023), 118 pp
ISBN: 978-3-95806-710-3

Band / Volume 9-03
Technical Design Report HBS
Volume 3 – Instrumentation
K. Lieutenant, J. Voigt (Vol. Eds.), T. Brückel, T. Gutberlet (Ser. Eds.)
(2023), 163 pp
ISBN: 978-3-95806-711-0

Band / Volume 9-04
Technical Design Report HBS
Volume 4 – Infrastructure and Sustainability
T. Gutberlet (Vol. Eds.), T. Brückel, T. Gutberlet (Ser. Eds.)
(2023), 137 pp
ISBN: 978-3-95806-712-7

Band / Volume 9-Overview
Opportunities for Research with Neutrons at the Next Generation Facility HBS
Overview of the High Brilliance neutron Source (HBS) Technical Design Report
T. Brückel, T. Gutberlet (Eds.) (2023), 44 pp
ISBN: 978-3-95806-713-4

Allgemeines / General
Band / Volume 9-02
ISBN 978-3-95806-710-3

Mitglied der Helmholtz-Gemeinschaft

JÜLICH
Forschungszentrum